Qualifying the Saturated Hydraulic Conductivity and Corresponding Infiltration Processes

by

Zuhier Alakayleh

A dissertation submitted to the Graduate Faculty of
Auburn University
in partial fulfillment of the
requirements for the Degree of
Doctor of Philosophy

Auburn, Alabama
December 14, 2019

Keywords: groundwater, forward modeling, clay-sand mixtures, hydraulic barrier, infiltration technique, soil moisture content.

Approved by

Xing Fang, Co-Chair, Professor of Civil Engineering
T. Prabhakar Clement, Co-Chair, Professor of Civil Engineering
Lauren Beckingham, Assistant Professor of Civil Engineering
Ming-Kuo Lee, Professor of Geosciences

ABSTRACT

Many engineering systems such as the hydraulic barriers and infiltration practices are designed based on the understanding of water infiltration through the subsurface. Among the soil hydraulic properties, the saturated hydraulic conductivity K_s is the most important parameter that controls the water seepage processes through the soil profile.

Clay-sand mixtures that have low K_s values are often used to construct hydraulic barriers. Several empirical models are available in the literature that can be used to predict reductions in K_s value of coarse sand due to the presence of clay and other fine minerals. However, all these models require measurements of multiple physical properties of the porous media. The resulting empirical expressions have several parameters that need to be individually evaluated using multiple soil characterization tests. In this study, a single parameter model was proposed and used to capture the variations in K_s value of different types of porous media mixtures using a scalable modeling framework. Several laboratory tests were conducted to measure K_s values of a variety of coarse and fine mixtures using synthetic porous media, natural clay-sand mixtures, and also using multiple literature-derived datasets to test the validity of the proposed model.

Infiltration practices are designed to have a high K_s value to enhance water infiltration into the underlying soil. During the construction and operational period, the hydraulic properties of the system have to be carefully measured at multiple locations and at multiple suction conditions. A technique that is inexpensive, easy to use, and requires a minimal amount of water to estimate the in situ K_s and the Green–Ampt suction head Ψ at

the wetting front is the Modified Philip–Dunne Infiltrometer (MPDI). In this study, a novel forward modeling algorithm was developed and used to investigate the performance of the MPDI. The forward model was used to simulate water level changes inside the infiltrometer with time when the soil hydraulic properties K_s and Ψ are known. The model was used to generate 30,000 water level datasets using randomly generated values of K_s and Ψ values. These data were then compared against field-measured drawdown data collected for three types of soil. The Nash–Sutcliffe efficiency (NSE) was used to assess the quality of the fit. Results show that multiple sets of the model parameters K_s and Ψ can yield drawdown curves that can fit the field-measured data equally well. Interestingly, all the successful sets of parameters (delineated by NSE $\geq$ the threshold value) give K_s values that converged to a valid range that is fully consistent with the tested soil texture class. However, the Ψ values varied significantly and did not converge to a valid range. Based on these results, we conclude that the MPDI is a useful field method to estimate K_s values, but it is not a robust method to estimate Ψ values.

The effect of the initial soil moisture content θ_{in} on the drawdown data measured using the MPDI and consequently on the estimated K_s and Ψ values were also investigated. Several laboratory tests were conducted using three types of porous media. Results show that the drawdown curve is different for each soil under varying θ_{in}. The estimated K_s values of every soil varied with θ_{in}, and the variation in K_s, however, could be minimized using a correction factor that is related to θ_{in} The estimated Ψ values in all the experiments did not correctly reflect the changes in soil texture classes and soil moisture content.

ACKNOWLEDGMENTS

I would like to express my sincere gratitude to my academic advisors, Professors Xing Fang and T. Prabhakar Clement, who have been tremendously supportive and patient during my PhD research. Without their guidance, encouragement, and valuable input throughout my research, I could not have completed my dissertation. I have been extremely lucky to have the opportunity to work with both of them.

I would like to extend a special thanks to my dissertation committee members, Professors Lauren Beckingham and Ming-Kuo Lee, for their valuable time to review my dissertation and provide their insightful comments and suggestions. I would also like to thank Dr. Yanzhao Cao for serving as a university reader of this dissertation.

I would also like to thank my friends and colleagues at Auburn and away for their continuous support through my academic. I wish to express my gratitude to Mutah University in Jordan for financial support toward my graduate study at Auburn University.

I'm deeply and forever thankful to my parents (Tawfiq and Rida), siblings, daughters (Sila and Retaal), and wife (Aseel) for their great love, support, and encouragement. I'm fortunate enough to have them in my life.

TABLE OF CONTENTS

LIST OF TABLES

LIST OF FIGURES

Chapter 1. Introduction and Objectives

1.1 Background

Water infiltration into the soil is the most important factor that affects many of the hydrological processes including groundwater recharge levels and the rate of surface runoff. When the infiltration increases the groundwater recharge increases and surface runoff decreases (Liu et al. 2011; Schiff and Dreibelbis 1949). Water infiltration into the soil can also directly affect the amount of water available for plant growth and erosion. With the increase in the infiltration of water, the water storage available for plant growth increases and erosion will decrease (Lipiec et al. 2006). Because of its important role in many fields, several models have been developed to describe and quantify the water infiltration into the soil including Green and Ampt (1911), Philip (1957), and Horton (1938).

Many engineering applications are designed based on the understanding of water infiltration through the subsurface. Some of these applications include the design of low permeability barriers, which are used to prevent contaminated water leaching from landfills and other waste disposal areas from polluting local groundwater aquifers. In contrast, some applications such as bioretention facilities and infiltration trenches or swales are designed to enhance water infiltration into underlying soil in order to attenuate runoff volume and accordingly increase groundwater recharge. In order to design these effective engineering applications, proper knowledge of the factors that affect water infiltration into the soil is needed. Some of the factors that affect water infiltration include the type of soil and its

physical/chemical properties. Soil properties such as hydraulic properties, fine content, and initial moisture content will greatly affect water infiltration into the soil.

Among the soil hydraulic properties, the saturated hydraulic conductivity K_s is the most important parameter that controls the water seepage processes through the soil profile (Alagna et al. 2016; Gregory et al. 2006; McKenzie and Jacquier 1997; Mohanty et al. 1994; Reynolds et al. 2000; Sivapullaiah et al. 2000; Zhang and Schaap 2019). Without having the proper knowledge of K_s value, it is impossible to design any effective engineering applications.

The infiltration of water into the soil will decrease with the increase in fine mineral percentage within the soil. Engineers use this fact to design low conductivity barriers that can prevent contaminated wastewater leaching from landfills and other waste disposal areas from polluting local groundwater aquifers. When an aquifer formation is highly permeable with no natural impervious soil layer, engineers add fine minerals such as clay to the locally available soil to achieve a mixture with a low conductivity value. The hydraulic conductivity of a clay-sand mixture will decrease with the increase in clay percentage (Abeele 1986; Chapuis 1990; Daniel 1993; Garlanger et al. 1987; Komine 2008; Sällfors and Öberg-Högsta 2002; Sivapullaiah et al. 2000). However, the consequence of adding an access amount of clay can affect the clay-sand mixtures in many ways. The swelling and shrinkage upon wetting and drying of the high-level clay mixture can eventually result in cracking and increase the risk of leakage through preferential flow paths (Dixon et al. 1985; Mollins et al. 1996). Also, the clay-sand mixture with increasing

clay content becomes more plastic and extremely difficult to compact (Sällfors and Öberg-Högsta 2002). Furthermore, the overall cost of the mixture will increase with increasing clay content (Akgün et al. 2006; Chapuis 1990; Lundgren 1981; Mollins et al. 1996). Therefore, the amount of clay required to achieve the desired hydraulic conductivity value of the mixture has to be carefully evaluated by performing laboratory-scale conductivity tests, and these efforts can be time consuming and cost prohibitive for most projects (Abichou et al. 2002; Chapuis 1990; Ebina et al. 2004).

Several studies have been conducted to develop mechanistic models that can predict the hydraulic conductivity values of clay-sand mixtures. Chapuis (1990) introduced an empirical equation to predict the hydraulic conductivity values of the soil-bentonite mixtures. Several physical parameters were used to develop the model including porosity, bentonite content, degree of saturation at the end of the test, grain-size distribution, and compaction level estimated from the Proctor curve. Benson et al. (1994) developed a five-variable regression model to estimate the hydraulic conductivity of compacted soil liners. Results from their regression analysis indicated five variables that were significantly correlated with the hydraulic conductivity value. These variables included: compactor weight, plasticity index, percent gravel, initial saturation, and percent clay. Another empirical model for predicting the hydraulic conductivity value of the clay-sand mixture was proposed by Benson and Trast (1995). The model parameters included the clay content, plasticity index, initial saturation, and compactive effort. Mollins et al. (1996) proposed a model that can predict the hydraulic conductivity of the clay-sand mixture based on the clay content, its properties, and sand porosity and tortuosity. Sivapullaiah et al.

(2000) model for predicting the hydraulic conductivity of bentonite-sand mixtures was based on measuring the void ratio and liquid limit of the mixture.

Our review indicated that there are several models available in the literature for predicting the reduction in the hydraulic conductivity of a porous medium due to the presence of clay and other fine minerals. However, all these attempts are based on measuring multiple physical properties of the porous media used for developing the mixture. Therefore, several soil characterization tests are needed to evaluate the multiple soil parameters included in the model. It will be desirable if one can develop a model based on an effective scaling parameter that can capture the combined effects of multiple soil parameters.

Another type of engineering applications, designed based on the understanding of water infiltration through the subsurface, is used to enhance water infiltration into the underlying soil. These types of applications, known as infiltration practices, are designed to have a high saturated hydraulic conductivity value. There are several examples of infiltration practices including infiltration basin, rain gardens, grassed swales, and porous pavement (Olson et al. 2013; Pitt et al. 1999). These practices are often called the low impact development (LID) or green infrastructures (GI) (in comparison to gray infrastructures for curb inlets and underground stormwater pipelines) because they intend to maintain or restore the predevelopment hydrology of the property and minimize the impact of urban development. The effectiveness of the infiltration practices is subjected to decrease due to many factors including clogging and compaction (Gregory et al. 2006;

Siriwardene et al. 2007). Therefore, the in situ saturated hydraulic conductivity of the infiltration practices has to be carefully measured at multiple locations (considering soil heterogeneous) throughout the infiltration practices during the construction and operation of the GI system.

Several field techniques have been developed to measure the in situ saturated hydraulic conductivity of the soil (Figure 1.1 shows some of them). A popular device for determining the in situ saturated hydraulic conductivity of the soil is the Disc infiltrometer which was described in detail by Perroux and White (1988). The rate at which water infiltrates into the soil is controlled by a suction applied at the soil surface. The analysis requires two infiltration measurements using two different tensions to estimate the saturated hydraulic conductivity of the soil. Another common device used in situ is the Guelph permeameter that was developed by Reynolds and Elrick (1986). This technique can measure the in situ saturated hydraulic conductivity using the constant head permeameter principle. This method employs a borehole (typically 31 cm depth and 3 cm radius) and uses the Mariotte principles to obtain a constant flow rate regardless of the decreasing water level within the permeameter. Philip (1993) introduced an approximate analysis based on the Green–Ampt theory to estimate the saturated hydraulic conductivity and the Green–Ampt suction head at the wetting front from the drawdown data of a falling-head permeameter. This method, known as the Phillip-Dunne permeameter, uses a cylindrical tube that is vertically inserted into a borehole at a given depth, typically 15 cm, within an unsaturated soil profile. Water is rapidly introduced into the system and the initial height H_{in} is recorded at time $t=0$. The data analysis procedure employs the Green–Ampt

model after transforming the actual three-dimensional flow system into an equivalent spherically symmetrical flow configuration. Ahmed et al. (2014) introduced a modified version of the Philip–Dunne permeameter (Philip 1993), known as the Modified Philip–Dunne Infiltrometer (MPDI). The MPDI involves applying the device near the surface rather than in a borehole that results in changing the flow configuration of the infiltrated water. The MPDI device (Figure 1.1d) includes a transparent plastic open-ended tube of internal radius r_1 (typically 5 cm) attached to a metal ring beveled from the edge for vertically inserting the system into an unsaturated soil for a distance of L_{max} (typically at about 5 cm). When the infiltrometer is placed on the soil surface, the wood ring is then placed on the top of the tube and a hammer is used to force the infiltrometer base (the metal ring) into the soil. Each user can buy these components and assemble them into the MPDI (not patented). The device is inexpensive, easy to use, and requires a minimal amount of water. These advantages make it a cost-effective and time-saving method to rapidly determine the in situ saturated hydraulic conductivity at the surface from multiple locations within the infiltration practices. The procedure for data collection and analysis is also described in ASTM-D8152-18 (2018). Following Philip's approximation, the infiltrated water into the soil is treated as primarily driven by pressure and capillarity forces. The absence of the gravity force results in the spherically symmetrical flow configuration.

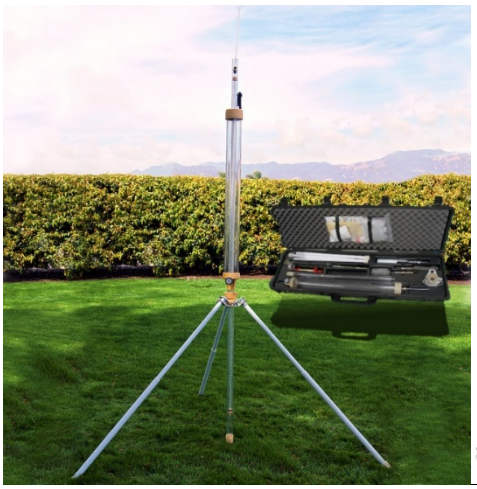

(a) Guelph permeameter.

(b) Disk infiltrometer.

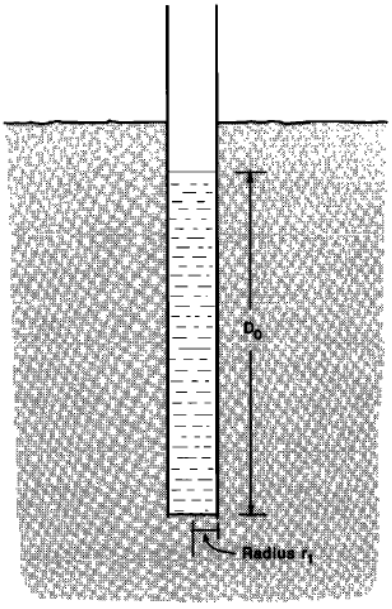

(c) Philip–Dunne permeameter.

(d) Modified Philip–Dunne infiltrometer.

Figure 1.1. Different types of infiltration techniques. (a) Guelph permeameter (Soil Moisture Corp. 2012), (b) Disk infiltrometer (Soil Measurement Systems 2005), (c) Philip–Dunne permeameter (Philip 1993), (d) Modified Philip–Dunne infiltrometer.

The spatial variability of the soil properties and limitations of the field techniques such as sample size and flow geometry could result in inaccurate estimation of the field-scale hydraulic properties (Mallants et al. 1997; Reynolds et al. 2000; Wessolek et al. 1994). Several studies are available in the literature that are aimed at evaluating the performance of different field techniques used for measuring the field-scale soil hydraulic properties. Mohanty et al. (1994) evaluated the relative performance of the Guelph permeameter, the velocity permeameter (Merva 1987), the disk permeameter, and the double-tube method (Bouwer 1964). The saturated hydraulic conductivity was measured using these methods at five different locations and at four soil depths. Undisturbed soil cores were also collected from all the locations to determine the saturated hydraulic conductivity in the laboratory to compare with the field-measured techniques. Reynolds et al. (2000) compared the saturated hydraulic conductivity values estimated using the tension infiltrometer (Perroux and White 1988) and the pressure infiltrometer (a single-ring, steady-flow technique) (Reynolds and Elrick 1990) with laboratory measurements. Muñoz-Carpena et al. (2002) compared the performance of the Philip-Dunne permeameter with the constant head permeameter and the Guelph permeameter. Nestingen et al. (2018) compared the accuracy and precision of the modified Philip-Dunne infiltrometer, the double-ring infiltrometer, and the minidisk infiltrometer (Zhang 1997). Controlled laboratory measurements of the saturated hydraulic conductivity for three types of media with different grain size distribution were completed. To determine the accuracy of each device, the mean hydraulic conductivity value was compared with the value obtained by using the falling-head test.

Our review indicates that several recent studies, including Weiss and Gulliver (2015), García-Serrana et al. (2017), Kristvik et al. (2018), and Taguchi et al. (2018), have used the Modified Philip-Dunne infiltrometer approach to measure the in situ soil hydraulic parameters. None of these studies have evaluated the sensitivity of the MPDI theory to the variations of the soil hydraulic parameters.

The initial moisture content is another soil property that affects the rate at which water infiltrated into the soil. The rate of water infiltration into a given soil varies between the maximum value when the soil is dry and the minimum value when the soil is wet (Horton 1933; Philip 1957; Ruggenthaler et al. 2016). Ruggenthaler et al. (2016) carried out a study to investigate the infiltration behavior in eight sites under dry, median, and wet conditions using the double-ring infiltrometer. The dry run was performed at the welting point, the median run was at the field capacity, and artificial sprinkling was used to produce the wet condition. Results showed that the infiltration rate decreased with increasing the initial soil moisture content. Previous studies have shown that water moves into the soil by the effect of two major forces: gravity and capillary forces (Gray and Norum 1967). Under a high soil moisture content (wet condition), a low wetting front suction exists and therefore the effect of capillary force decreases and the gravity force increases (Gray and Norum 1967; Hino et al. 1988; Regalado et al. 2005). Therefore, data collected using the MPDI under wet condition should be carefully evaluated since the assumption that the flow is primarily driven by pressure and capillarity is no longer valid.

1.2 Objectives of the Study

The study is divided into three parts and each of them is presented in a single chapter (Chapter 2, Chapter 3, and Chapter 4) in the dissertation. These chapters consist of independent introduction, materials and methods, results and discussion, and conclusions.

The objective of Chapter 2 is to develop a single parameter model that can be used to capture the variations in hydraulic conductivity value of coarse porous media due to the presence of different percentages of fine using a scalable modeling framework. All the current literature models are based on measuring multiple physical properties of the porous media within the mixture. The resulting empirical expressions have several parameters that need to be individually evaluated by multiple soil characterization tests. The main objective of this chapter is to propose a model that can estimate the hydraulic conductivity values of coarse-fine mixtures with fine content varying between 0 and 100 percent without using multiple experimental data points. Chapter 2 (Alakayleh et al. 2018) has been published as a journal paper in *Water,* a peer-reviewed journal covering multidisciplinary topics related to water such as hydrological and hydraulic studies.

In Chapter 3, the Modified Philip–Dunne infiltrometer (MPDI) is described in detail. The objective of this chapter is to further our understanding of the fundamentals of the MPDI theory and identify some of its advantages and limitations. Our review indicated that none of the studies that have used the MPDI to measure the in situ hydraulic properties of the soil have evaluated the sensitivity of the MPDI theory to the variations of the soil hydraulic parameters. This chapter is to complete a comprehensive investigation of the

sensitivity of the MPDI theory using a forward-modeling algorithm that can be used to simulate water level changes inside the infiltrometer with time. Chapter 3 (Alakayleh et al. 2019) has also been published in *Water* under the special issue "Soil and Water-Related Ecosystem Services" as the second journal paper.

The objective of Chapter 4 is to explore the effect of varying initial soil moisture content on the drawdown curve measured using the MPDI. This chapter aims to investigate the effect of varying initial soil moisture content of a given soil on the drawdown curves measured using the MPDI and use the data to study the uniqueness of the estimated saturated hydraulic conductivity and suction head values.

Chapter 5 provides a summary of the key findings of this dissertation.

Chapter 2. Understanding the Changes in Saturated Hydraulic Conductivity Values of Coarse- and Fine-Grained Porous Media Mixtures

2.1 Introduction

The contamination of groundwater systems by landfill leachates is one of the common environmental problems. When an aquifer formation is highly permeable with no natural impervious soil layer, engineers use low permeability clay-sand mixtures to construct hydraulic barriers that can prevent contaminated wastewater leaching from landfills and other waste disposal areas from polluting local groundwater aquifers (Akgün et al. 2006; Daniel 1993; Kenney et al. 1992; Mollins et al. 1996; Sällfors and Öberg-Högsta 2002). The amount of clay required to achieve the desired level of low permeability mixture is evaluated by performing laboratory-scale conductivity tests, and these efforts can be time consuming and cost prohibitive (Abichou et al. 2002; Chapuis 1990; Ebina et al. 2004).

Past studies have shown that the hydraulic conductivity of a clay-sand mixture will decrease with the increase in clay percentage (Abeele 1986; Chapuis 1990; Garlanger et al. 1987; Komine 2008; Sällfors and Öberg-Högsta 2002; Sivapullaiah et al. 2000). However, adding an excess amount of clay can lead to swelling and shrinkage that can eventually result in cracking and increase the risk of leakage through preferential flow paths (Dixon et al. 1985; Mollins et al. 1996). Also, at high clay levels, the mixture becomes more plastic and extremely difficult to compact (Sällfors and Öberg-Högsta 2002). Furthermore, the overall cost of the mixture will increase with increasing clay content (Akgün et al. 2006; Chapuis 1990; Lundgren 1981; Mollins et al. 1996).

The most important parameter that controls the groundwater seepage processes through subsurface aquifers is the hydraulic conductivity of the system (Shackelford and Javed 1991; Sivapullaiah et al. 2000). Without having a proper knowledge of the hydraulic conductivity value, it is impossible to design effective engineering barriers. Therefore, many investigators have conducted studies to develop mechanistic models that can predict the hydraulic conductivity value of clay-sand mixtures. Almost all currently available models are based on empirical formulations that use various physical properties of the materials used to develop the mixture and relate them to the effective hydraulic conductivity value of the mixture.

Chapuis (1990) introduced an empirical equation to predict the saturated hydraulic conductivity values of soil-bentonite mixtures. Several physical parameters were used to develop the model including porosity, bentonite content, degree of saturation at the end of the test, grain-size distribution, and the compaction level estimated from the Proctor curve. Permeameter tests were performed to evaluate the conductivity values. The results of the study indicated that there is an inverse relation between saturated hydraulic conductivity and amount of bentonite used in the mixture. No obvious correlation could be observed between the saturated hydraulic conductivity and porosity values of the mixture. However, saturated hydraulic conductivity correlated better with “efficient” porosity, which is related to the pore space available for fast-moving water. Note that the efficient porosity value is different from effective porosity, since it does not include the portion of immobile water that is retained at the surface of fine particles.

A five-variable regression model was developed by Benson et al. (1994) to estimate the saturated hydraulic conductivity of compacted soil liners. Results from the regression analysis indicated the five variables that were significantly correlated with the saturated hydraulic conductivity value (analyzed using the natural logarithmic scale); the variables included: compactor weight, plasticity index, percent gravel, initial saturation, and percent clay. The coefficient of determination (R^2) of their regression model was 78%. The authors stated that the model can be used to understand the conditions needed to achieve required saturated hydraulic conductivity values, however, it should not be used to avoid performing saturated hydraulic conductivity tests in the field or laboratory.

Another empirical model for predicting the saturated hydraulic conductivity values was developed by Benson and Trast (1995). This model can determine the saturated hydraulic conductivity of clay-sand mixture based on clay content, plasticity index, initial saturation, and compactive effort. The results from the falling-head saturated hydraulic conductivity test indicated an inverse relationship between saturated hydraulic conductivity and plasticity index, initial saturation, and compactive effort.

Mollins et al. (1996) used the compaction permeameter falling head permeability test and an indirect test based on consolidation data to measure the saturated hydraulic conductivity values of low and high clay content mixtures. Results showed that saturated hydraulic conductivity values of the clay-sand mixture linearly correlated with the clay void ratio when plotted on a logarithmic scale. This study proposed a model that can predict

the saturated hydraulic conductivity of the mixture based on the clay content, its properties, sand porosity and tortuosity.

Sivapullaiah et al. (2000) developed an equation aimed at predicting the saturated hydraulic conductivity of bentonite-sand mixtures based on the void ratio and liquid limit of the mixture. The consolidation cell permeameter test was used to measure the saturated hydraulic conductivity value. A linear relationship was established between the saturated hydraulic conductivity of the mixture (used in the logarithmic scale) and the void ratio. Other studies have also explored the similar type of empirical relationship between saturated hydraulic conductivity to the net void ratio of a mixture (Abeele 1986; Taylor 1948). In contrast to these studies, Kenney et al. (1992) and Castelbaum and Shackelford (2009) presented a relation between saturated hydraulic conductivity and void ratio of the bentonite rather than the net void ratio for mixtures present with a sufficient bentonite content to be uniformly distributed to fill all the void spaces between sand particles.

Abichou et al. (2002) conducted a study aimed at understanding the changes in microstructure and the saturated hydraulic conductivity value of sand-bentonite mixtures at varying bentonite content. Simulated sand-bentonite mixtures were prepared using glass beads, to simulate sand particles, which were then mixed with powdered and granular bentonite. The use of glass beads helped to improve the visual properties of the mixtures. Results showed that pores available for water flow decreased as the bentonite content increased in the mixture, and this resulted in the reduction of saturated hydraulic conductivity. In the case of mixtures prepared with powdered bentonite, the bentonite

coated the glass bead particles, swelled, and later filled the pores. Little glass bead particles were coated with bentonite if mixtures were prepared using granular bentonite. In this case, granular bentonite particles occupied the pores between the glass bead particles and then absorbed the introduced water and swelled. In both cases, when sufficient bentonite was available to fill all the pores between glass bead particles, the saturated hydraulic conductivity of the mixture was primarily controlled by the saturated hydraulic conductivity of bentonite.

Dias et al. (2008) investigated the effect of volume fraction and particle size ratio for binary mixtures of glass beads on the tortuosity coefficient. This was done because of the sensitivity of the tortuosity coefficient in estimating permeability values using the Kozeny–Carman equation that relates permeability with porosity, tortuosity, and grain size. Previous studies correlate tortuosity with porosity using a simplified formula, $T = \varepsilon^n$, where T is tortuosity, ε is porosity, n is a power factor, which was proposed to be 0.04 by Mota et al. (2001). This simplified formula and the Kozeny–Carman equation were combined together and then a new formula for n factor was developed. Permeability tests were conducted and the data was used to measure the experimental values of n using the new formula. The measured n values were found to range between 0.4 and 0.5 and a model was used to correlate the changes of n with the changes in volume fraction and particle size ratio. The developed model helped to improve the accuracy of permeability values calculated using the Kozeny–Carman equation.

Our review indicates that while there are several types of models available for predicting the reduction in the saturated hydraulic conductivity of a porous medium due to the presence of clay and other fine minerals, all these models are based on measuring multiple physical properties of the porous media used to develop the mixture. The resulting empirical expressions have several parameters that need to be individually evaluated by multiple soil characterization tests. It will be desirable if one can develop a model based on an effective scaling parameter that can capture the combined effects of multiple soil parameters. Therefore, the objective of this study is to develop an integrated scaling parameter that can be used to fully capture the variations in different types of physical properties into a unified framework. In this study, we have hypothesized that the changes in saturated hydraulic conductivity values of fine- and coarse-grained mixtures can be corrected to the amount of fine material in the mixture. We collected several sets of laboratory data and also assembled multiple sets of literature-derived data to develop a scalable framework for modeling the changes in saturated hydraulic conductivity values due to the presence of fine material.

2.2 Materials and Methods

2.2.1 Synthetic Coarse-Fine and Fine-Coarse Mixtures

Three sets of experiments with two using synthetic media and other using natural media were completed in this study. Materials used in the synthetic media experiments were different types of uniform coarse and fine glass beads. The coarse glass beads were used to simulate sand minerals and small glass beads were used to simulate fine minerals

such as silt and clay. Our approach is similar to studies by Abichou et al. (2002) and Dias et al. (2008) that used glass beads to simulate clay-sand mixtures.

Figure 2.1 shows the two sets of synthetic media experiments completed in this study. First, a coarse porous medium was mixed with three different sized fine porous media to develop three different dry mixtures. The saturated hydraulic conductivity (K_{sc}) of the coarse porous medium is 920 m/d, and the saturated hydraulic conductivity values (K_{sf}) of the three fine porous media are: 228, 57, and 9 m/d. In the second set of experiments, a fine porous medium was mixed with three different coarse porous media. The saturated hydraulic conductivity of the fine porous medium is 9 m/d, and the saturated hydraulic conductivity values of the three coarse porous media are: 920, 228, and 57 m/d.

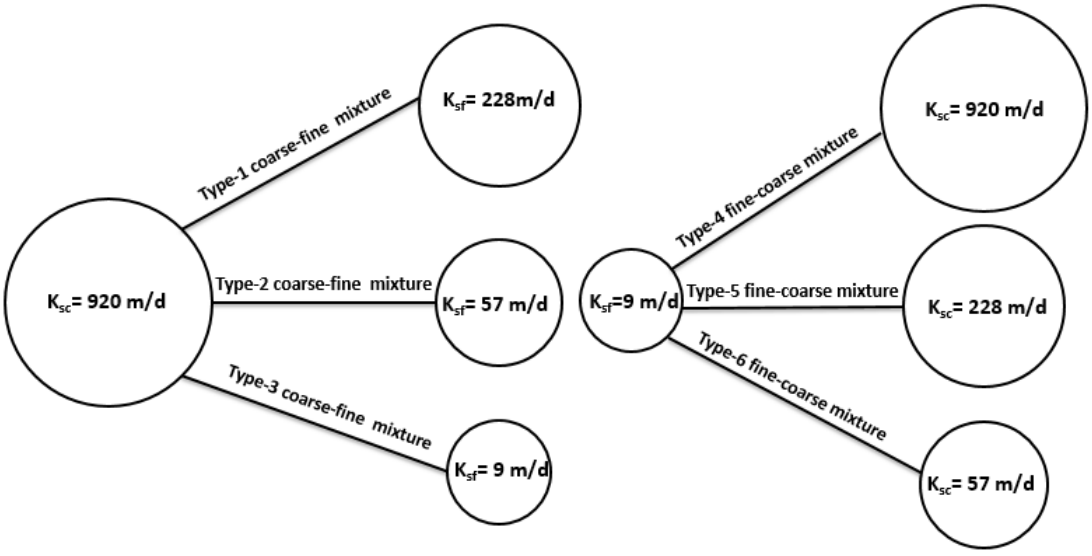

Figure 2.1. Schematic diagram illustrating the two sets of coarse-fine and fine-course porous media mixtures used in our laboratory experiments. K_s is saturated hydraulic conductivity in m/day, the subscripts *c* and *f* stand for the coarse and fine particles. Each type of mixture was prepared with seven different fine percent levels: 0%, 5%, 10%, 15%, 20%, 25%, and 30%.

Before mixing, the porous media were washed in tap water to remove any dust and then dried in an oven. Samples were prepared by mixing coarse porous media with the following amount (percent dry weights) of fine porous media (0%, 5%, 10%, 15%, 20%, 25%, and 30%). An innovative mixing procedure used by Dias et al. [22] was employed to thoroughly mix the coarse and fine glass beads. In this method, glycerol is used as a binder to fully mix the glass beads of different sizes. After packing the mixture, the glycerol was washed out by flushing water through the column. The use of glycerol allowed us to pack a uniform mixture within the column.

Saturated hydraulic conductivity tests for glass bead mixtures were conducted by closely following the method described in ASTM-D2423-68 (1968). This method uses the constant head permeameter test to determine the saturated hydraulic conductivity of materials with values greater than 1×10^{-5} m/s (ASTM-D5084-16a 2016). Two transparent plastic columns of diameter 1.9 cm, but different lengths were used to construct the permeameter. The length of the short column is 25 cm and the long column is 75 cm. A wire mesh was used at the bottom of the short column then the soil sample was added over this mesh and was compacted gradually. While packing, the column was kept under water to maintain fully saturated conditions. To avoid segregation, the column was gradually lowered into the water bucket as it was packed. After packing the short column, a long transparent column was connected to the short column using a rubber coupling.

Tap water was used as the permeant liquid, and prior to its use, the water was allowed to reach the lab temperature. This was done to avoid gas exchanges and air trapping

while running the test. After the sample was compacted, a high hydraulic gradient was applied to wash out the glycerol before running the saturated hydraulic conductivity tests. To ensure consistency, a pump was used to introduce the water flow into the sample. The flow rate, sample length, column cross-section area, and head loss were measured, and Darcy's law was applied to calculate the effective saturated hydraulic conductivity value of the mixture.

2.2.2 Natural Clay-Sand Mixtures

Natural clay was sieved on mesh No. 60 and was used in this study. The saturated hydraulic conductivity value of this clay is 1.12×10^{-3} m/d. Fine sand with a saturated hydraulic conductivity value of 46.5 m/d was used. Aged deaired water equilibrated to laboratory conditions was used to avoid gas exchanges during the test. All the mixtures were prepared under saturated conditions.

Samples were prepared by mixing the sand with varying amount (percent weights) of clay (0%, 5%, 6%, 8%, 10%, 11%, 13%, 15%, 20%, 25%, and 30%). These mixtures were prepared based on the dry weight of the material. To obtain complete mixing, deaired water was added to the mixture and it was then physically stirred to prepare a well-mixed saturated slurry (glycerol was not added in this case). The clay-sand slurry was left in the mixing pan and covered for a period of about 48 h to let the clay fully saturate with water. During this period, water was added and the mixture was periodically stirred, whenever it is needed, to ensure complete mixing and full saturation.

A falling head permeameter was used; the test procedure closely followed the method described in ASTM-D5084-16a (2016). Within the permeameter, the clay-sand mixture was packed in between two sand layers. The bottom sand layer helped prevent the fine material from washing away through the bottom screen. The top sand layer helped us to better compact the mixture. After the sample was packed, the falling head permeameter test was performed to determine the saturated hydraulic conductivity value of the sample.

2.3 Results

2.3.1 Results of Coarse-Fine Porous Media Mixtures

Test results for the first set of synthetic coarse-fine porous media mixtures indicated that the saturated hydraulic conductivity decreased as the fine percentage increased in the mixture (Figure 2.2). The reduction in saturated hydraulic conductivity was significant when we started to add fines to the coarse material; however, the reductions became less significant when the percentage of the fine was greater than about 15%. Interestingly, the overall saturated hydraulic conductivity of the mixture was almost close to the saturated hydraulic conductivity of the fine particles when the percent of the fine was above 30%.

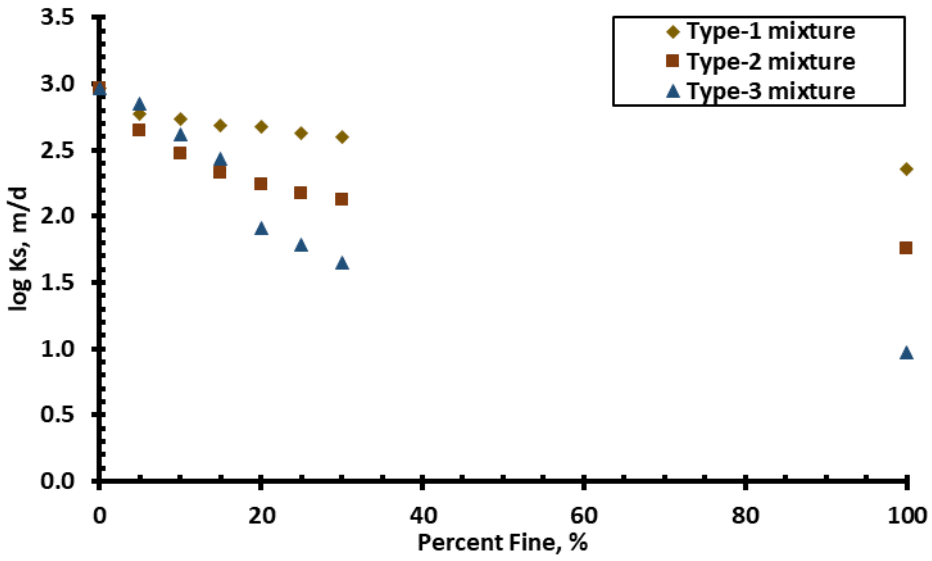

Figure 2.2. Decrease in the effective saturated hydraulic conductivity values (K_s values plotted in log scale) of Type-1 (K_{sc} = 920 m/day and K_{sf} = 228 m/day), Type-2 (K_{sc} = 920 m/day and K_{sf} = 57 m/day), and Type-3 (K_{sc} = 920 m/day and K_{sf} = 9 m/day) coarse-fine mixtures. The seven mixtures for each type were prepared by varying the fine porous media content (percentage by weight) as: 0%, 5%, 10%, 15%, 20%, 25%, and 30%.

This trend of decrease in saturated hydraulic conductivity with increasing percent fines is similar to the observations made by others for different types of clay and sand mixtures (Benson et al. 1994; Garlanger et al. 1987; Kenney et al. 1992; Komine 2008; Sivapullaiah et al. 2000).

We have developed and used the following empirical equation to describe the reductions in the saturated hydraulic conductivity values of all our coarse-fine porous media mixtures.

$$\log K_s(p) = (\log K_{sc} - \log K_{sf}) \times e^{(-s \times p)} + \log K_{sf} \quad (2.1)$$

where p is the percent of fine (e.g., 10 for 10 percent of fine, ranging 0–100), $K_s(p)$, K_{sc}, and K_{sf} are the saturated hydraulic conductivity values of the mixture, coarse porous media, and fine porous media, respectively. The model uses a single fitting constant s, which is an empirical parameter employed to scale the results based on the percentage of fines in the mixture. The empirical model was fitted to the dataset shown in Figure 2.2 and the optimal values of the scaling parameter for Type 1, 2, and 3 mixtures that best fit all the experimental data are 0.04, 0.05, and 0.03 (see Figure 2.3), respectively. The nonlinear Solver Add-in available in Excel was used to evaluate these fitting parameters. Saturated hydraulic conductivity values obtained by Equation (2.1) in comparison with experimental values for the first set of the three different types of mixtures are plotted in Figure 2.3 as a function of percent fine. The root mean square error (RMSE) values of log K_s calculated between the fitted model and experiment are summarized in Table 2.1. The coefficients of determination (R^2) values are 93.4%, 98.6%, and 95.4% for Type 1, 2, and 3 mixtures, respectively.

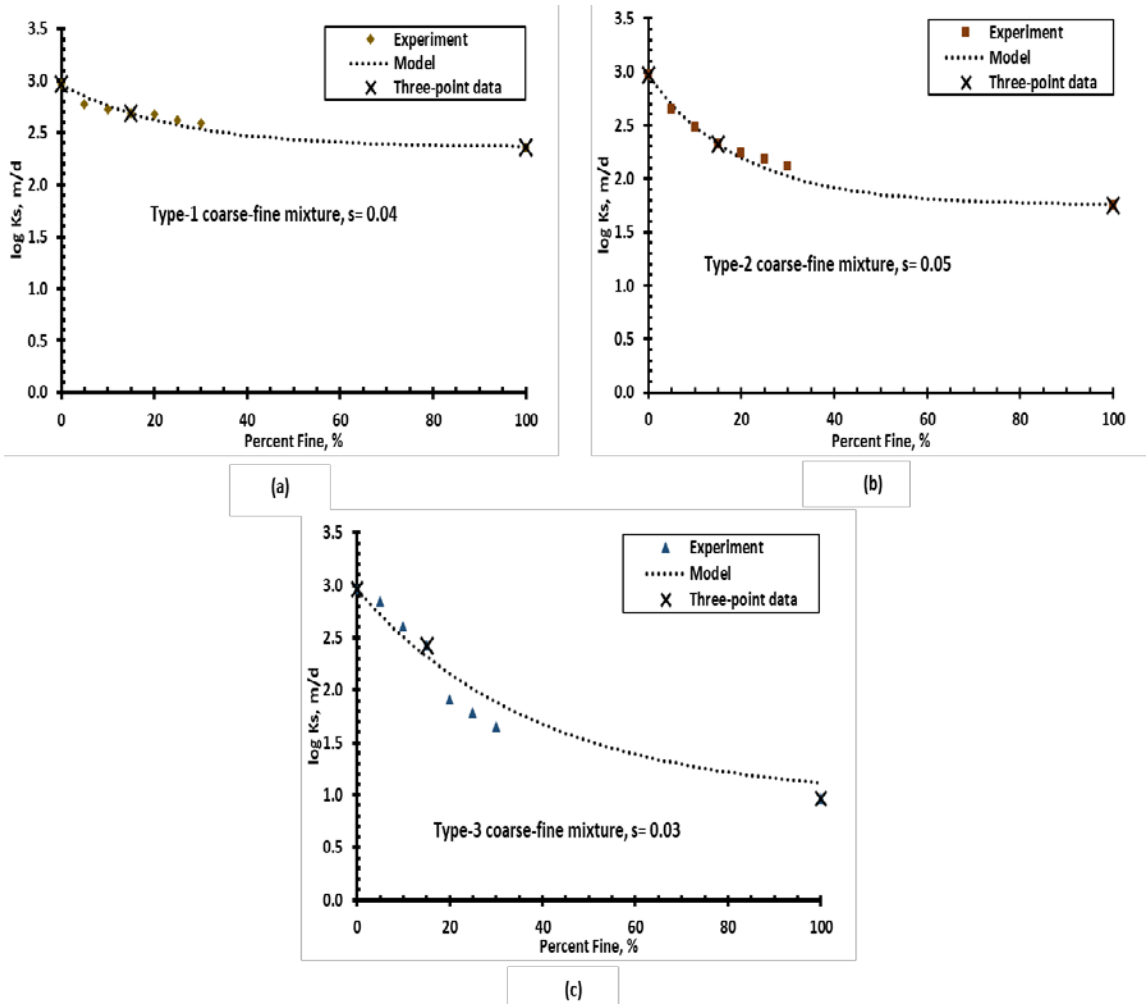

Figure 2.3. Comparison of fitted model results with experimental data for all three types of coarse-fine mixtures: (**a**) Type-1 (K_{sc} = 920 m/day and K_{sf} = 228 m/day), (**b**) Type-2 (K_{sc} = 920 m/day and K_{sf} = 57 m/day), and (**c**) Type-3 (K_{sc} = 920 m/day and K_{sf} = 9 m/day). The effective saturated hydraulic conductivity K_s values are plotted on the *y*-axis in the log scale. The cross symbol is used to identify the data points used in the three-point method discussed in Section 2.3.5.

Table 2.1 Summary of the scaling factor (s) values estimated for all the samples tested in this study and literature-derived experimental datasets.

Type of Mixture	s Estimated Using the Entire Dataset	s Evaluated Using the Three-Point Method [4]
Type-1 coarse-fine mixture	0.037 (RMSE [1]= 0.041, R^2 = 93.4%)	0.041 (RMSE = 0.045, R^2 = 92.3%)
Type-2 coarse-fine mixture	0.046 (RMSE = 0.041, R^2 = 98.6%)	0.050 (RMSE = 0.050, R^2 = 97.8%)
Type-3 coarse-fine mixture	0.031 (RMSE = 0.138, R^2 = 95.4%)	0.026 (RMSE = 0.169, R^2 = 93.0%)
Type-4 fine-coarse mixture	0.031 (RMSE = 0.138, R^2 = 95.4%)	0.026 (RMSE = 0.169, R^2 = 93.0%)
Type-5 fine-coarse mixture	0.040 (RMSE = 0.043, R^2 = 99.9%)	0.041 (RMSE = 0.044, R^2 = 98.7%)
Type-6 fine-coarse mixture	0.054 (RMSE = 0.046, R^2 = 95.6%)	0.056 (RMSE = 0.047, R^2 = 95.4%)
Clay-sand mixture	0.079 (RMSE = 0.188, R^2 = 97.3%)	0.077 (RMSE = 0.191, R^2 = 97.2%)
Montmorillonite-sand mixture [2]	0.074 (RMSE = 0.051, R^2 = 99.9%)	0.074 (RMSE = 0.051, R^2 = 99.9%)
Kaolinite-sand mixture [2]	0.034 (RMSE = 0.041, R^2 = 99.7%)	0.034 (RMSE = 0.041, R^2 = 99.7%)
Bentonite-silt mixture [3]	0.030 (RMSE = 0.134, R^2 = 99.4%)	0.032 (RMSE = 0.168, R^2 = 99.1%)

Note: [1] All root mean square errors (RMSEs) and coefficients of determination R^2 of log K_s were calculated using the entire dataset for each fitted model; [2] Data from Denson et al. (1968); [3] Data from Doley et al. (2016); [4] The details of the three-point method are described in Section 2.3.5.

2.3.2 Results of Fine-Coarse Porous Media Mixtures

The second set of experiments were completed using three different types of fine-coarse mixtures, where a uniform fine porous medium was mixed with three different types of coarse porous media at different dry weight percentages levels. Figure 2.4 shows the increase in saturated hydraulic conductivity values as we increased the percentage of coarse material in the mixture. Similar to the coarse-fine mixtures, the amount of fines in the system controlled the effective saturated hydraulic conductivity value of the mixture. The addition of coarse material into the fine porous media had little impact until about 85% of coarse material was added to the system, after which the system was highly influenced by the conductivity of the coarse material used to prepare the mixture.

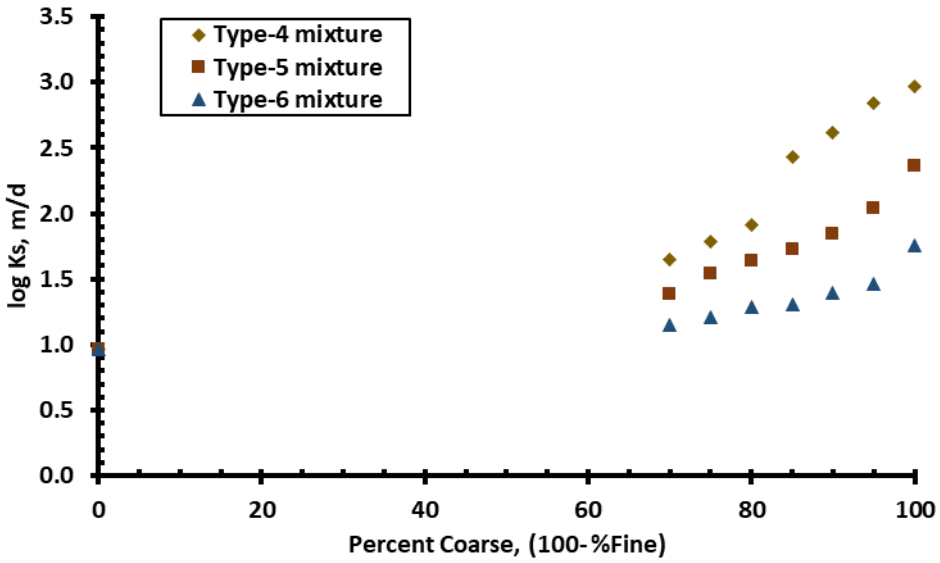

Figure 2.4. Increase in the effective saturated hydraulic conductivity values (K_s values plotted in log scale) of Type-4 (K_{sc} = 920 m/day and K_{sf} = 9 m/day), Type-5 (K_{sc} = 228 m/day and K_{sf} = 9 m/day), and Type-6 (K_{sc} = 57 m/day and K_{sf} = 9 m/day) fine-coarse mixtures. The seven mixtures for each type were prepared by varying the coarse porous media content (percentage by weight) as: 0%, 70%, 75%, 80%, 85%, 90%, and 95%.

The empirical model used to describe the coarse-fine Type 1, 2, and 3 mixtures was also used to analyze the fine-coarse Type 4, 5, and 6 mixtures. The fitted values of the scaling parameter for Type 4, 5, and 6 mixtures are 0.03, 0.04, and 0.05, respectively. Figure 2.5 shows the experimental and modeled saturated hydraulic conductivity values for the three types of fine-coarse mixtures characterized in this study. The coefficients of determination (R^2) values are 95.4%, 99.9%, and 95.6% for the three types of mixtures.

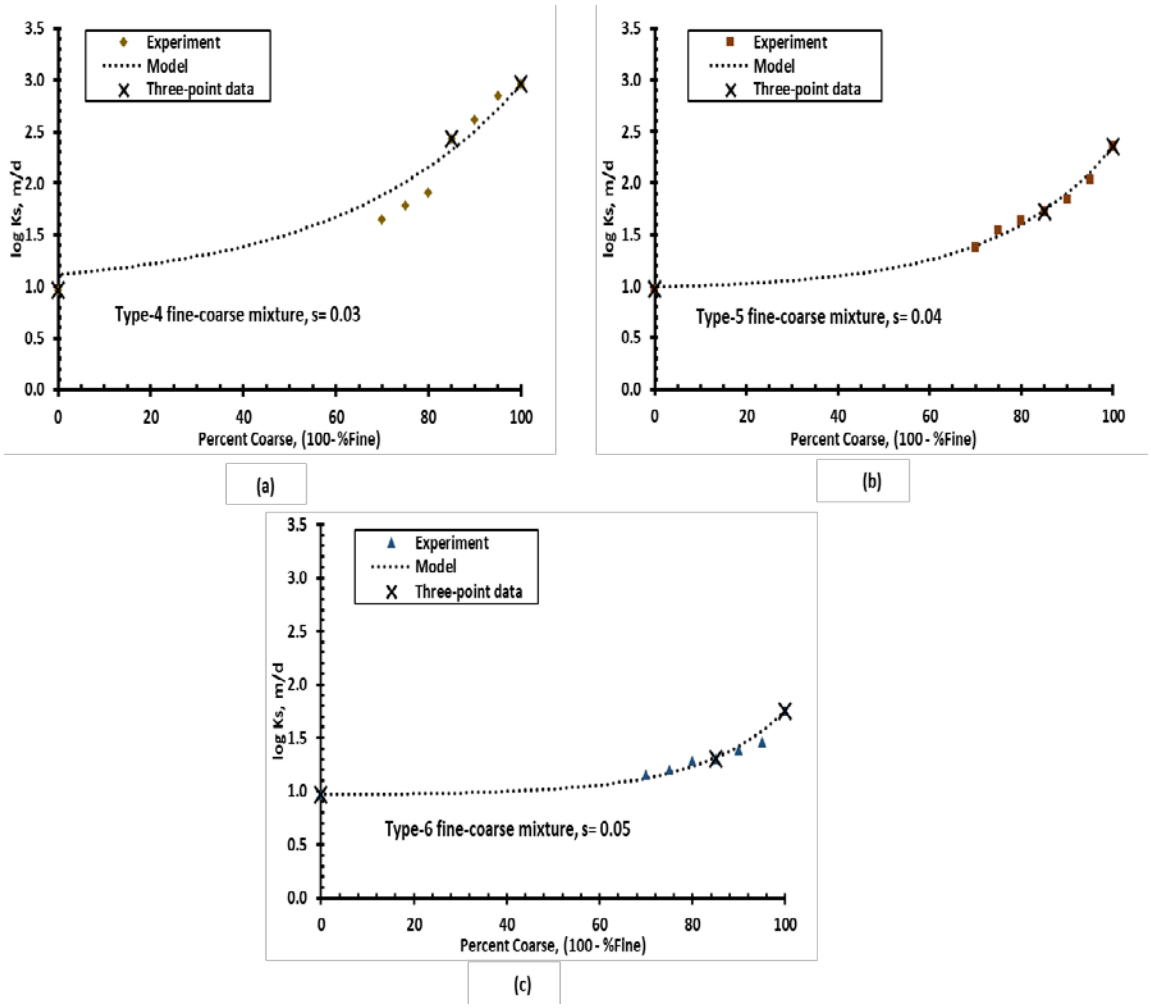

Figure 2.5. Comparison of fitted model results with experimental data for all three types of fine-coarse mixtures: (**a**) Type-4 (K_{sc} = 920 m/day and K_{sf} = 9 m/day), (**b**) Type-5 (K_{sc} = 228 m/day and K_{sf} = 9 m/day), and (**c**) Type-6 (K_{sc} = 57 m/day and K_{sf} = 9 m/day). The cross symbol is used to identify the data points used in the three-point method discussed in Section 2.3.5.

2.3.3 Results of Clay-Sand Mixtures

The performance of the model was tested using an exploratory dataset collected using natural clay and sand. Figure 2.6 shows both experimental data and model results for a natural sand, with saturated hydraulic conductivity value of 46.5 m/day, mixed with a

natural clay with saturated hydraulic conductivity value of 1.1×10^{-3} m/day. The behavior of the mixture at varying clay content was similar to the behavior of the different types of synthetic mixtures discussed in the previous sections. The optimal fitted value of the scaling parameter s for the clay-sand system was estimated to be 0.08. This result gave a value of 97.3% for the coefficient of determination R^2.

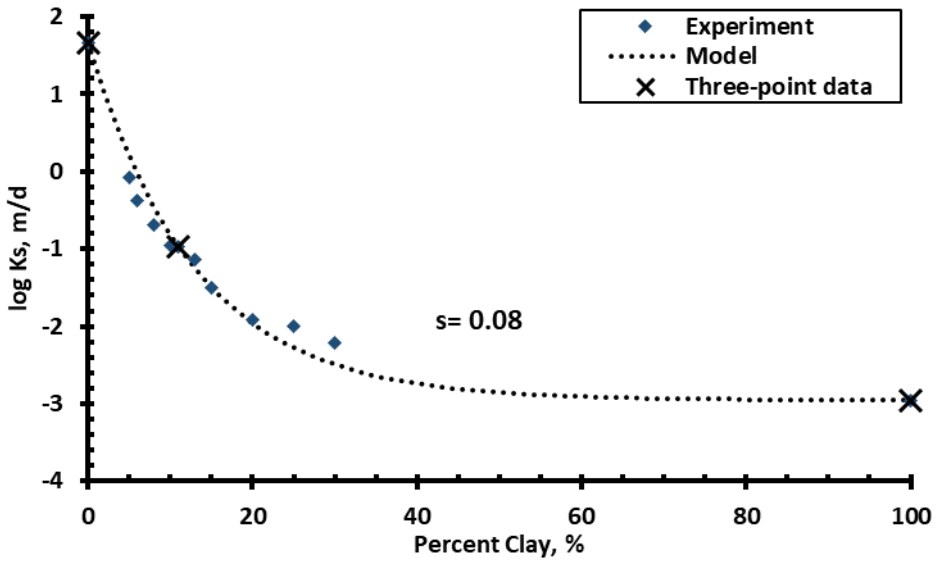

Figure 2.6. Comparison of fitted model results with experimental data for the natural clay and sand mixture. The cross symbol is used to identify the data points used in the three-point method discussed in Section 2.3.5.

2.3.4 Comparison of Model Results with Literature-Derived Experimental Datasets

The validity of the model in representing the changes in saturated hydraulic conductivity of the clay-sand mixtures at varying clay content levels was further tested using data from previous studies. Denson et al. (1968) reported the saturated hydraulic conductivity of clay-sand mixtures at varying clay content for both montmorillonite and kaolinite clay. The purpose of their study was to investigate the reduction in saturated

hydraulic conductivity of a sand by introducing different amount of clay. The saturated hydraulic conductivity of the clay-sand mixture reduced to practically zero when montmorillonite and kaolinite content were about 3 and 16 percent, respectively. Figure 2.7 shows both model results and experimental data from Denson et al. (1968) for montmorillonite and kaolinite mixed with sand. These results indicate that experimentally measured saturated hydraulic conductivity values at different clay contents are well described by our model—Equation (2.1).

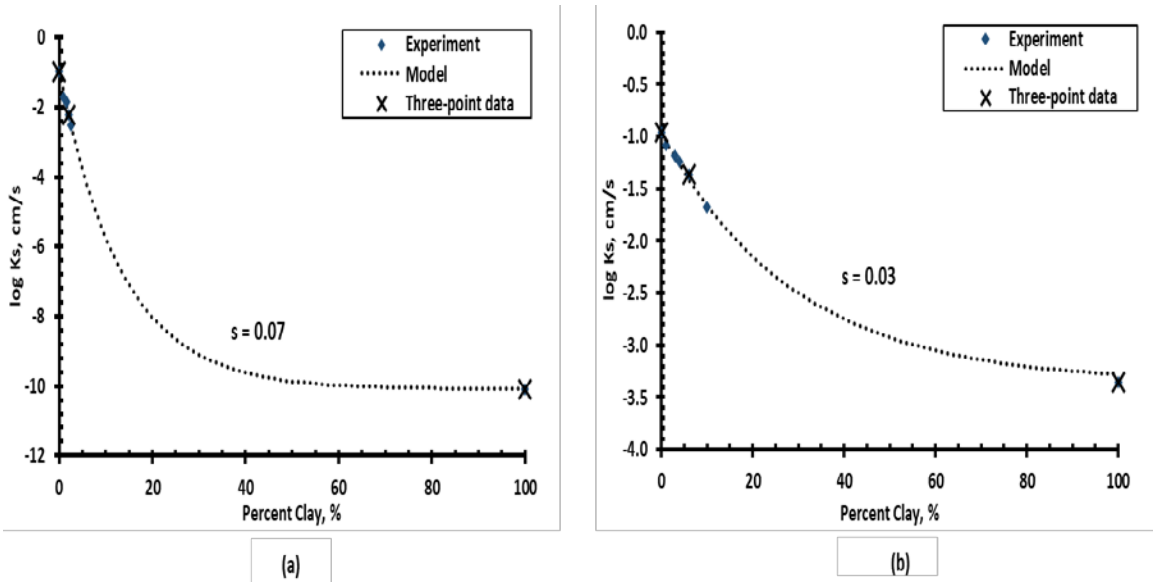

Figure 2.7. Comparison of our fitted model results with experimental data from Denson et al. (1968) for clay-sand mixtures: (**a**) montmorillonite clay, and (**b**) kaolinite clay. The cross symbol is used to identify the data points used in the three-point method discussed in Section 2.3.5.

Also, the dataset from a study carried out by Doley et al. (2016) was used to test the validity of the proposed model. Figure 2.8 shows both experimental data and model results for bentonite mixed with locally available silty soil in Brahmaputra, India. Several

saturated hydraulic conductivity tests were performed to investigate the effect of bentonite content at various percentages on the locally available soil in order to find the optimum percentage that can be used to get the required low saturated hydraulic conductivity value. The study recommended mixing the available soil with 20 to 30 percent dry weight of bentonite to modify and use the available soil as a low conductivity liner material.

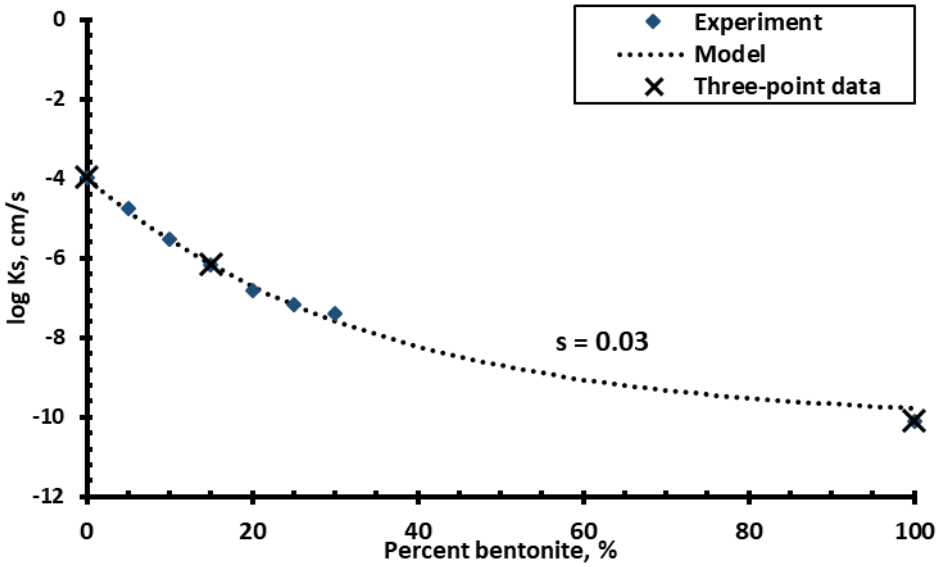

Figure 2.8. Experimental saturated hydraulic conductivity values for bentonite-silt mixtures (Doley et al. 2016) at different bentonite content in comparison with fitted model results using the proposed model—Equation (2.1). The cross symbol is used to identify the data points used in the three-point method discussed in Section 2.3.5.

2.3.5 A Simple Three-Point Method to Estimate the Scaling Parameter

In all of the above discussions, the model fitting exercise was completed using all available data points. Based on further analysis we have found that in order to approximately estimate the value of the model parameter (the scaling factor *s*), one would

at least need three data points. Fortunately, two of these points are end members (fine and coarse material) and therefore all we need is the value of one coarse-fine mixture. As an example, if our model is used to describe the Doley et al. (2016) dataset, there is no need to measure the saturated hydraulic conductivity values for many bentonite-silt mixtures in order to find the bentonite percentage that would yield the required low conductivity value. All one needs to measure is the saturated hydraulic conductivity value of just one mixture of sand and bentonite. In order to save the time required to perform the saturated hydraulic conductivity tests, we recommend using an optimal mixture with the lowest possible bentonite content required to achieve evenly distributed bentonite throughout the mixture. A good rule of thumb is to use about 10 to 20 percent of bentonite. The saturated hydraulic conductivity value of this mixture coupled with the saturated hydraulic conductivity of the end members (sand and bentonite) are sufficient to adequately fit and determine the scaling factor *s*. The fitted model can then be used to estimate the saturated hydraulic conductivity values for any bentonite content ranging from 0 to 100 percent. We applied this approach to estimate the scaling factor *s* for all our laboratory datasets and for all literature-derived datasets. The estimated values of the scaling parameter and the corresponding RMSE values are summarized in Table 2.1. The three experimental data points used for this approach are shown in Figures 2.3, 2.5, 2.6, 2.7 and 2.8 for each dataset; note these three data points are marked with a cross symbol. All root mean square errors (RMSEs) and coefficients of determination R^2 of log K_s in Table 2.1 were calculated using the entire dataset for fitted models developed using the three-point method; therefore, these RMSEs and R^2 values can be compared with the values of corresponding fitted model developed

using the entire dataset. For all different types of mixtures, very little difference was observed between RMSE and R^2 values for fitted models developed using the entire dataset and using the three-point method. Therefore, the three-point method is an acceptable approach for estimating the value of the model parameter *s*.

2.4 Discussion and Conclusions

In typical engineering projects, a soil mixture with a saturated hydraulic conductivity value of at least 1×10^{-7} cm/s is required to construct hydraulic liners (Benson et al. 1999; Benson et al. 1994; Gleason et al. 1997). The percentage of clay and sand to be used vary based on the properties of the materials used to develop the mixture and compaction conditions during the construction of the liner. A laboratory test conducted by Garlanger et al. (1987) recommended a minimum bentonite content of 6% to be mixed with locally available material, for a landfill site in central Florida, to achieve a saturated hydraulic conductivity value of 1×10^{-8} cm/s or less. In another study, Gleason et al. (1997) stated that a bentonite content of ≤15% is able to achieve a bentonite-sand mixture with a saturated hydraulic conductivity value of less than 1×10^{-7} cm/s. The required bentonite percentage was varied based on the type of bentonite, sodium or calcium bentonite, and sand type. Usually, the bentonite content ranged between 5 and 15 percent (Chapuis 1990). In all these studies, multiple laboratory experiments were conducted to determine the bentonite content required to achieve the target saturated hydraulic conductivity value. The model proposed in this study can estimate the saturated hydraulic conductivity values of coarse-fine mixtures with fine content varying between 0 and 100 percent without using multiple experimental data points. In practical applications, in order to estimate the value

of the model parameter (the scaling factor *s*), one would need at least three data points. In the proposed three-point method these values can include the saturated hydraulic conductivity values of the two end members (pure coarse material and pure fine material), and at least one critical mixture. We recommend using a mixture with the lowest possible fine (or clay material) percentage required to achieve a uniform, well-mixed mixture. A good rule of thumb is to use about 10 to 20 percent of fine material. These three data can be used to fit the model and estimate the value of the scaling parameter *s*, and then the fitted model can be used to calculate the saturated hydraulic conductivity of mixtures with various amounts of fines. Table 2.1 compares the values of *s* evaluated using the three-point method against the values estimated using the entire dataset. The refitted *s* values for all synthetic coarse-fine and fine-coarse mixtures, clay-sand mixtures, and literature-derived experimental datasets using this three-point approach were close to the values estimated using the full set of data.

To summarize, in this study, we have investigated the performance of a scalable model that used for predicting the changes in the saturated hydraulic conductivity value of coarse and fine porous media mixtures due to the presence of different amounts of fines. Several laboratory experiments that represented the percentage of fines ranging from 0 to 30 were conducted using simulated coarse-fine and fine-coarse synthetic porous media mixtures. The value of the saturated hydraulic conductivity of the coarse porous media decreased as the percent fine increased in the mixture. The reduction in saturated hydraulic conductivity was significant when we started to add fine material to the coarse material; however, the reductions became less significant when the percentage of fine exceeded

about 15%. Typically, the overall saturated hydraulic conductivity value of the mixture was almost close to the saturated hydraulic conductivity of the fine particles when the percent of the fine was above 30%.

In the past, others have attempted to predict reductions in the saturated hydraulic conductivity of coarse sand due to the presence of clay material and other fine minerals. However, all available models require measurement of multiple physical properties of the porous media mixture. The resulting empirical expressions have several model parameters that need to be individually calibrated by conducting multiple soil characterization tests. In this study, we have proposed a simpler model that uses a single model parameter to estimate the saturated hydraulic conductivity values of different types of mixtures. The proposed model successfully correlated the changes in saturated hydraulic conductivity values of a variety of coarse-fine mixtures with the amount of fine material in the mixture. We have tested the model performance using several new laboratory datasets, and also using multiple literature-derived datasets. It is important to note that this method is suitable only for modeling artificial mixtures and should not be used to predict the saturated hydraulic conductivity value of undisturbed, heterogeneous natural porous media. The proposed framework is a useful tool for modeling the hydraulic properties of various types of engineered mixtures. The model can help design optimal mixtures without conducting multiple experiments that could be time consuming and cost prohibitive.

Chapter 3. A Comprehensive Performance Assessment of the Modified Philip–Dunne Infiltrometer

3.1 Introduction

Saturated hydraulic conductivity K_s is one of the most important parameters that control the water seepage processes through the soil profile (Ahmed et al. 2014; Alagna et al. 2016; Kanwar et al. 1990; Mohanty et al. 1994; Reynolds et al. 2000). The value of K_s depends on the size and type of mineral present in the soil; for example, the presence of fine minerals such as silt and clay can greatly reduce K_s values (Alakayleh et al. 2018; Komine 2008; Sällfors and Öberg-Högsta 2002; Sivapullaiah et al. 2000). In addition, the value of K_s decreases with a reduction in the effective porosity of the system (Abeele 1986; Francisca and Glatstein 2010; Sivapullaiah et al. 2000).

Analyzing the undisturbed soil core taken from the field is a common method to determine K_s in the laboratory using either the constant- or falling-head permeameter (ASTM-D5084-16a 2016). The soil core method has some challenges including macropores created by insertion of the ring, and relatively small sample size that may not yield a representative K_s value (Lee et al. 1985; Reynolds et al. 2000). To overcome these disadvantages, several field techniques have been developed to measure the in situ saturated hydraulic conductivity of the soil. However, natural variability of the soil properties and limitations of the field techniques such as sample size and flow geometry could also result in inaccurate estimation of the field-scale hydraulic properties (Mallants et al. 1997; Reynolds et al. 2000; Wessolek et al. 1994).

One of the common devices used in the field is the Guelph permeameter that was developed by Reynolds and Elrick (1986). This technique can measure the in situ saturated hydraulic conductivity using the constant head permeameter principle. This method employs a borehole (typically 31 cm depth and 3 cm radius) and uses the Mariotte principles to obtain a constant flow rate regardless of the decreasing water level within the permeameter.

Another simplified falling-head method that requires a small volume of water and short duration was developed by Bagarello et al. (2004). This permeameter is a ring, typically 20 to 30 cm diameter, inserted a short distance into the soil and then filled with a known volume of water. The time needed for the total volume of water to infiltrate is measured along with the initial and final water contents of the soil to estimate the value of K_s.

Philip (1993) introduced an approximate analysis based on the Green–Ampt theory to estimate K_s and the Green–Ampt suction head Ψ at the wetting front from the drawdown data of a falling-head permeameter. This method, known as the Phillip-Dunne permeameter, uses a cylindrical tube that is vertically inserted into a borehole at a given depth, typically 15 cm, within an unsaturated soil profile. Water is rapidly introduced into the system and the initial height H_{in} is recorded at time $t=0$. The data analysis procedure employs the Green–Ampt model after transforming the actual three-dimensional flow system into an equivalent spherically symmetrical flow configuration.

Ahmed et al. (2014) introduced a modified version of the Philip–Dunne permeameter (Philip 1993), known as the Modified Philip–Dunne Infiltrometer (MPDI). The MPDI involves applying the device near the surface rather than in a borehole that results in changing the flow configuration of the infiltrated water. The device is inexpensive, easy to use, and requires a minimal amount of water. These advantages make it a cost-effective method to rapidly determine K_s at the surface to evaluate the infiltration capacity of the soil. The procedure for data collection and analysis is also described in ASTM-D8152-18 (2018). This method will be further reviewed in detail in the background and governing equations section since the focus of this study is to further understand the MPDI theory.

Several studies are available in the literature that are aimed at evaluating the performance of different field techniques used for measuring the field-scale soil hydraulic properties. The saturated hydraulic conductivity was measured at five different locations and at four soil depths by Mohanty et al. (1994) to evaluate the relative performance of the Guelph permeameter, the velocity permeameter (Merva 1987), the disk permeameter (Perroux and White 1988), and the double-tube method (Bouwer 1964). Undisturbed soil cores were also collected from all the locations to determine the saturated hydraulic conductivity in the laboratory. The measured K_s values were the lowest when Guelph permeameter was used, while the larger values were measured by the disk permeameter and the double-tube method. The velocity permeameter gave hydraulic conductivity values closer to the values estimated in the laboratory. Reynolds et al. (2000) compared the K_s values estimated using the tension infiltrometer (Perroux and White 1988) and the pressure

infiltrometer (a single-ring, steady-flow technique) (Reynolds and Elrick 1990) with laboratory measurements and found that the K_s values were significantly different even though the sample size was the same. Gómez et al. (2001) determined K_s and Ψ values using different field techniques. The primary goal of their study was to compare the performance of the falling head, the single ring, the rainfall (Connolly et al. 1991), and the tension infiltrometer for the assessment of infiltration rate at a field site. The differences in measured K_s values using different techniques were smaller than the differences observed for the Ψ values. The Ψ values varied considerably and relatively large Ψ values obtained using the analysis of Philip (1993) for the falling-head infiltrometer. The authors did not provide an explanation for obtaining large Ψ values. However, since the Ψ values were higher than the average values for soils with the same textural class reported by others, the authors recommended using another method to estimate Ψ rather than the Philip (1993) method. Muñoz-Carpena et al. (2002) compared the performance of the Philip–Dunne permeameter with the constant head permeameter and the Guelph permeameter. The measured K_s values by the Philip–Dunne permeameter were greater than those values obtained using the Guelph permeameter by an order of magnitude. The laboratory constant head permeameter method gave K_s values that ranged between the values estimated using the Philip–Dunne and Guelph permeameters. The authors explained that the variations were due to differences in water infiltration geometries and sample wetted volumes of the methods. Controlled laboratory measurements of K_s for three types of media with different grain size distribution were completed by Nestingen et al. (2018) in order to compare the accuracy and precision of the Modified Philip–Dunne Infiltrometer, the double-ring

infiltrometer, and the minidisk infiltrometer (Zhang 1997). To determine the accuracy of each device, the mean hydraulic conductivity value was compared with the value obtained by using the falling-head test. Results showed that the MPDI gave the correct trend of decreasing K_s values by increasing the fine content of the media. The estimated K_s values from the three methods were close to the values of the falling-head test. The most precise method was the double-ring method, followed by the MPDI, and the minidisk infiltrometers.

Our review indicates that several recent studies, including Weiss and Gulliver (2015), García-Serrana et al. (2017), Kristvik et al. (2018), and Taguchi et al. (2018), have used the MPDI approach to measure the in situ soil hydraulic parameters. None of these studies have evaluated the sensitivity of the MPDI theory to the variations of the soil hydraulic parameters. The objective of this study is to complete a comprehensive investigation of the sensitivity of the MPDI theory used for determining K_s and Ψ from the drawdown data collected using the MPDI.

3.2 Methods

3.2.1 Background and Governing Equations

Figure 3.1 shows the conceptual diagram of the MPDI. This modified version of the Philip–Dunne permeameter was originally developed by Ahmed et al. (2014). The apparatus is a transparent plastic open-ended tube of internal radius r_1 (typically 5 cm) attached to a metal ring beveled from the edge for vertically inserting the system into an unsaturated soil for a distance of L_{max} (typically at about 5 cm). Water is rapidly poured to

the system and the initial height is H_{in} at time $t=0$, and the water is allowed to infiltrate into the soil. During infiltration, the changes in water height in the tube $H(t_j)$ is recorded with time (t_j, j=1,2,..,n). The soil volumetric moisture content θ_{in} at the beginning of the test, and θ_s at the end of the test are also recorded.

To analyze the drawdown data, Ahmed et al. (2014) modified the procedure introduced by Philip (1993) to account for the difference in the flow configuration due to the installation of the device closer to the surface, rather than inside a borehole. The wetted soil is represented as a capped sphere with a radius of $R(t_j)$ instead of the actual three-dimensional flow configuration. Another simplification that was applied by Philip (1993) and followed by Ahmed et al. (2014) is replacing the actual disk infiltration surface (of radius r_1) by a sphere with radius $r_0 = 0.5 \times r_1$. The surface area of the actual disk infiltration surface (of radius r_1) and the assumed sphere (of radius $r_0 = 0.5 \times r_1$) is the same.

Figure 3.1 shows the notations used to develop the governing equations for the MPDI. The geometry of the wetting front which is a capped sphere of radius $R(t_j)$ is used to express the cumulative infiltration at a given time using the initial and final volumetric moisture content of the soil enclosed within the sphere. A mass balance statement (Equation (3.1)) that equates the volume of water left in the infiltrometer at a given time $\left[H_{in} - H\left(t_j\right)\right]\pi r_1^2$ with the cumulative infiltration that occurred during the same time is used to compute $R(t_j)$ as a function of $H(t_j)$. This equation is only valid where the geometric

shape of the wetting front remains constant at the sphere, typically at $R(t_j)$ with values greater than $\sqrt{r_1^2 + L_{max}^2}$.

$$\left[H_{in} - H(t_j)\right]\pi r_1^2 = \frac{\pi}{3}(\theta_s - \theta_{in})\left[2R^3(t_j) + 3R^2(t_j)L_{\max} - L^3{}_{\max} - 4r_o{}^3\right] \quad (3.1)$$

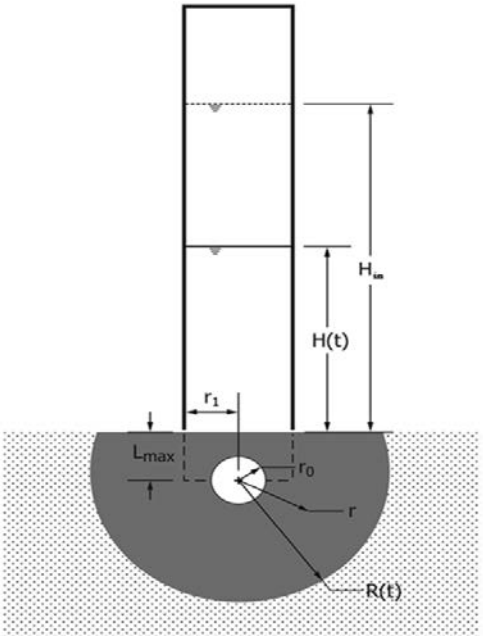

Figure 3.1. Notations used in the governing equations of the Modified Philip–Dunne Infiltrometer (Nestingen 2007).

The flow velocity at the spherical infiltration surface v_{co} is given by differentiating Equation (3.1) with respect to time. Following Philip's approximation, the velocity is only driven by pressure and capillarity forces since they dominate over gravity during the short duration of the test. The pressure-capillary flow velocity across the spherical surface $v_c(r)$ of radius $r(r_0 \leq r < R)$ is given as (Ahmed et al. 2014):

$$v_c(r) = v_{co}\left[\frac{2r_o^{\,2}}{r^2 + rL_{\max}}\right] = \left[(\theta_s - \theta_{in})\left(R^2(t_j) + R(t_j)L_{\max}\right)\frac{dR(t_j)}{dt} - 2r_o^{\,2}K_s\right]\left[\frac{1}{r^2 + rL_{\max}}\right] \quad (3.2)$$

The pressure-capillarity potential drop ΔP from the spherical source $r = r_0$ to the wetting front $r = R(t_j)$ is given by applying Darcy's law: $\Delta P = \beta \int_{r_0}^{R(t_j)} [v_c(r)/K_s]\, dr$. Substituting Equation (3.2) into Darcy's law yields the following equation (note, the exploratory factor β, equal to $\pi^2/8$, is used to account for the change of flow path efficiency resulting from the replacement of the actual flow configuration) (Ahmed et al. 2014):

$$\Delta P = \frac{\pi^2}{8}\left[(\theta_s - \theta_{in})\frac{R^2(t_j) + R(t_j)L_{\max}}{K_s}\frac{dR(t_j)}{dt} - 2r_0^{\,2}\right] \times \frac{\ln\dfrac{R(t_j)(r_0 + L_{\max})}{r_0(R(t_j) + L_{\max})}}{L_{\max}} \quad (3.3)$$

The pressure-capillarity potential drop from the spherical source to the wetting front is also given by $\Delta P = \Psi - P(t_j)$, where $P(t_j)$ is the pressure at the sphere source. $P(t_j)$ is determined by applying Darcy's law for the flux in the cylinder of soil encased within the infiltrometer $q = -K_s[dp/dz + 1]$. This flux is the same as the rate of drop in the water height inside the infiltrometer $q = -\Delta H(t_j)/\Delta t_j$. Equating these two fluxes and integrating with z will result in $P(t_j) = H(t_j) + L_{max} - [\Delta H(t_j)/\Delta t_j](L_{max}/K_s)$. This leads to another expression for the pressure-capillarity potential drop between the spherical source to the wetting front (Ahmed et al. 2014).

$$\Delta P = \Psi - P(t_j) = \Psi - H(t_j) - L_{\max} + \frac{\Delta H(t_j)}{\Delta t_j}\frac{L_{\max}}{K_s} \tag{3.4}$$

By equating the previous two expressions of the pressure-capillarity potential drop from the spherical source to the wetting front (Equations (3.3) and (3.4)), Ahmed et al. (2014) obtained the following equation that quantifies the temporal drop in the water height inside the infiltrometer as a function of the soil hydraulic properties K_s and Ψ:

$$\Delta H_s(t_j) = \frac{K_s}{L_{\max}}\Delta t_j \left\{ \begin{array}{l} \frac{\pi^2}{8}(\theta_s - \theta_{in})\frac{R^2(t_j) + R(t_j)L_{\max}}{K_s}\frac{\Delta R(t_j)}{\Delta t_j}\frac{\ln\frac{R(t_j)(r_o + L_{\max})}{r_o(R(t_j) + L_{\max})}}{L_{\max}} \\ -\frac{\pi^2}{4}r_o{}^2\frac{\ln\frac{R(t_j)(r_o + L_{\max})}{r_o(R(t_j) + L_{\max})}}{L_{\max}} - \Psi + H(t_j) + L_{\max} \end{array} \right\} \tag{3.5}$$

Where $dR(t_j)/dt$ in Equations (3.2) and (3.3) are calculated as $\Delta R(t_j)/\Delta t_j$ in Equations (3.5) and (3.6), and $\Delta R(t_j) = R(t_j) - R(t_{j-1})$. For each application of the MPDI, one measures the water height $H(t_j)$ at different time t_j or records t_j at different specified $H(t_j)$ until most of the water infiltrates into the soil. $R(t_j)$ is solved first using Equation (3.1) based on measured $H(t_j)$ values, and then $dR(t_j)/dt$ can be estimated. Equation 3.5 was used by Ahmed et al. (2014) to fit K_s and Ψ values by minimizing the absolute difference between the time series of calculated head drop $\Delta H_s(t_j)$ and measured $\Delta H(t_j)$ data using the solver function available in Excel. Another method for setting the optimization procedure is to solve for K_s and Ψ using the following equation, which is a

rearrangement of Equation (3.5), written to evaluate Δt_{sj} and it can be used to fit with measured time intervals Δt_j data.

$$\Delta t_{sj} = \frac{\frac{\pi^2}{8}(\theta_s - \theta_{in})\frac{R^2(t_j) + R(t_j)L_{\max}}{K_s}\frac{\ln\frac{R(t_j)(r_0 + L_{\max})}{r_0(R(t_j) + L_{\max})}}{L_{\max}}\Delta R(t_j) - \frac{L_{\max}}{K_s}\Delta H(t_j)}{\Psi - H(t_j) - L_{\max} + \frac{\pi^2}{4}r_0^2\frac{\ln\frac{R(t_j)(r_0 + L_{\max})}{r_0(R(t_j) + L_{\max})}}{L_{\max}}} \tag{3.6}$$

Based on time-series data of t_j and $H(t_j)$ $(j=1, 2, \ldots, n)$, $\Delta t_j = t_j - t_{j-1}$ and $\Delta H(t_j) = H(t_j) - H(t_{j-1})$ are estimated as observed/measured time intervals and head drops, respectively. $\Delta H_s(t_j)$ and Δt_{sj} are the changes in the head drop and time intervals, computed using Equations (3.5) and (3.6), respectively. Therefore, one has a choice of fitting either (3.5) or (3.6) to fit the K_s and Ψ values, and in this study, we will fit both equations to understand their relative sensitivities. Also, since both (3.5) and (3.6) are nonlinear, the system can yield multiple combinations of K_s and Ψ that could fit the observations equally well. The question then is which of these solutions are feasible solutions? And can we accept or reject these values? What is the range of the accepted values of K_s and Ψ? The goal of this study is to answer these questions to better understand the advantages and disadvantages of using the MPDI.

3.2.2 Forward-Modeling Algorithm and Its Applications

A forward-modeling code was developed and written in Visual Basic for Applications (VBA) available within Excel. The details of the algorithm which was used

are summarized in Figure 3.2. Table 3.1 shows various applications of the forward-modeling code that are discussed in this study.

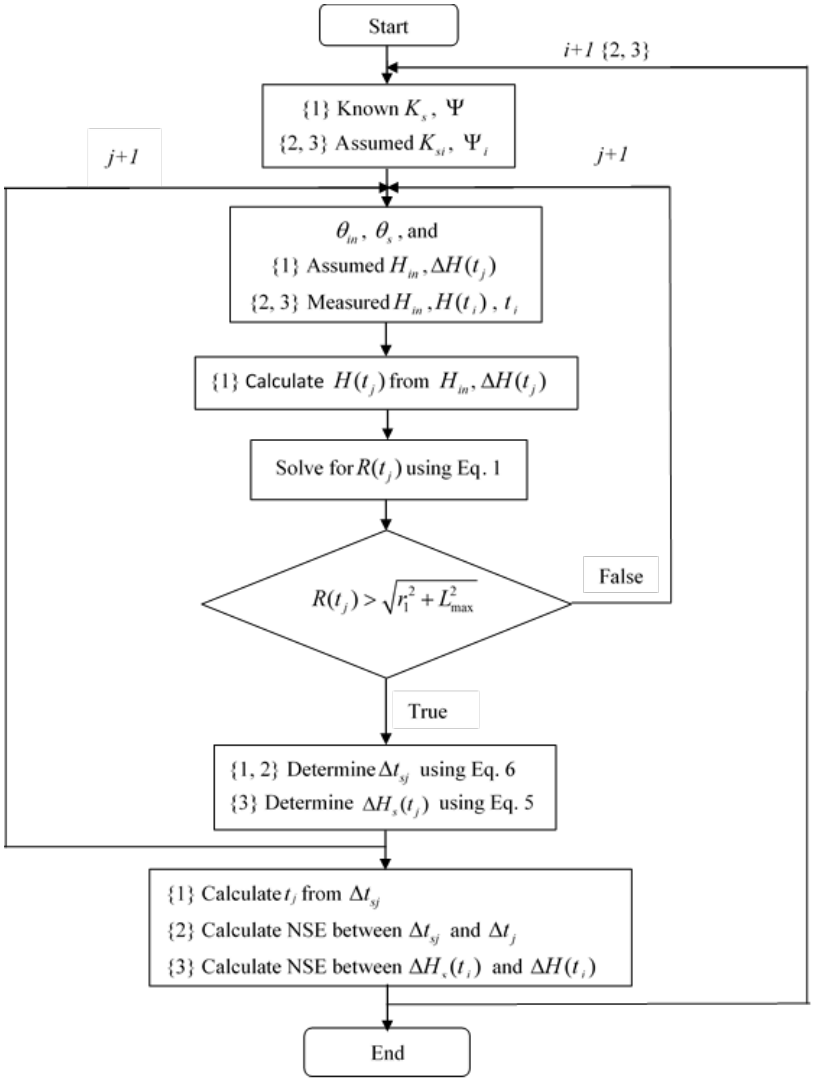

Figure 3.2. Flowchart for the analysis procedure using the forward-modeling code used to generate the drawdown data and to estimate K_s and Ψ for values from measurements of head $H(t_j)$ versus time t_j.
Note: Between { } is the application number (e.g., Application 1, 2, and/or 3) that the corresponding parameter or a step is only used for that application/applications.

Table 3.1 The three different applications of the forward model.

Forward-Modeling Application	Measured/Input	Simulated	Calculated/Output
Application 1	Assumed H_{in} and $\Delta H(t_j)$, known K_s and Ψ	Δt_{sj} using $\Delta H(t_j)$ and $H(t_j)$	$t_j = t_{j-1} + \Delta t_{sj}$, and $H(t_j) = H(t_{j-1}) - \Delta H(t_j)$
Application 2	Measured H_{in}, $H(t_j)$, t_j, assumed K_{si} and Ψ_i	Δt_{sj} using $H(t_j)$, and $\Delta H(t_j)$	NSE between Δt_{sj} and $\Delta t_j = t_j - t_{j-1}$
Application 3	Measured H_{in}, $H(t_j)$, t_j, assumed K_{si} and Ψ_i	$\Delta H_s(t_j)$ using $H(t_j)$, and Δt_j	NSE between $\Delta H_s(t_j)$ and $\Delta H(t_j)$

In Application 1, the forward-modeling code is used to develop a synthetic drawdown data ($H(t_j)$ versus t_j), using Equation (3.6) that was obtained by Ahmed et al. (2014), if the soil hydraulic properties (K_s and Ψ) and the initial value of head H_{in} are known, and $\Delta H(t_j)$ are then assumed. The water height drop $\Delta H(t_j)$ could be assumed to have constant value (we have used 1 cm in this study, this value is free to be selected by the user). The code will then compute $H(t_j) = H(t_{j-1}) - \Delta H(t_j)$ with $H(t_0) = H_{in}$ or $H(t_j) = H_{in} - j \times \Delta H(t_j)$ since $H(t_j)$ is necessary for solving $R(t_j)$ using Equation (3.1) and then determines $\Delta R(t_j)$. Then Equation (3.6) is used to determine Δt_{sj} from which we can estimate $t_j = t_{j-1} + \Delta t_{sj}$. Note in this type of purely forward application (namely Application 1) one must assume initial head H_{in} and $\Delta H(t_j)$ values and use Equation (3.6) to find Δt_{sj}. One cannot assume initial time and Δt_j and employ Equation (3.5) to compute $H(t_{sj})$ because the right-hand side of Equation (3.5) has $H(t_j)$ (which is the values we are trying to estimate), whereas the right-hand side of Equation (3.6) does not require the values of t_j. Also, $H(t_j)$ values are required to determine $R(t_j)$ using Equation (3.1) because the right-hand side of Equations (3.5) and (3.6) have $R(t_j)$.

For Applications 2 and 3, we used field infiltration measurement data collected using the MPDI method for three different soil textures. The MPDI was inserted 5 cm into the soil surface and was rapidly filled with water to an initial height H_{in}. The changes of water height inside the tube $H(t_j)$ was recorded with time (t_j, j=1,2,..,n). The soil moisture content prior the test was measured by collecting soil samples from three different locations around the tube. The soil moisture content after the test was also measured by collecting three different soil samples from the location where the tube was inserted. These soil moisture measurements were made gravimetrically in accordance with the test method ASTM-D2216-10 (2010). Then the soil bulk density was measured closely following the procedure described in ASTM-F1815-11 (2011) to convert the gravimetric moisture content into the volumetric soil moisture content.

The sensitivity of the MPDI theory for predicting Δt_{sj} (using Equation (3.6), which is our Application 2) or for predicting $\Delta H_s(t_j)$ (using Equation (3.5), which is our Application 3) for various values of K_s and Ψ was evaluated. For the applications 2 and 3, the field-measured water height $H(t_j)$ inside the tube was used in the model. To understand the sensitivity, we randomly generated a large number of datasets (e.g., m = 30,000 used in this study) to test different sets of parameters K_{si} and Ψ_i (i = 1, 2, …, m) then the drawdown data were predicted for each set. The predicted drawdown data using each set of parameters K_s and Ψ were compared with the measured drawdown data to determine what values of K_s and Ψ are acceptable. The field recorded measurements for the drop of water height inside the MPDI with time, i.e., $H(t_j)$ and t_j (j=1,2, …, n) were used as a part of input data (see Figure 3.2) in the sensitivity study.

The two soil parameters of the MPDI model were sampled randomly using a uniform distribution within the range of 1×10^{-4} cm/s to 1×10^{-1} cm/s and −85 cm to −1 cm for K_s and Ψ, respectively; these ranges include all the soil types as reported in Clapp and Hornberger (1978). Note the value of Ψ will also be a function of the moisture content and it can vary with the soil type. The total 30,000 sets of generated parameters were checked graphically to make sure that the generated parameter sets cover all possible random combinations of K_s and Ψ values. The Nash–Sutcliffe efficiency (NSE) (Nash and Sutcliffe 1970) was used to rank and evaluate the acceptability of each set of model parameters K_s and Ψ. For Application 2, predicted Δt_{sj} and measured $\Delta t_j = t_j - t_{j-1}$ were compared to compute the NSE value; note that the forward-modeling code outputs modeled Δt_{sj} between the measured water heights $H(t_j)$. For Application 3, predicted $\Delta H_s(t_j)$ and measured $\Delta H(t_j) = H(t_j) - H(t_{j-1})$ were compared to compute the NSE value. In this case, the forward-modeling code outputs modeled $\Delta H_s(t_j)$ at measured water height $\Delta H(t_j)$ and Δt_j for $\Delta H(t_j) = H(t_j) - H(t_{j-1})$.

A detailed flowchart for the analysis procedure used in the forward model is shown in Figure 3.2 for all the three applications (also see Table 3.1). The Newton-Raphson's method was used to solve for the wetting front radius $R(t_j)$ using the mass balance relation (Equation (3.1)). To evaluate the quality of the fit, the NSE values could be calculated between simulated and measured values of Δt_j, $\Delta H(t_j)$, t_j, or $H(t_j)$. However, to be consistent with the analysis procedure introduced by Ahmed et al. (2014), Δt_j and $\Delta H(t_j)$

data were used in this study to determine the NSE values. The NSE was calculated only for data when the MPDI analysis is valid, i.e., $R(t_j) > \sqrt{r_1^2 + L_{max}^2}$.

3.3 Results and Discussion

3.3.1 Example of the Use of Application 1: Forward Simulation of Drawdown Curves for Different Types of Soil

The forward-modeling code was used to predict the drawdown curves of the MPDI (Application 1), using Equation (3.6) that was obtained by Ahmed et al. (2014), for three types of soils using the soil properties reported by Rawls et al. (1982). To show the variations of the drawdown curves predicted using the MPDI theory, at varying soil hydraulic properties, three types of soil (silt loam, sandy loam, and sand, see Table 3.2) were considered. Following the procedure for Application 1 described in the methods section, H_{in} was assumed as 51 cm, and $\Delta H(t_j)$ as 1.0 cm (j = 2 , 3, …, n). The moisture deficit $\Delta\theta$ was assumed to be the same for all the three soils and fixed at 0.05 (assumed wet soil). Then at $\Delta\theta_{max}$ (assumed dry soil) for each soil when θ_{in} was set at the field capacity (minimum θ) and θ_s at the saturated moisture content or effective porosity (see Table 3.2). The Brook and Corey model (Brooks and Corey 1966) was used to determine Ψ for each θ_{in} value and the results are summarized in Table 3.2. Note, in Table 3.2, θ_r is the residual saturation, θ_e is the effective porosity, Ψ_b is the bubbling pressure, and λ is the pore size distribution; the values reported were selected from the ranges recommended by Rawls et al. (1982).

Table 3.2 The soil hydraulic properties for silt loam, sandy loam, and sand (Rawls et al. 1982) and statistical summary of predicted Δt_{sj} (seconds).

Soil Type	K_s[a] (cm/s)	θ_r[a]	θ_e[a]	Ψ_b[a] (cm)	λ[a]	$\Delta\theta$[b] ($\theta_e - \theta_{in}$)	Ψ[c] (cm)	Δt_{sj} (Seconds) Max	Min	Avg	SD
Silt loam	1.89×10^{-4}	0.027	0.501	−17	0.36	0.050 (wet)	−24	1615	526	899	302
						0.217 (dry)	−86	459	274	361	53
Sandy loam	7.19×10^{-4}	0.025	0.412	−15	0.61	0.050 (wet)	−19	530	148	270	104
						0.222 (dry)	−61	169	88	124	23
Sand	5.83×10^{-3}	0.010	0.417	−8	1.09	0.050 (wet)	−9	123	21	47	26
						0.355 (dry)	−53	23	12	17	3

[a] Data from Rawls et al. (1982); [b] Assumed small and maximum soil moisture deficits; [c] Determined for every θ_{in} value using the Brook and Corey model (Brooks and Corey 1966).

The forward-modeling code considers that the MPD theory is only valid when the geometric shape of the wetting front remains constant at the sphere; typically, at $R(t_j)$ values greater than $\sqrt{r_1^2 + L_{max}^2}$. The corresponding first water height $H(t_1)$ when the MPDI theory is valid can be computed from Equation (3.1), which is the mass balance equation for determining necessary water needed to satisfy a given moisture deficit $\Delta\theta = \theta_s - \theta_{in}$.

$$\Delta H_1 = H_{in} - H(t_1) = 16.928\,\Delta\theta$$
$$\text{when } R(t_1) = \sqrt{r_1^2 + L_{\max}^2} = 2\sqrt{5}\ cm \quad \text{since} \quad r_1 = L_{\max} = 5\,cm \tag{3.7}$$

Equation (3.7) clearly shows that the first water height or head drop ΔH_1 after which the model starts to be valid is independent of the soil texture class (not related to K_s and Ψ) but only depends on $\Delta\theta$. When assuming H_{in} is equal to 51.0 cm and $\Delta H(t_j)$ as 1.0 cm (j = 2 ,3, …, n), and when the value of $\Delta\theta = \theta_s - \theta_{in}$ was set to be the same value for all the three types of soil at 0.05 (wet soil), the calculated ΔH_1 values for all the three soils is found to be 0.8 cm. Therefore, the water height $H(t_1)$ at which the Modified Philip–Dunne

model starts to be valid for silt loam, sandy loam, and sand is 50.2 cm. When we used $\Delta\theta_{max}$ (assuming dry soil) values of 0.217, 0.222, and 0.355, the calculated ΔH_1 values are 3.7, 3.8, and 6.0 cm for silt loam, sandy loam, and sand, respectively. Therefore, the water height $H(t_1)$ at which the MPDI model starts to be valid for silt loam, sandy loam, and sand are 47.3 cm, 47.2 cm, and 45.0 cm, respectively.

The corresponding results of the drawdown curves are given in Figure 3.3, which starts from $H(t_1)$ to 0. When $\Delta\theta$ was assumed the same for all the soil types at 0.05 (wet soils), the total drawdown time t_n of $H(t_1)$ = 50.2 cm water within the MPDI for silt loam, sandy loam, and sand were predicted as 45011.3 sec (750.2 min), 13531.6 sec (225.5 min), and 2353.3 sec (39.2 min), respectively. When the forward-modeling code was applied for $\Delta\theta_{max}$ of each soil (dry conditions), the total drawdown time t_n of $H(t_1)$ = 47.3, 47.2, and 45.0 cm water within the MPDI for silt loam, sandy loam, and sand were predicted as 17028.9 sec (283.8 min), 5843.9 sec (97.4 min), and 755.3 sec (12.6 min), respectively. Statistical summary (maximum, minimum, average, and standard deviation) of predicted Δt_{sj} for each 1.0 cm drop is listed in Table 3.2 for each soil. The smallest Δt_{sj} occurs at the earliest drawdown interval and the largest Δt_{sj} at the last drawdown interval.

The total drawdown time t_n values needed to infiltrate $H(t_1)$ cm water within the MPDI are 57 to 68% shorter when $\Delta\theta$ was assumed the same for all the soil types at 0.05 (wet soils) than when $\Delta\theta_{max}$ (dry soils) was assumed. Please note that $H(t_1)$ values are different when $\Delta\theta_{max}$ and $\Delta\theta$ = 0.05 were assumed for every soil type; therefore, the time needed to infiltrate the first drawdown ΔH_1 was excluded from the calculation since the

Modified Philip–Dunne theory is not valid. This means that the total drawdown time t_n needed to infiltrate $H(t_1)$ cm water from the MPDI into wet soil is much more than the time need to infiltrate into dry soil. This is similar to the observations from previous studies that showed that the rate at which water infiltrates into dry soil can be higher than wet soil (Gray and Norum 1967; Philip 1957; Ruggenthaler et al. 2016).

Since $H(t_1)$ values are different as it depends on the assumed value of $\Delta\theta$ and to facilitate an easy comparison, the time t_n needed to infiltrate 45.0 cm (the height at which the model is valid for the three soils) water inside the MPDI was determined for all the three soil types. When $\Delta\theta_{max}$ was assumed, t_n were predicted as 16392.0 sec (273.2 min), 5644.9 sec (94.1 min), and 755.3 sec (12.6 min) for silt loam, sandy loam, and sand, respectively. The corresponding total drawdown time when $\Delta\theta = 0.05$ were also calculated as 42220.3 sec (703.7 min), 12742.7 sec (212.4 min), and 2239.7 sec (37.3 min) for silt loam, sandy loam, and sand systems, respectively. For each of the three soil, the total drawdown time for 45.0 cm of water under $\Delta\theta_{max}$ is 56 to 66% shorter than one observed using $\Delta\theta = 0.05$, but the total drawdown time for silt loam is about 20 times larger than one observed for the sand system.

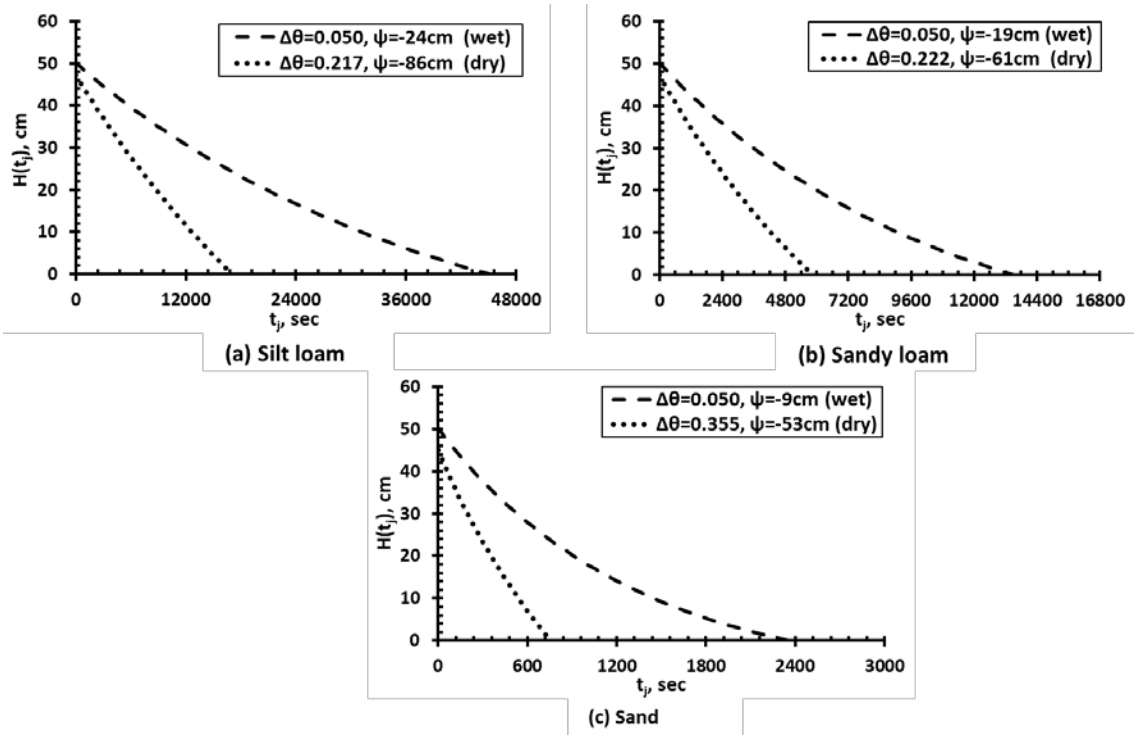

Figure 3.3. Drawdown curves for (**a**) silt loam, (**b**) sandy loam, and (**c**) sand estimated by the forward-modeling code using the soil properties K_s and Ψ reported in Table 3.2 for two different values of $\Delta\theta$ representing wet and dry conditions. Three graphs (a, b, and c) have different scales for the x-axis (time in sec).

3.3.2 Example of the Use of Application 2: Simulation Using Δt_{sj} Determined by Equation (3.6) and Compare with the Measured Time Intervals Δt_j

A field-measured drawdown data [$H(t_j)$ versus t_j] were collected using the MPDI for three types of soil (silt loam, sandy loam, and sand). The data for sandy loam were collected in an infiltration basin in Stillwater, Minnesota and provided by Farzana Ahmed (Ahmed 2014). The data for silt loam and sand were collected in an agriculture experimental field and a pile of construction sand, respectively, in Auburn, Alabama. These three soils were selected to represent a relatively wide range of low to high K_s and Ψ values.

The collected data were used in the sensitivity analysis procedure, which uses the forward-modeling code for Application 2 as described in the flowchart (see Figure 3.2). For every set of the 30,000 randomly generated parameters, the drawdown curves similar to Figure 3.3 were developed and the NSE values were then calculated using Δt_{sj} determined by Equation (3.6) and the measured time intervals Δt_j. Even though the two soil parameters K_s and Ψ were sampled 30,000 times randomly using a uniform distribution in the range 1×10^{-4} cm/s to 1×10^{-1} cm/s and −85 cm to −1 cm, respectively, Figure 3.4 only shows the sets of parameters with NSE values greater than zero, which are 3.4%, 32.2%, and 16.2% of the 30,000 sets of parameters for silt loam, sandy loam, and sand, respectively. Figure 3.4 clearly indicates that a large number of the randomly generated parameters K_s and Ψ combinations for each type of soil produced the drawdown curves that did not match well (NSE < 0) with the corresponding observed drawdown data. For example, the x-axes of Figure 3.4 for the three soils have different scales (0.005, 0.05, and 0.5) for K_s in cm/s, all parameter combinations with K_s > 0.0018 cm/s for silt loam (Figure 3.4a), K_s > 0.01 cm/s for sandy loam (Figure 3.4b), and K_s > 0.082 cm/s for sand (Figure 3.4c) would produce drawdown curves with NSE < 0 in comparison to the measured drawdown data. It means that the Modified Philip–Dunne theory can eliminate any unrealistic K_s but not for Ψ since the full range of Ψ would produce drawdown curves with NSE > 0 as long as K_s is within a reasonable range (Figure 3.4). This is an important conclusion of the study. Therefore, we used wide ranges for K_s and Ψ to randomly generate 30,000 parameter sets; if narrow rages were used, it may not allow us to obtain this

important result. In Appendix A, we present the results shown in Figure 3.4 using the three–dimensional plots.

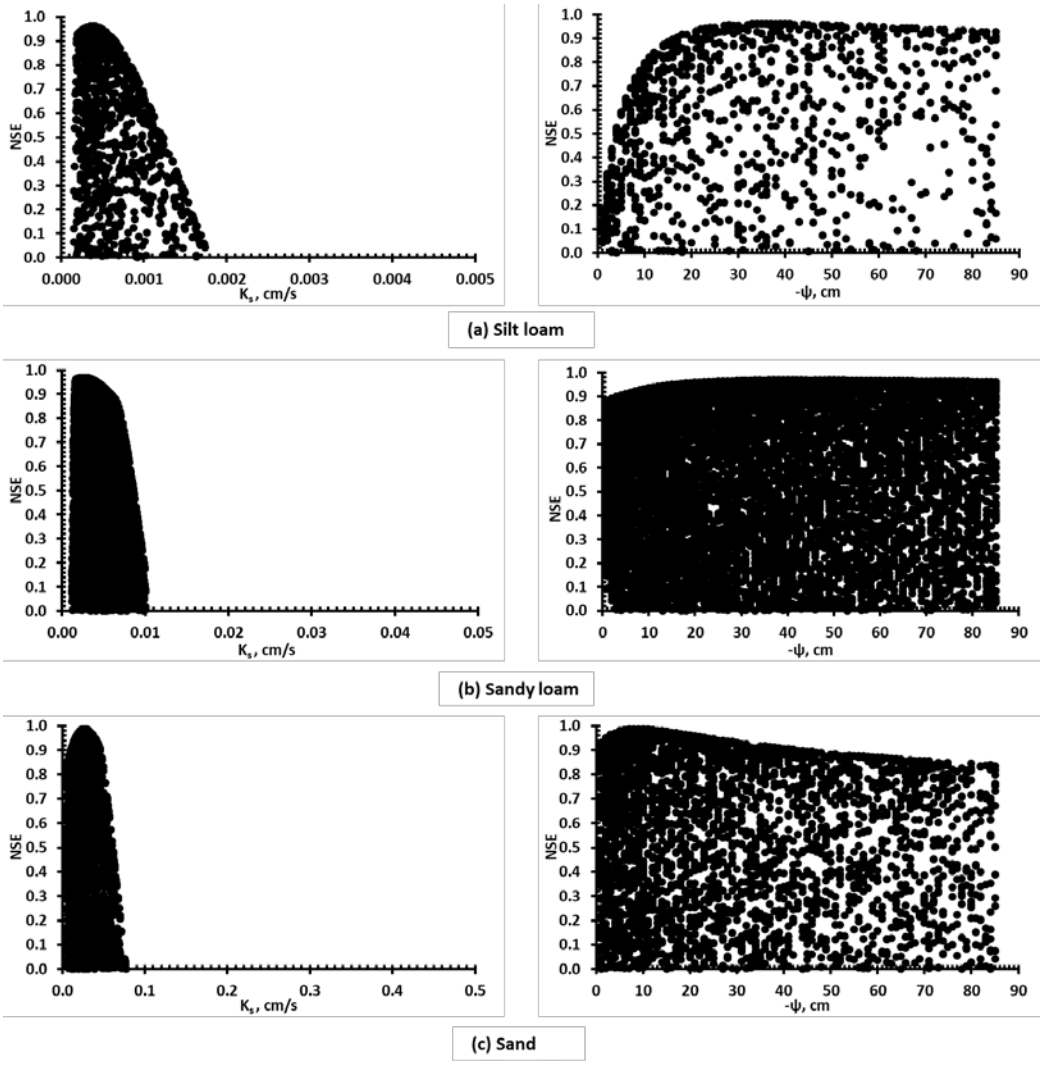

Figure 3.4. Scatter plots for the NSE calculated between Δt_{sj} determined by Equation 3.6 and the measured time intervals Δt_j, on the left is NSE versus K_s (cm/s) and NSE versus - Ψ (cm) is on the right. (**a**) silt loam, (**b**) sandy loam, and (**c**) sand. The scales for K_s are different for each of the three soils.

Figure 3.4 shows that the saturated hydraulic conductivity K_s is strongly correlated with the NSE but the Green–Ampt suction head Ψ at the wetting front is not. The highest

NSE values for the most optimal set of parameters are 0.961, 0.968, and 0.986 for silt loam, sandy loam, and sand, respectively. An NSE threshold was adopted to delineate the successful sets of parameters (Figure 3.5) that produce the drawdown curve matching well with the observed drawdown data. The NSE threshold was determined as a ratio (0.98 was used in this study) of the highest NSE values of the most optimal set of parameters. The selected NSE thresholds were checked and show a well matching with the field-measured drawdown data for all the three types of soil (Figure 3.5). Please note that we have not used a fixed NSE (e.g., 0.9 or 0.95) as the threshold to identify the successful sets of parameters since NSE also depends on which variable (e.g., Δt_j or ΔH_j) is used to compute NSE (see Section 3.3.3), and the range between the highest NSE and the fixed threshold may vary for each test based on the value of the highest NSE.

The successful values of K_s (with NSE $\geq$ the threshold) are ranged within the same order of magnitude that are consistent with the tested soil texture class: 2.4–5.3×10^{-4} cm/s, 1.6–4.3×10^{-3} cm/s, and 1.9–3.5×10^{-2} cm/s for silt loam, sandy loam, and sand, respectively (Figure 3.6). Previous studies have shown that the measured K_s values may vary among the measurement methods by two or more orders of magnitude (Durner and Lipsius 2005; Muñoz-Carpena et al. 2002).

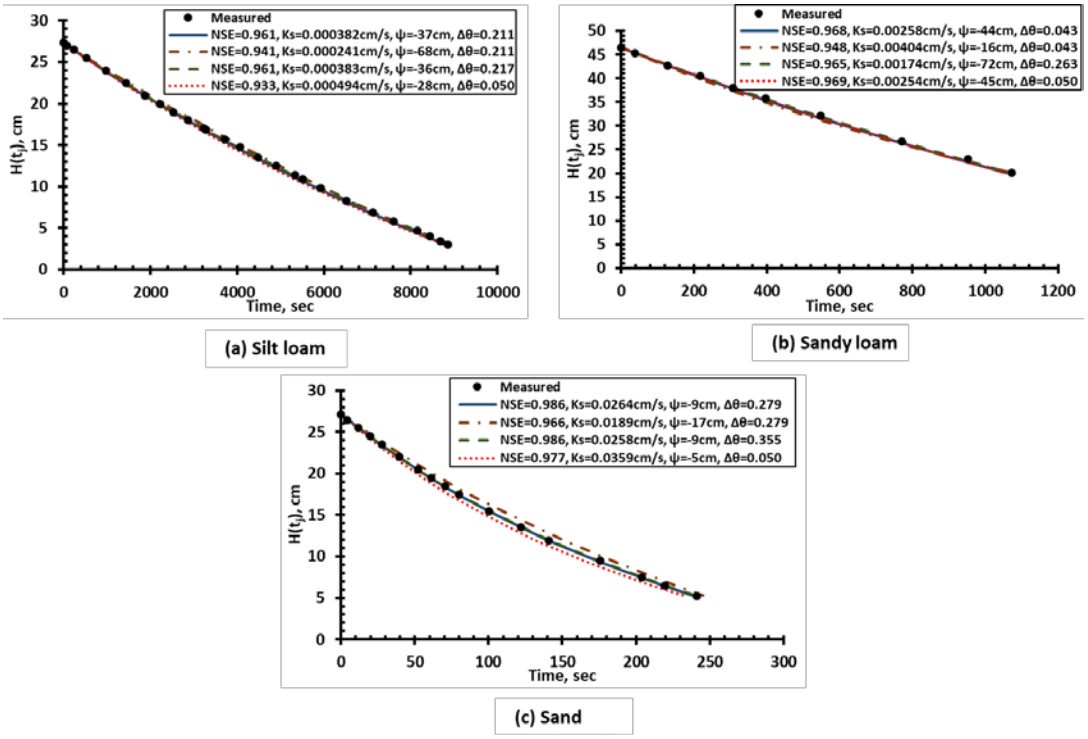

Figure 3.5. Field-measured and simulated drawdown curves using the sets of parameters with the highest and threshold NSE values (determined using Δt) and for K_s and Ψ back-fitted using the same measured drawdown curve of each soil and two assumed $\Delta\theta$ values: (**a**) silt loam, (**b**) sandy loam, and (**c**) sand. Note, the dots show measured drawdown data, the blue lines give the drawdown curves with the highest NSE (e.g., 0.961 for silt loam), and brown dash-dotted lines give the drawdown curves with the selected NSE threshold (e.g., 0.941 = 0.98×0.961 for silt loam).

On the other hand, the successful Ψ (with NSE ≥ the threshold) values do not converge to a specific range as in the case of K_s. The Ψ values ranged between −68 cm and −23 cm, −85 cm and −15 cm, and −18 and −4 for silt loam, sandy loam, and sand, respectively (Figure 3.6). The successful sets of parameters K_s and Ψ (with NSE ≥ the threshold) for the three types of soil are plotted together in Figure 3.6.

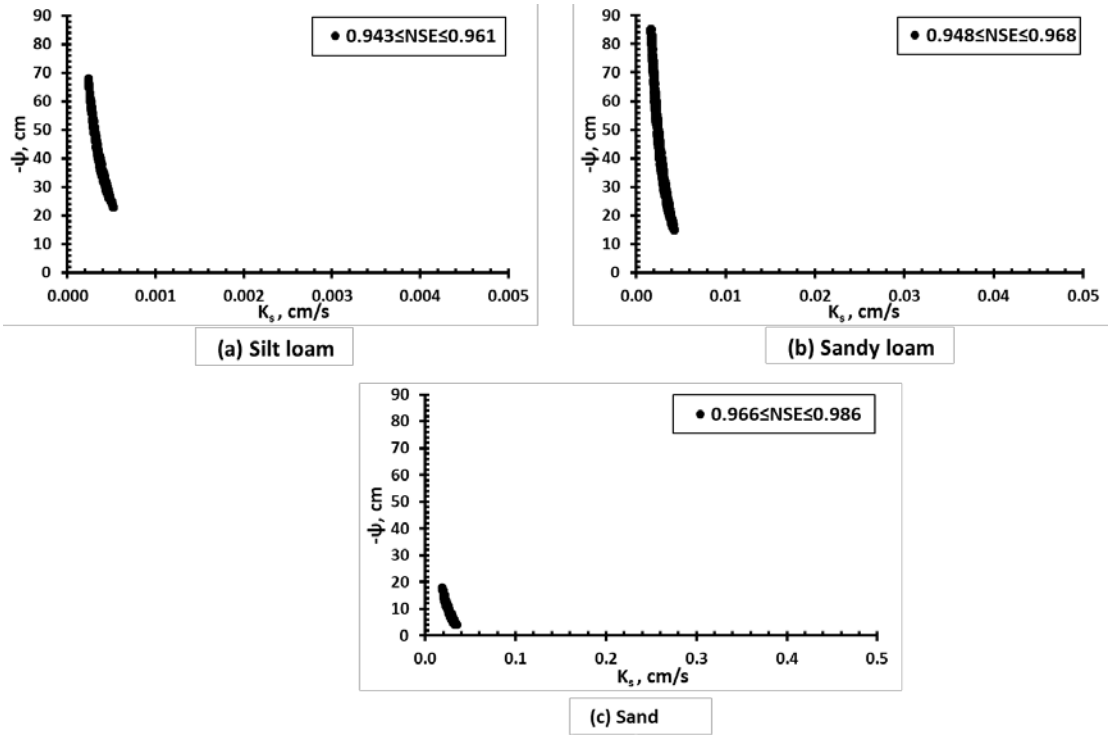

Figure 3.6. The successful sets of parameters K_s versus – Ψ (delineated by NSE ≥ the threshold value) determined from simulation using Δt_{sj} determined by Equation 3.6 and the measured time intervals Δt_j: (**a**) silt loam, (**b**) sandy loam, and (**c**) sand. Note: The limits for K_s (or x-axis) are different for the three soils.

The most optimal set of parameters (with the highest NSE values) determined using Application 2 and 3 (see Section 3.3.3) are reported in Table 3.3. Using the backward-fitting analysis procedure introduced by Ahmed et al. (2014), the fitted optimal parameters of K_s and Ψ using Δt_j are 3.96×10^{-4} cm/s and −37 cm for silt loam with NSE of 0.961; 2.59×10^{-3} cm/s and −44 cm for sandy loam with NSE of 0.968; and 2.66×10^{-2} cm/s and −9 cm for sand with NSE of 0.986.

Please note that all the synthetic drawdown data that were developed following the procedure of Application 1 (data of Figure 3.3) were also used in the sensitivity analysis procedure, which uses the forward-modeling code for Application 2 as described in the flowchart (see Figure 3.2). Results were similar to Figures 3.4–3.6 determined using the measured drawdown data described earlier in this section.

Table 3.3 The most optimal sets of K_s and Ψ (with the highest NSE values) determined using Application 2 and 3 as described in the flowchart (see Figure 2) with measured $\Delta\theta$, H_{in}, θ_{in}, and θ_s (input data) for the three tested soils (silt loam, sandy loam, and sand).

Soil Type	H_{in}	θ_{in}	θ_s	$\Delta\theta$	K_s **(cm/s)**		**Ψ (cm)**	
	(cm)				Application 2	Application 3	Application 2	Application 3
Silt loam	31.0	0.238	0.449	0.211	3.82×10^{-4}	3.88×10^{-4}	−37	−36
Sandy loam	51.0	0.339	0.382	0.043	2.58×10^{-3}	2.83×10^{-3}	−44	−37
Sand	33.5	0.096	0.375	0.279	2.64×10^{-2}	2.74×10^{-2}	−9	−8

3.3.3 Example of the Use of Application 3: Simulation Using $\Delta H_s(t_j)$ Determined by Equation 3.5 and Compare with the Changes in Measured Head Values $\Delta H(t_j)$

The collected data for the three types of soil were also analyzed using the forward-modeling code of the Application 3 mode (see Figure 3.2), which is based on estimating $\Delta H_s(t_j)$ determined by Equation (3.5) and comparing with measured head changes, $\Delta H(t_j)$ values. Figure 3.7 shows the results out of the 30,000 sets of randomly generated parameters K_s and Ψ with corresponding NSE values greater than zero for the three types of soil. The number of parameter sets with NSE > 0 are 1.8%, 12.5%, and 5.0% of the 30,000 sets of the parameters for silt loam, sandy loam, and sand, respectively. In

the Appendix A, we present the results shown in Figure 3.7 using the three–dimensional plots.

Results from the simulation using ΔH supported the strong correlation between NSE and K_s and the weak correlation with Ψ. The highest NSE values for the most optimal set of parameters are 0.914, 0.872, and 0.940 for silt loam, sandy loam, and sand, respectively. The NSE threshold was determined using the same ratio (0.98) of the highest NSE value applied in Section 3.3.2. Please note that the NSE calculated from ΔH is lower than the NSE calculated from Δt. This difference comes from the definition of the NSE proposed by Nash and Sutcliffe (1970) that is equal to one minus the sum of the absolute squared differences between predicted and observed values normalized by the variance of observed values. The variance of observed ΔH_j is typically less than the variance of Δt_j (see Figures 3.3 and 3.5); therefore, it leads to a lower value of NSE when NSE was determined using ΔH_j.

Similar to the results from Section 3.3.2, the successful values of K_s (with NSE ≥ the threshold) were ranged within the same order of magnitude that are consistent with the tested soil texture class: 2.9–4.7×10^{-4} cm/s, 2.0–3.5×10^{-3} cm/s, and 2.4–3.0×10^{-2} cm/s for silt loam, sandy loam, and sand, respectively (Figure 3.8). The successful values of Ψ (with NSE ≥ the threshold) still do not converge to a specific range as in the case of K_s. The successful values of Ψ (with NSE ≥ the threshold) ranged between −52 cm and −27 cm, −64 cm and −24 cm, and −11 and −6 for silt loam sandy loam, and sand, respectively (Figure 3.8).

The most optimal set of parameters (with the highest NSE values) determined using Application 3 are reported in Table 3.3. Using the analysis procedure introduced by Ahmed et al. (2014), the backward-fitted optimal parameters of K_s and Ψ using ΔH_j are 3.88×10^{-4} cm/s and −37 cm for silt loam with NSE of 0.914; 2.80×10^{-3} cm/s and −38 cm for sandy loam with NSE of 0.872; and 2.7×10^{-2} cm/s and −8 cm for sand with NSE of 0.940.

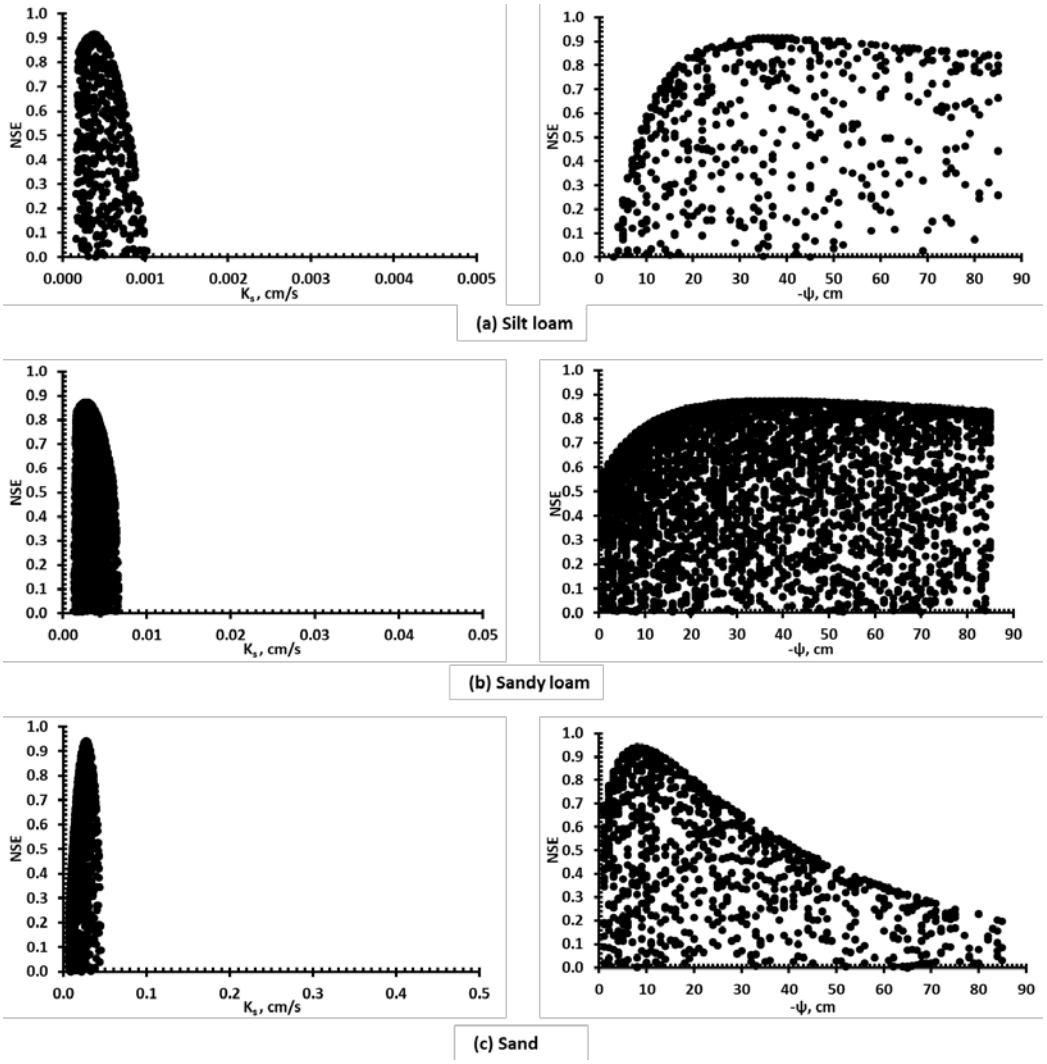

Figure 3.7. Scatter plots for the NSE calculated between $\Delta H_s(t_j)$ determined by Equation 3.5 and the changes in measured head $\Delta H(t_j)$, on the left is K_s

versus NSE and –Ψ versus NSE is on the right. (**a**) Silt loam, (**b**) Sandy loam, and (**c**) Sand.

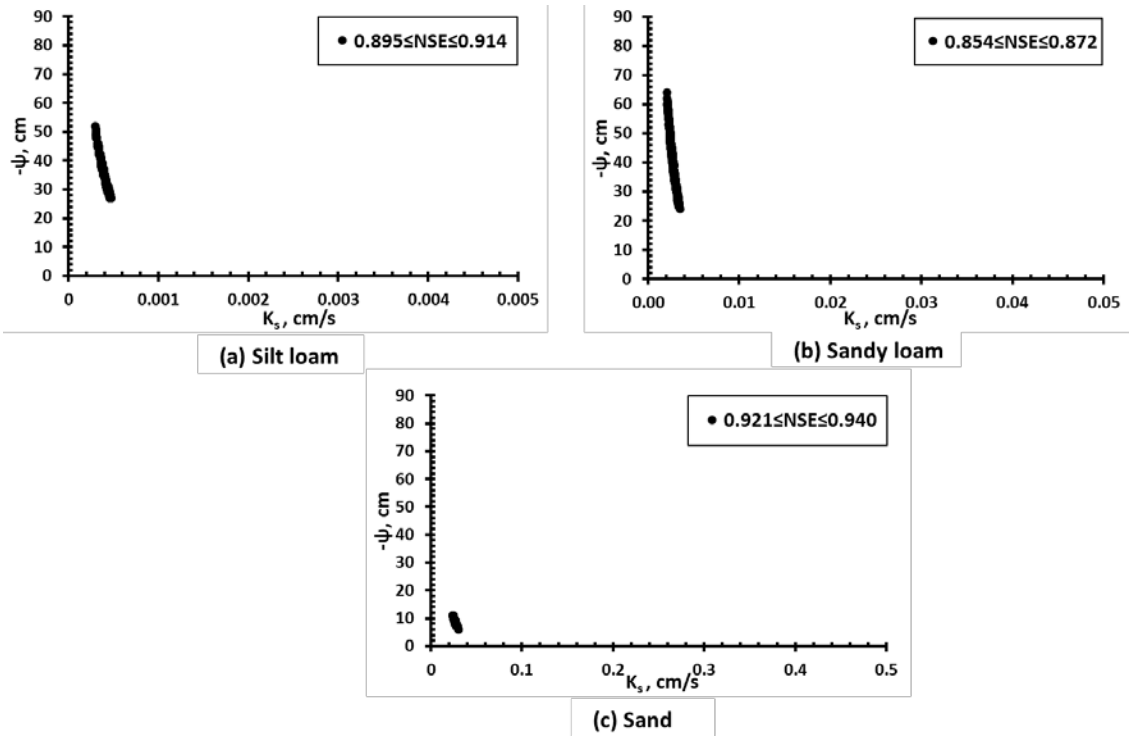

Figure 3.8. The successful sets of parameters K_s versus - Ψ (delineated by NSE ≥ the threshold value) determined from simulation using $\Delta H_s(t_j)$ determined by Equation 3.5 and the changes in measured head $\Delta H(t_j)$. (**a**) silt loam, (**b**) sandy loam, and (**c**) sand. Note: The limits for K_s (or x-axis) are different for the three soils.

3.3.4 Effects of Applying Varying Moisture Deficit $\Delta\theta$ on the Back-Fitted K_s and Ψ

Results from Figure 3.3 show that the drawdown curve predicted using the MPDI theory is different under varying soil moisture deficit $\Delta\theta$ when Ψ is changed with θ_{in}. To examine the sensitivity of the MPDI theory (Equations 3.5 and 3.6) to varying $\Delta\theta$, the soil properties K_s and Ψ were back-fitted using the measured drawdown data for silt loam, sandy loam, and sand using different $\Delta\theta$ (assumed) values including the maximum $\Delta\theta_{max}$

and a very low $\Delta\theta$ of 0.05 and the results are summarized in Table 3.4. Figure 3.5 shows that the simulated drawdown curves with the back-fitted K_s and Ψ using the maximum and a small $\Delta\theta$ match well with the observed drawdown data for three types of soil. The back-fitted K_s and Ψ determined using different assumed $\Delta\theta$ values are basically the same as the back-fitted K_s and Ψ using measured $\Delta\theta$ if one considers their variations determined in the laboratory or the field. This means that the back-fitted K_s and Ψ using all the drawdown data are not sensitive to $\Delta\theta$, which is the same conclusion obtained by Regalado et al. (2005) using the Philip–Dunne permeameter; they only measured two infiltration times when the permeameter was half full and empty. This does not mean that the Modified Philip–Dunne drawdown curves are not sensitive to the initial moisture contents, as indicated by Figure 3.3.

Therefore, above sensitivity analysis has two implications. First, in practices of using MPDI, the user may assume/estimate $\Delta\theta$ based on the field condition (wet or dry) to determine K_s and Ψ with a good accuracy if the user did not measure θ_{in} and/or θ_s. For example, $\Delta\theta$ can be set at 0.05, $\Delta\theta_{max}/4$, $\Delta\theta_{max}/2$, $3\Delta\theta_{max}/4$, and $\Delta\theta_{max}$ depending on the observed wet to dry soil condition (Table 3.4). Since the moisture content θ values at the field capacity (for the lowest θ_{in}) and saturated condition are available for many reference books, $\Delta\theta_{max}$ can be found for each soil. It is important to note that the same measured drawdown data of each type of soil were used to back-fit K_s and Ψ reported in Table 3.4 under different assumed $\Delta\theta$ values. Second, MPDI theory has a certain deficiency in counting the change of the initial moisture content since Figure 3.3 and 4.4 clearly

indicate the drawdown curves are different for the same soil when measured under different initial moisture contents, which will be further studied in Chapter 4.

Table 3.4 Values of saturated hydraulic conductivity K_s and Green–Ampt suction head Ψ at the wetting front for silt loam, sandy loam, and sand back-fitted using the same measured drawdown curve of each soil with different assumed moisture deficits $\Delta\theta$ including the measured $\Delta\theta$ values.

Soil Type	$\Delta\theta$	K_s (cm/s)	Ψ (cm)	$H(t_1)$ (cm)	NSE
Silt loam	0.211 (measured)	3.96×10^{-4}	−37	27.4	0.961
	0.217 (maximum)	3.82×10^{-4}	−37	27.3 [a]	0.961
	0.050 (assumed)	4.94×10^{-4}	−28	30.2	0.933
	$\Delta\theta_{max}/4$ (assumed)	4.91×10^{-4}	−28	30.1	0.934
	$\Delta\theta_{max}/2$ (assumed)	4.06×10^{-4}	−35	29.2	0.966
	$3\Delta\theta_{max}/4$ (assumed)	3.95×10^{-4}	−36	28.2	0.965
Sandy loam	0.043 (measured)	2.59×10^{-3}	−44	50.3	0.968
	0.222 (maximum)	1.79×10^{-3}	−70	47.2 [a]	0.965
	0.050 (assumed)	2.54×10^{-3}	−45	50.2	0.969
	$\Delta\theta_{max}/4$ assumed)	2.51×10^{-3}	−46	50.1	0.964
	$\Delta\theta_{max}/2$ (assumed)	2.21×10^{-3}	−53	49.1	0.965
	$3\Delta\theta_{max}/4$ (assumed)	2.08×10^{-3}	−57	48.2	0.964
Sand	0.279 (measured)	2.64×10^{-2}	−9	28.8	0.986
	0.355 (maximum)	2.58×10^{-2}	−9	27.5 [a]	0.986
	0.050 (assumed)	3.59×10^{-2}	−5	32.7	0.977
	$\Delta\theta_{max}/4$ (assumed)	3.40×10^{-2}	−5	32.0	0.961
	$\Delta\theta_{max}/2$ (assumed)	2.88×10^{-2}	−8	30.5	0.986
	$3\Delta\theta_{max}/4$ (assumed)	2.78×10^{-2}	−8	29.0	0.986

Note: [a] Minimum $H(t_1)$ at $\Delta\theta_{max}$ that is used in Figure 3.5.

3.4 Conclusions

We have developed a forward model that was used to further our understanding of the fundamentals of the MPDI theory and identify some of its advantages and limitations. The forward model can be used to simulate synthetic drawdown curves that describe the changes in the water height $H(t_j)$ with time t_j when the values of K_s and Ψ are known. These

simulation results can be used to design the MPDI surveys under different types of field conditions. The forward model can also be used later to determine K_s and Ψ values by fitting the synthetic drawdown data against field-measured drawdown data. In this study, the model was used in this curve fitting mode to evaluate the quality of fit of 30,000 sets of randomly generated values of K_s and Ψ against the field-measured drawdown datasets compiled for three types of soil. Results show that the model is highly nonlinear and therefore it does not yield a unique best fit. There are multiple sets of parameters that can be used to fit the field-measured drawdown data equally well. The quality of the fit is quantified using an NSE threshold value. Our results show that for the good fits (which are delineated by NSE $\geq$ the threshold value), the predicted values of K_s are within the expected order of magnitude value for the tested soil. However, the value of Ψ can vary considerably even for good fits, especially for soils with low K_s. Based on these results, we conclude that the MPDI is a useful method to estimate K_s but not a robust method to estimate Ψ. This finding is similar to the results from Gómez et al. (2001) who also recommended to use alternative approaches to estimate the Green–Ampt suction head Ψ at the wetting front rather than using the Philip (1993) method. In addition, we found that the model fitted K_s and Ψ values are not sensitive to the assumed value of the moisture deficit $\Delta\theta$, therefore, the user of the MPDI can estimate $\Delta\theta$ based on qualitative field observations (i.e., wet or dry soil). For example, $\Delta\theta$ can be set at 0.05 for wet soils, and $\Delta\theta_{max}/4$, $\Delta\theta_{max}/2$, $3\Delta\theta_{max}/4$, or $\Delta\theta_{max}$ for different levels of partially dry to fully dry soils, respectively. The sensitivity analysis also indicates that MPDI theory has a certain deficiency in counting the change of the initial moisture content. Further studies are needed to understand/recheck or

possibly revise the current MPDI theory to fit only the K_s values when $\Delta\theta$ and Ψ values are known, or to improve the experimental procedures that can yield more sensitive datasets that can help uniquely identify K_s and Ψ values.

Chapter 4. Effect of Initial Moisture Content on the Drawdown Curve Measured Using the Modified Philip-Dunne Infiltrometer

4.1 Introduction

Water movement into the soil is the most important factor that affects many of the hydrological processes including groundwater recharge and the rate and amount of surface runoff (Liu et al. 2011; Schiff and Dreibelbis 1949). Soil properties such as the fine content, initial moisture content, and saturated hydraulic conductivity affect the water movement into the soil. The infiltration rate into the soil will decrease with the increase in fine mineral percentage within the soil (Alakayleh et al. 2018; Komine 2008; Sällfors and Öberg-Högsta 2002).

The effect of the initial soil moisture content on the infiltration has been studied by several investigators. The rate at which water infiltrates into a given soil varies between the maximum value when the soil is dry and the minimum value when the soil is wet (Horton 1933; Philip 1957; Ruggenthaler et al. 2016). Ruggenthaler et al. (2016) investigated the infiltration behavior in eight sites under dry, median, and wet soil moisture conditions using the double-ring infiltrometer. The dry run was performed at the welting point, the median run was at the field capacity, and artificial sprinkling was used to produce the wet condition. Results showed that the infiltration rate decreased with increasing the initial soil moisture content. Hino et al. (1988) investigated the effect of the initial soil moisture content on the vertical water movement through the soil using a one-dimensional vertical infiltration system. The system is a small cylindrical lysimeter supplied with artificial rainfall and two tensiometers at different depths. Results showed that as the initial

soil moisture content increases, the faster the downward water movement through the soil. Fan et al. (2018) investigated the wetting front pattern characteristics for different soil texture classes under an initial moisture content of 40%, 50%, and 60% field capacity. A vertical line-source moistube, which contained uniformly and densely distributed nano-pores that work as a subsurface source of water, was used to introduce a constant flow of water. Their results showed that the coarser the soil texture, the greater the gravitational force. On the contrary, the finer the soil texture the stronger the capillary action. This results in a uniform wetting front migration in the vertical direction for fine soil. The wetting front downward movement rate increases with the increase in the initial water content of the soil.

The saturated hydraulic conductivity K_s is one of the crucial parameters that govern the flow rate of water into the soil profile. Therefore, an accurate measurement of the soil saturated hydraulic conductivity is very important for the investigation of the hydrological processes (Alagna et al. 2016; McKenzie and Jacquier 1997; Mohanty et al. 1994; Reynolds et al. 2000; Zhang and Schaap 2019). Many field and laboratory methods for measuring the saturated hydraulic conductivity K_s are available. However, measuring K_s for a large-field scale requires multiple determinations on many locations which could be time consuming when a laboratory measurement by taking soil cores is used. A variety of field methods were developed to measure in situ K_s including the Guelph permeameter (Reynolds and Elrick 1986), the tension infiltrometer (Perroux and White 1988), the minidisk infiltrometer (Zhang 1997), and the Philip–Dunne permeameter (Philip 1993).

A modified version of the Philip–Dunne permeameter, known as the Modified Philip–Dunne Infiltrometer (MPDI), was developed by Ahmed et al. (2014). The MPDI is a suitable technique to measure the near-surface soil saturated hydraulic conductivity at a large field scale because of its ease of operation and requires a minimal amount of water. The device is a transparent open-ended tube with a radius of 5 cm beveled from one side for vertically inserting the tube 5 cm into the soil, however, these values are free to be selected by the user. Applying the device 5 cm into the soil rather than tightly inserting into a 15 cm borehole like the Philip–Dunne permeameter results in changing the flow configuration of the infiltrated water. Water is rapidly introduced into the device to an initial height H_{in} at time $t = 0$ and then the change in water height inside the tube is monitored with time. The soil volumetric moisture content is measured at the beginning (i.e., the initial soil moisture content θ_{in}) and at the end of the test (i.e., the saturated soil moisture content θ_s). The soil moisture content can be measured gravimetrically then the bulk density is measured and used to convert the gravimetric moisture content into volumetric moisture content. Or directly measure the volumetric moisture content using a moisture probe. The analysis is based on applying the Green-Ampt theory to estimate the saturated hydraulic conductivity K_s and the Green-Ampt suction head Ψ at the wetting front from the drawdown data of water inside the MPDI. The actual disk infiltration surface (with a radius r_1 of 5 cm, Figure 4.1a) is substituted by a sphere with equivalent surface area (with a radius $r_0 = 0.5 \times r_1$). The flow from the tube into the soil is primarily treated as driven by pressure and capillarity. The absence of the gravity component results in the spherically symmetrical flow configuration. The assumed spherically symmetrical

configuration is approximated to the actual three-dimensional flow configuration by applying a geometrical coefficient. Based on exploratory calculations using conformal mapping, Philip (1993) (see Figure 4.1a) and later Ahmed et al. (2014) have used $\beta = \pi^2/8$ in the governing equations of their methods. This coefficient was applied since the assumed flow paths are more hydraulically efficient than the actual flow paths.

Previous studies have shown that water moves into the soil by the effect of two major forces: gravity and capillary forces (Gray and Norum 1967). The coarser the soil texture, the greater the gravitational force. On the contrary, the finer the soil texture the stronger the capillary action. Under a high soil moisture content (wet condition), a low wetting front suction exists and therefore the effect of capillary force decreases and the gravity force increases (Gray and Norum 1967; Hino et al. 1988; Regalado et al. 2005). Therefore, data collected using the MPDI under wet conditions should be carefully evaluated since the assumption that the flow is primarily driven by pressure and capillarity is no longer valid. Regalado et al. (2005) have also stated that data collected using the Philip–Dunne permeameter under wet conditions of a low suction head at the wetting front must be taken with care for the same reason.

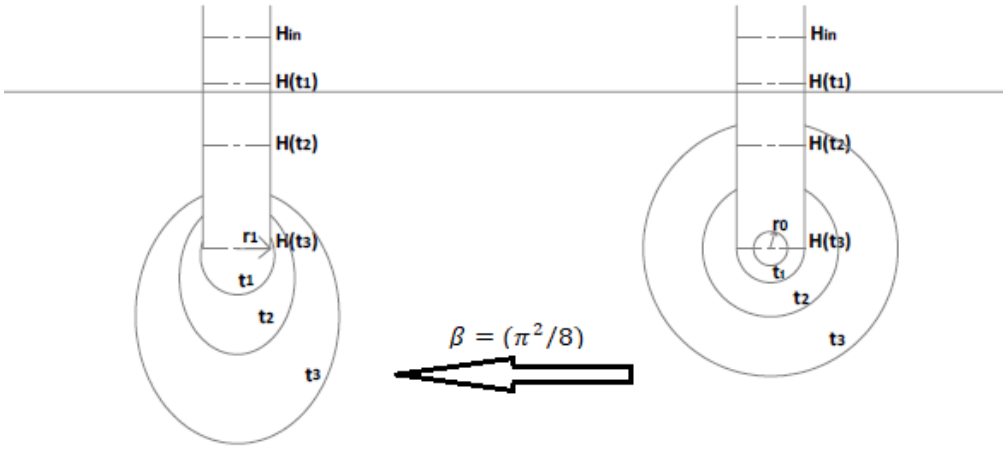

(a)

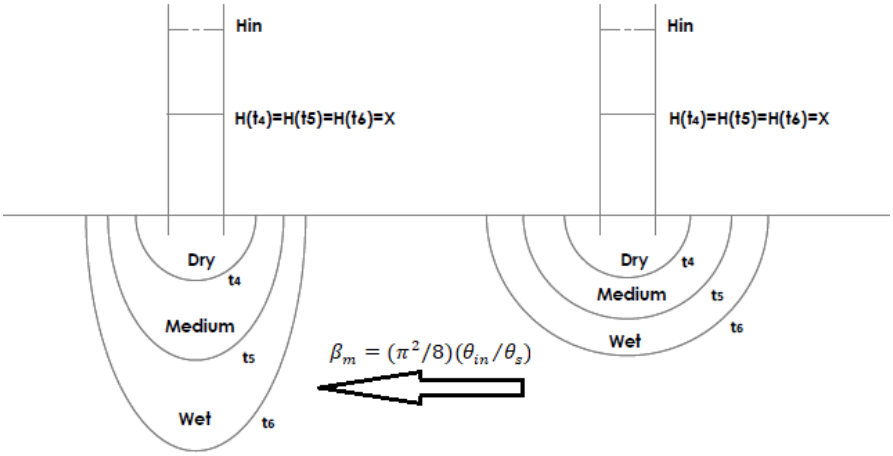

(b)

Figure 4.1. (a) Geometrical analog of the wetting fronts of water infiltrated from the Philip-Dunne permeameter (revised from Regalado et al. 2005) where H_{in}, H_1, H_2, and H_3 are the water levels inside the permeameter with corresponding time t_0, t_1, t_2, and t_3, respectively; the soil has a certain soil moisture content. (b) Geometrical analog of the wetting fronts of water infiltrated from the Modified Philip-Dunne Infiltrometer for a soil with three initial soil moisture contents (dry, medium, and wet) when the same drawdown $H(t_4) = H(t_5) = H(t_6) = X$ cm occurs at different time t_4, t_5, and t_6, respectively. On the right is the assumed spherically symmetrical configuration and the actual three-dimensional flow configuration is on the left.

Alakayleh et al. (2019) investigated the performance of the MPDI using a forward modeling algorithm. Results showed that the MPDI is a useful field method to estimate K_s but is not an accurate method to estimate Ψ. Gómez et al. (2001) have also recommended using another method rather than the Philip–Dunne permeameter (Philip 1993) to estimate the Green-Ampt suction head Ψ at the wetting front. Alakayleh et al. (2019) found out that the back-fitted K_s and Ψ values were not sensitive to the measured soil moisture deficit ($\Delta\theta = \theta_s - \theta_{in}$); therefore, the user of the MPDI can pre-estimate $\Delta\theta$ based on the field observations (i.e., wet or dry soil). Consequently, the estimated K_s and Ψ are only sensitive to the drawdown data measured using the MPDI. Regalado et al. (2005) explored similar results of the high sensitivity of K_s and Ψ estimated using the Philip–Dunne permeameter (Philip 1993) to the measured drawdown data and the small sensitivity to the moisture deficit $\Delta\theta$. Since the drawdown curve can vary for a given soil under different field conditions (i.e., wet or dry soil), one has to carefully analyze the collected drawdown data and correlate it with the soil moisture condition in order to get a unique estimate of K_s and Ψ.

In this study, we performed several experiments in the laboratory and in situ on different soil texture classes to investigate the effect of varying soil moisture content on the drawdown curve measured using the MPDI and consequently on the uniqueness of the estimated K_s and Ψ values. Note that the MPDI was developed by Ahmed et al. (2014) and used by others to evaluate the surface infiltration rate parameters for stormwater infiltration practices which are designed to have relatively high saturated hydraulic conductivity

values. Therefore, we haven't done tests and verified the results using soil with very low K_s values such as clay.

4.2 Materials and Methods

4.2.1 Laboratory Experiments

A mini MPDI with a radius of 1.27 cm that is driven 1.27 cm into the soil was constructed and used in the laboratory to estimate K_s and Ψ for three sets of experiments (Figure 4.2a). Three different types of soil were used in laboratory experimental testing. The three types of soil were obtained by mixing fine sand with a varying amount (percent dry weights) of No. 52 SilCoSil silt (8%, 15%, and 30%). The silt was made of ground quartz and was purchased from the U.S. Silica Company. The soil texture class and the particle size distributions of the three soils were measured using the Mastersizer 3000 made by Malvern Panalytical (2018). After the soil mixture was prepared by mixing the fine sand with silt at a specific percentage, the produced soil mixture was packed in a testing bucket with a diameter of 29 cm and a depth of 37 cm. Initial soil moisture content was measured gravimetrically by taking three soil samples during the packing of the middle and surface parts of the bucket where the process of infiltration occurs. The MPDI was inserted 1.27 cm into the soil surface near the center of the bucket. Then water was rapidly poured to fill the MPDI to an initial height H_{in} at time $t = 0$. During infiltration, the water level inside the MPDI was recorded with time. Immediately after all the water has infiltrated, the infiltrometer was removed from the testing bucket and soil samples were collected from the location where the tube was inserted to measure the final gravimetric soil moisture content. Then the soil bulk density was measured by taking a soil core, closely following

the procedure described in ASTM-F1815-11 (2011), in order to convert the gravimetric moisture content into volumetric soil moisture content. The collected data were analyzed using the procedure proposed by Ahmed et al. (2014) to estimate K_s and Ψ. The total volume of soil was removed from the testing bucket to a bigger bucket and was mixed manually with water in order to obtain a different and higher initial soil moisture content. The same volume of soil was then repacked again in the same volume of the testing bucket in order to get a similar dry bulk density. The MPDI was used again to determine K_s and Ψ by measuring the water height drop inside the MPDI with time using the same procedure mentioned above. Figure 4.2 shows the mini MPDI and the experimental testing setup that were used in this study.

(a) Mini MPDI. (b) Experimental setup.

Figure 4.2. (a) Mini MPDI, and (b) experimental setup.

For comparison, a minidisk infiltrometer made by Meter Group Inc. (2018) was used to estimate K_s of the three soil types that were tested using the mini MPDI. The same packing and mixing procedure used for the MPDI was used. The device is a transparent tube with a radius of 1.55 cm that is divided into two chambers. The lower chamber contains the volume of water (about 90 cm^3) that infiltrates into the soil. The upper chamber controls the suction and therefore the rate at which water infiltrates into the soil. A stainless steel porous disk is attached to the bottom of the infiltrometer to prevent water from leaking in the open air. After both chambers were filled with water, the suction was set to 6 cm and the bottom of the infiltrometer was placed on the soil and then water started to infiltrate into the soil. During infiltration, the volume of water inside the infiltrometer was recorded with time. The test was repeated for different initial soil moisture content for every soil. The procedure for data collection and analysis were made following the procedure described in Meter Group Inc. (2018).

4.2.2 Field Experiments

A standard MPDI with a radius of 5 cm that is driven 5 cm into the soil was used to estimate the in situ K_s and Ψ. Data were collected in situ for the water-height drop inside the tube over time, initial and final gravimetric soil moisture contents, and soil bulk density. The drawdown data were collected at the same location using the MPDI for the same soil under dry and wet conditions. Data for the dry condition were collected after several sunny days and directly after rainy days for wet condition.

The minidisk disk infiltrometer was used to estimate the in situ K_s in the same location where the MPDI was used. Results were compared with the one obtained using the MPDI. The suction head of the infiltrometer was set to 5 cm for both dry and wet conditions.

4.3 Results and Discussion

4.3.1 Laboratory Experiments

The laboratory-measured drawdown data were collected using the mini MPDI for the three soil mixtures (fine sand mixed with 8%, 15%, and 30% silt). This results in three different soil texture classes including loamy sand, sandy loam, and silt loam, respectively. Figure 4.3 shows the particle size distribution of the three soils that were measured using the Mastersizer 3000 made by Malvern Panalytical (2018).

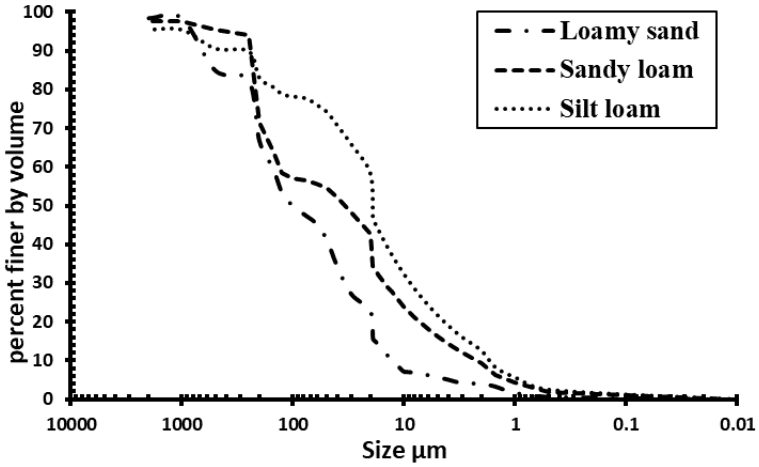

Figure 4.3. Particle size distributions of the three soils that were used in the laboratory testing.

Figure 4.4 shows the drawdown curves measured using the mini MPDI, which starts from H_{in} to $H(t)$ = 2 cm (the support base for the mini MPDI would not allow us to

read the depth of complete empty tube), for the three soils under varying initial soil moisture content. The mini MPDI (Fig. 4.2) was used in the laboratory since the soil is more homogenous than in the field where a standard MPDI with a radius of 5 cm was used.

Results show that the total drawdown time t_2, which was recorded when $H(t) = 2$ cm, varied with the soil type. For example, under dry conditions, t_2 values were 70, 492, and 2652 seconds for the loamy sand, sandy loam, and silt loam, respectively (note that H_{in} was 32, 30, and 29.5 cm for loamy sand, sandy loam, and silt loam, respectively). Figure 4.4 shows that the measured drawdown curves are significantly different for the same soil under varying initial soil moisture content. The dry soil has θ_{in} of 0.001–0.002, about 0.69–1.40% of the wet soil (θ_s = 0.138–0.144). Results show that for every soil the total drawdown time t_2 is greater under wet condition than dry condition. The total drawdown time t_2 values under dry and wet conditions were 70 and 465 seconds, 492 and 2722 seconds, and 2652 and 12118 seconds for loamy sand, sandy loam, and silt loam, respectively. The t_2 values under dry condition were 395, 2230, and 9466 seconds shorter than that observed under wet condition for loamy sand, sandy loam, and silt loam respectively. This is similar to the observations made by others who have shown that the rate of water infiltration into dry soil can be higher than wet soil (Gray and Norum 1967; Philip 1957; Ruggenthaler et al. 2016). This is because there are more voids in dry soil that allow water to fill relatively fast, but wet soil has much less voids to allow water fill and therefore takes more time to infiltrate. Mathematically, Richard's equation described water movement by diffusion and advection terms. The capillary potential is responsible for diffusion term and hydraulic conductivity is responsible for the advection term. As an

example, when clay soil is wet the capillarity potential is low and the hydraulic conductivity of the clay is also low, therefore, the summation of both diffusion and advection terms is low. When the soil is dry, the capillarity potential of the clay is high and the hydraulic conductivity is low, therefore, summation of both diffusion and advection terms of dry soil would be higher than under wet condition. Since the summation of both terms is greater under dry condition than wet condition, therefore, water movement into dry soil will be faster than into wet soil. The clay soil has been considered in the example to explain the variation in the infiltration rate with varying soil moisture conditions since the effect of the initial soil moisture content on the infiltration rate is greater with increasing the fine content of the soil.

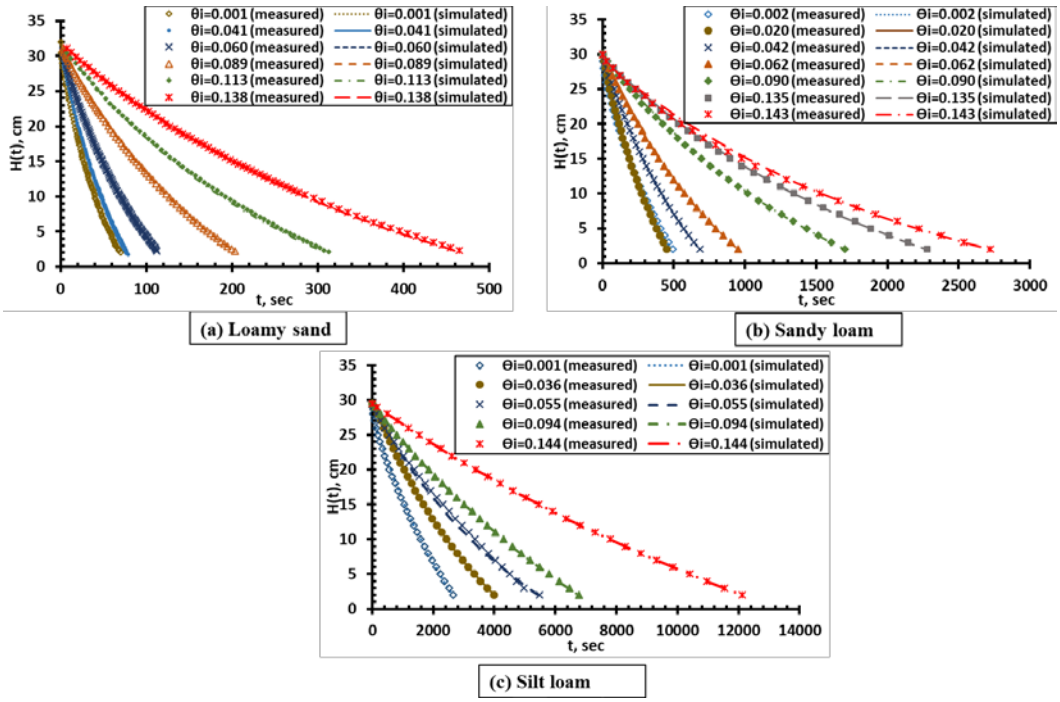

Figure 4.4. Laboratory-measured drawdown data for the three soil types under varying initial soil moisture content versus the simulated drawdown curves using the Modified Philip–Dunne theory and back-fitted K_s and Ψ proposed by Ahmed et al. (2014): (a) loamy sand, (b) sandy loam, and (c) silt loam.

The collected drawdown data for the three soils under varying initial soil moisture content and the corresponding initial and final volumetric soil moisture content were analyzed using the analysis procedure proposed by Ahmed et al. (2014) and the back-fitted K_s and Ψ are reported in Table 4.1.

Table 4.1. Back-fitted saturated hydraulic conductivity K_s and Green-Ampt suction head Ψ at the wetting front estimated using the Modified Philip-Dunne theory under varying initial soil moisture content with and without applying the correction factor.

Soil type	θ_{in}	θ_s	Bulk density	K_s	Ψ	K_s [a]	Ψ [a]	$(\theta_{in}/\theta_s) \times s$
	%	%	g/cm^3	cm/s	cm	cm/s	cm	
Loamy sand (8% silt)	0.12	20.4	1.58	3.15×10^{-2}	-9	2.29×10^{-2}	-9	0.1
	4.10	20.4	1.58	2.60×10^{-2}	-15	1.74×10^{-2}	-15	1.7
	6.00	20.4	1.59	1.80×10^{-2}	-15	2.68×10^{-2}	-17	2.6
	8.90	20.4	1.58	1.05×10^{-2}	-13	2.04×10^{-2}	-14	3.8
	11.3	20.4	1.59	7.09×10^{-3}	-13	1.67×10^{-2}	-16	4.8
	13.8	20.4	1.58	4.63×10^{-3}	-13	1.26×10^{-2}	-18	5.9
Sandy loam (15% silt)	0.18	23.0	1.64	4.01×10^{-3}	-13	2.89×10^{-3}	-11	0.1
	2.00	23.0	1.65	3.79×10^{-3}	-18	4.13×10^{-3}	-19	1.3
	4.20	23.0	1.65	2.76×10^{-3}	-18	4.14×10^{-3}	-18	2.7
	6.20	23.0	1.64	1.96×10^{-3}	-16	3.87×10^{-3}	-19	4.0
	9.00	23.0	1.65	1.10×10^{-3}	-16	2.83×10^{-3}	-21	5.7
	13.5	23.0	1.65	9.01×10^{-4}	-13	3.27×10^{-3}	-20	8.6
	14.3	23.0	1.64	8.92×10^{-4}	-10	3.44×10^{-3}	-16	9.1
Silt loam (30% silt)	0.14	25.0	1.72	5.66×10^{-4}	-20	4.08×10^{-4}	-18	0.1
	3.60	25.0	1.71	4.28×10^{-4}	-18	7.00×10^{-4}	-21	2.6
	5.50	25.0	1.71	3.35×10^{-4}	-16	7.16×10^{-4}	-20	4.6
	9.35	25.0	1.72	1.78×10^{-4}	-31	5.55×10^{-4}	-40	7.8
	14.4	25.0	1.72	9.49×10^{-5}	-33	4.33×10^{-4}	-45	12.0

[a] Estimated when $\beta_m = (\pi^2/8)(\theta_{in}/\theta_s) \times s$ was used in the governing equations of the MPDI rather than using $\beta = (\pi^2/8)$.

Table 4.1 shows that the overall trend of back-fitted K_s values estimated using the MPDI was decreasing with increasing the fine content. This correct trend was also observed by Nestingen et al. (2018) for the K_s values estimated using the MPDI for three types of sand with different grain size distribution. For a given soil, the MPDI does not provide a unique estimate of K_s as it supposed to do when measured under varying initial soil moisture content. The estimated K_s values of every soil (Table 4.1) varied with the initial soil moisture content. This is directly related to the differences in observed drawdown curves when the MPDI tests were performed under varying θ_{in} for every soil and to the small sensitivity of K_s and Ψ estimated using the Modified Philip–Dunne theory to the soil moisture deficit. The lowest K_s value of every soil was observed when the MPDI was used in wet soil. Note that the flow from the MPDI into the soil is primarily treated as driven by pressure and capillarity and ignore the gravity force. Previous studies have shown that the higher is the initial soil moisture content the lower the effect of the capillary force and the higher is the gravity force (Hino et al. 1988). That means an underestimate of K_s is the consequence of neglecting the gravity force as the infiltrated water from the MPDI into the soil is primarily treated as driven by pressure and capillarity force. The estimated Ψ values (see Table 4.1) were arbitrary and did not reflect the changes in the soil texture class and initial soil moisture content of every soil. This is similar to the results from Alakayleh et al. (2019) who also explored that the MPDI is not a robust method to estimate the Ψ values.

It will be desirable to somehow account for the effect of the soil moisture content in the MPDI model to provide a unique estimate of K_s and correct Ψ values that reflect the

variation in θ_{in} of a given soil. In this study, we have developed and used a correction factor to be multiplied with the constant coefficient (β) that was proposed by Philip (1993) and also used by Ahmed et al. (2014) to approximate the spherically symmetrical configuration to the actual three-dimensional flow configuration. The correction factor is used in the MPDI governing equations to help in yielding a unique estimate of K_s whatever the initial soil moisture content at the time of performing the test. Equations 4.1 and 4.2 show the governing equation of the MPDI before and after applying the correction factor, respectively. Where $\beta = (\pi^2/8)$ and $\beta_m = (\pi^2/8)(\theta_{in}/\theta_s) \times s$ (Figure 4.1).

$$\Delta t = \frac{\beta(\theta_s - \theta_{in})\dfrac{R^2(t) + R(t)L_{\max}}{K_s}\dfrac{\ln\dfrac{R(t)(r_0 + L_{\max})}{r_0(R(t) + L_{\max})}}{L_{\max}}\Delta R(t) - \dfrac{L_{\max}}{K_s}\Delta H(t)}{\Psi - H(t) - L_{\max} + 4\beta r_0^{\,2}\dfrac{\ln\dfrac{R(t)(r_0 + L_{\max})}{r_0(R(t) + L_{\max})}}{L_{\max}}} \tag{4.1}$$

$$\Delta t = \frac{\beta_m(\theta_s - \theta_{in})\dfrac{R^2(t) + R(t)L_{\max}}{K_s}\dfrac{\ln\dfrac{R(t)(r_0 + L_{\max})}{r_0(R(t) + L_{\max})}}{L_{\max}}\Delta R(t) - \dfrac{L_{\max}}{K_s}\Delta H(t)}{\Psi - H(t) - L_{\max} + 4\beta_m r_0^{\,2}\dfrac{\ln\dfrac{R(t)(r_0 + L_{\max})}{r_0(R(t) + L_{\max})}}{L_{\max}}} \tag{4.2}$$

Ahmed et al. (2014) used equation 4.1 to solve for K_s and Ψ by minimizing the absolute difference between Δt determined using equation 4.1 and the measured time intervals. Another method for setting the optimization is to fit K_s and Ψ values by minimizing the absolute difference between the time series of calculated ΔH and measured

head drop data. One can calculate ΔH by rearranging equation 4.1 (put ΔH on the left side of the equation).

The geometrical coefficient β should reflect the changes in the actual three-dimensional flow configuration of a given soil under varying initial soil moisture content. Figure 4.1b shows the geometrical analog of the MPDI with considering varying initial soil moisture content. Previous studies have shown that the wetting front could advance to a deeper depth with the increase in the initial water content of the soil (Fan et al. 2018; Hino et al. 1988). The finer the soil texture the greater the effect of the initial soil moisture content. The proposed correction factor equals $(\theta_{in}/\theta_s) \times s$ where s was found to be similar to the absolute and nondimensional value of the bubbling pressure Ψ_b of the tested soil from Rawls et al. (1982). The bubbling pressure or the air-entry value of the soil is the matric suction that must be acceded before the entry of air into the soil voids. This value is a function of the largest pore in the porous medium. When the largest pore in the porous medium is small, the bubbling pressure will be large (Fredlund 2006). The bubbling pressure is 9, 15, and 21 cm for loamy sand, sandy loam, and silt loam, respectively. The geometrical coefficient in the governing equations of the MPDI is then multiplied with the correction factor and becomes $\beta_m = (\pi^2/8)(\theta_{in}/\theta_s) \times s$. The K_s and Ψ values estimated using the MPDI theory when the correction factor was used in the governing equation are reported in Table 4.1. Results show that K_s values of every soil measured under varying initial soil moisture content were consistent after applying the correction factor but Ψ is still arbitrary. Where a high variability in K_s values of a given soil was observed when estimated using the MPDI under varying initial soil moisture content before applying the

correction factor. The coefficients of variation (standard deviation divided by the mean value) of K_s for the loamy sand, sandy loam, and silt loam were 66.3%, 60.9%, and 59.1%, respectively. After the correction factor was used in the MPDI equations (see Equation 4.2) the coefficients of variation decreased to 25.9%, 15.7%, and 25.6% for the loamy sand, sandy loam, and silt loam, respectively. Figure 4.5 shows K_s values with and without applying the correction factor with the corresponding θ_{in} values. The exponential trendline was used to illustrate the decrease in K_s value estimated using the Modified Philip-Dunne theory with increasing the initial soil moisture content at the time when the test was performed. The coefficients of determination R^2 were ranged between 0.95 and 0.98.

The correction factor (Table 4.1) varies with θ_{in} for the same soil texture class (since θ_s and s are the same) and is much greater for the wet condition than for dry condition to account for the effect of the initial soil moisture content within a given soil. For example, for loamy sand (Table 4.1), θ_{in} changed from 0.12% to 13.8%, 115 times increase, and then the correction factor has the same increase. Also, the correction factor varies with the soil texture class, greater with the increase in the fine content of the soil to account for the greater effect of the initial soil moisture content on fine soil than coarse soil. For example, when the initial soil moisture content is the same for the three soil ($\theta_{in} \approx 0.09$) the correction factor equals 3.8, 5.7, and 7.8 for loamy sand, sandy loam, and silt loam, respectively.

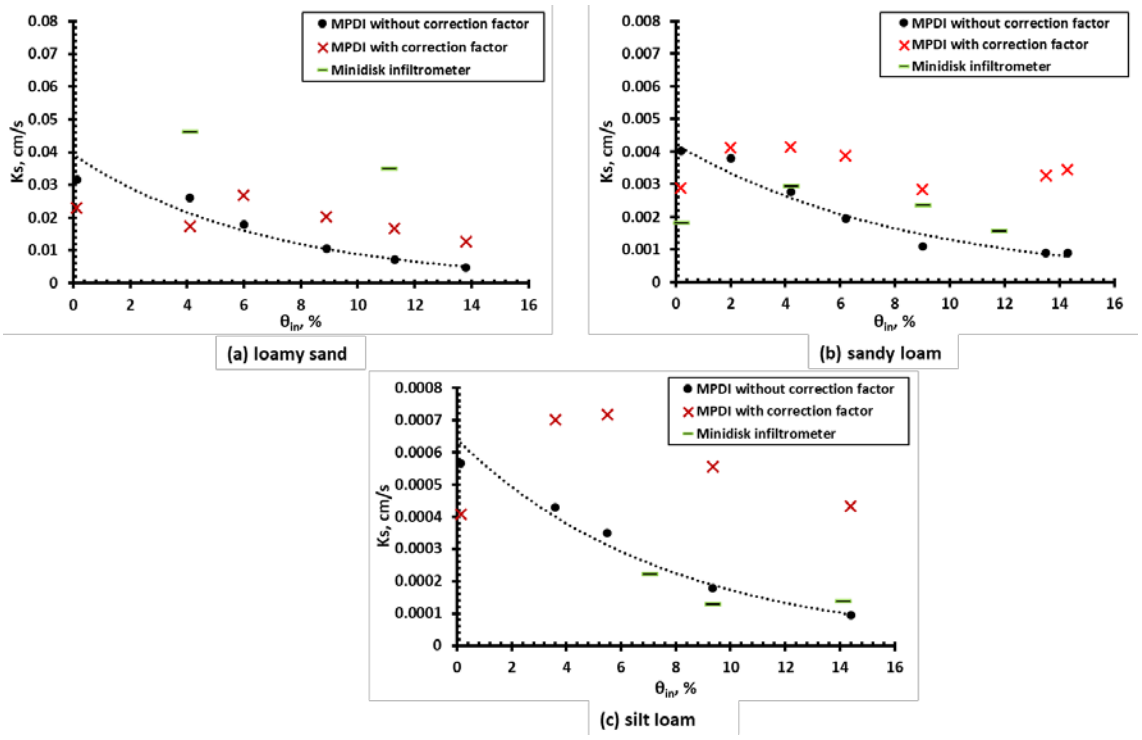

Figure 4.5. Comparing the saturated hydraulic conductivity K_s estimated using the Modified Philip-Dunne theory under varying initial soil moisture content before and after applying the correction factor and K_s estimated using the minidisk infiltrometer. Note: the scales for K_s in the y-axis are different for each of the three soils and the dashed lines are for the exponential trendlines.

The MPDI was then compared against the minidisk infiltrometer that was used to estimate K_s of the three soils under varying θ_{in} and the results are summarized in Table 4.2. The K_s values estimated using both methods have not been compared against any reference method such as the falling head test as completed by Nestingen et al. (2018). Therefore no error analysis was discussed. The coefficient of variation was used to determine and compare the precision (variation of K_s) and therefore the relative performance of the MPDI against the minidisk infiltrometer when both methods were used under varying θ_{in} of a given soil. The coefficients of variation of K_s estimated using the minidisk infiltrometer

were 19.5%, 28.0%, and 31.8% for the loamy sand, sandy loam, and silt loam, respectively, which are similar to the coefficients of variation after applying the correction factor in the MPDI equations.

Table 4.2. Saturated hydraulic conductivity K_s estimated using the Minidisk infiltrometer under varying initial soil moisture content.

Soil type	θ_{in}	**Bulk density**	K_s
	%	**g/cm^3**	**cm/s**
Loamy sand	4.10	1.58	4.62×10^{-2}
8% silt	11.1	1.59	3.50×10^{-2}
Sandy loam	0.18	1.64	1.82×10^{-3}
15% silt	4.20	1.64	2.93×10^{-3}
	9.00	1.65	2.35×10^{-3}
	11.8	1.64	1.56×10^{-3}
Silt loam	7.04	1.71	2.21×10^{-4}
30% silt	9.35	1.72	1.28×10^{-4}
	14.1	1.71	1.37×10^{-4}

4.3.2 Field Experiments

The field-measured drawdown data were collected using the standard MPDI for a silt loam soil in an agriculture experimental field in Auburn, Alabama. The drawdown data were collected at the same location using the MPDI under dry and wet conditions. Data for dry condition were collected after several sunny days and directly after rainy days for wet condition. Figure 4.6 shows the measured drawdown data, which starts from H_{in} = 31 cm to $H(t)$ = 3 cm.

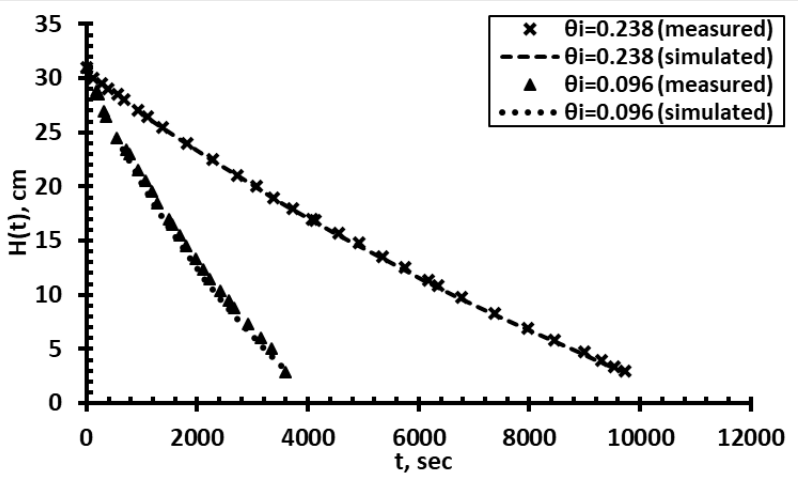

Figure 4.6. Field-measured drawdown data for a silt loam soil under dry and wet conditions versus the simulated drawdown curves using the Modified Philip-Dunne theory proposed by Ahmed et al. (2014).

Figure 4.6 shows that the measured drawdown curves are significantly different for the same soil under varying initial soil moisture content. The total drawdown time t_3, which was recorded when $H(t)$ = 3 cm, varied with initial soil moisture content. t_3 values were 3600 and 9720 seconds under the dry and wet conditions, respectively. Under the dry condition, t_2 value was 6120 seconds shorter than that observed under wet condition. The dry soil has θ_{in} of 0.096 and the wet soil has θ_{in} of 0.238 with about 21.5 and 53.2% of θ_s, respectively. The collected drawdown data under the dry and wet conditions and the corresponding initial and final volumetric soil moisture content were analyzed using the analysis procedure proposed by Ahmed et al. (2014) and the obtained K_s and Ψ are reported in Table 4.3.

Table 4.3. Saturated hydraulic conductivity K_s and Green-Ampt suction head Ψ at the wetting front estimated using the Modified Philip-Dunne theory under dry and wet conditions with and without applying the correction factor.

θ_{in}	θ_s	K_s	Ψ	K_s [a]	Ψ^a	$(\theta_{in}/\theta_s) \times s$
%	%	cm/s	cm	cm/s	cm	
9.57	44.4	1.40×10^{-3}	-20	2.59×10^{-3}	-32	4.5
23.8	44.9	3.80×10^{-4}	-37	1.03×10^{-3}	-90	11.0

Results (Table 4.3) show a similar trend to the laboratory-measured data of decreasing K_s value when the test was conducted under the relatively wet condition and the arbitrary Ψ. Then the correction factor was used in the MPDI equations where *s* is equal to 21 which is the absolute and nondimensional value of the bubbling pressure of the silt loam. The obtained K_s and Ψ after applying the correction factor are reported in Table 4.3. The coefficients of variation before and after applying the correction factor were 81.0% and 60.9%, respectively. The coefficient of variation value of the in situ tested soil is higher than the one of the laboratory tested soil reported in Section 4.3.1. This could be related to the difference in the soil homogeneity in the lab and in situ (Nestingen et al. 2018).

The minidisk infiltrometer was then used to in situ measure the saturated hydraulic conductivity K_s on the same location under dry and wet conditions. The measured K_s values were 3.4×10^{-3} and 3.0×10^{-3} cm/s for the dry and wet conditions, respectively. These values are similar to the one estimated using the MPDI under dry condition.

4.4 Conclusion

In this study, we have investigated the effect of initial soil moisture content θ_{in} on the drawdown curve measured using the Modified Philip-Dunne Infiltrometer and consequently on the estimated K_s and Ψ values. Three sets of laboratory experiments were conducted for three types of porous media (loamy sand, sandy loam, and silt loam). These types of porous media were obtained by adding varying amounts (percent dry weights) of No. 52 SilCoSil silt (8%, 15%, and 30%, respectively) to fine sand. Results showed that the overall trend of K_s values estimated using the MPDI was decreasing with increasing the fine content. For a given soil, the drawdown curve was different under varying θ_{in}. This results in different back-fitted K_s values for a given soil using measured drawdown curves under varying θ_{in}. The lowest K_s values were observed when the MPDI was used in wet soil. That means an underestimate of K_s is the consequence of neglecting the gravity force as the infiltrated water from the MPDI into the soil is primarily treated as driven by pressure and capillarity force. Previous studies have shown that the greater the effect of the gravitational force than the capillary force when the initial soil moisture content increases. Results from the MPDI were compared against the results from the Minidisk infiltrometer under varying initial soil moisture content for the laboratory and in situ experiments. K_s values estimated using the minidisk infiltrometer were similar to the one estimated using the MPDI under dry condition. Therefore, the minidisk infiltrometer is not sensitive to varying initial soil moisture content like the MPDI. In this study, we proposed a correction factor to be multiplied with the geometrical coefficient that is used in the governing equations of the MPDI. The correction factor can help to obtain a unique estimate of K_s

value for a given soil whatever the θ_{in} value at the time of performing the test. This correction factor varies within a given soil with the variation in θ_{in}. Also, the correction factor varies with the soil texture classes, greater with the increase in the fine content of the soil. A consistent estimate of K_s was obtained after the correction factor was used. The coefficients of variation of K_s decreased from 66.3%, 60.9%, and 59.1% to 25.9%, 15.7%, and 25.6% for the loamy sand, sandy loam, and silt loam, respectively. The coefficients of variation after applying the correction factor were similar to the one calculated for K_s values estimated using the minidisk infiltrometer under varying θ_{in}. The correction factor was also tested by collecting in situ drawdown data under dry and wet conditions for a silt loam soil. The coefficient of variation of K_s decreased from 81.0% to 60.9%. However, we recommend performing the MPDI tests in dry condition and avoid performing the test on a rainy or after rainy days. Results show that the estimated Ψ values in all the experiments were arbitrary and did not reflect the changes in soil texture classes and the soil moisture content. This is similar to the results from Alakayleh et al. (2019) how found that the MPDI is not a robust method to estimate Ψ.

Chapter 5. Summary, Conclusions, and Recommendations for Future Work

5.1 Summary

The design of many engineering systems requires a better understanding of water infiltration processes through subsurface soil. Among the soil hydraulic properties, the saturated hydraulic conductivity K_s is the most important parameter that controls the water seepage processes through the soil profile. Without having proper knowledge of the K_s value, it is difficult to design effective engineering systems. Some of the engineering systems involve the design of low conductivity barriers, known as hydraulic barriers, to prevent contaminated water leaching from landfills and other waste disposal areas from polluting local groundwater aquifers. In contrast, some applications are designed to have high conductivity areas to enhance water infiltration into the underlying soil to attenuate runoff volume and to increase groundwater recharge.

The low saturated hydraulic conductivity clay-sand mixtures are often used to construct hydraulic barriers. While there are several empirical models available in the literature that can be used to predict reductions in K_s values of coarse sand due to the presence of clay and other fine minerals, all these models require measurement of multiple physical properties of the porous media. The resulting empirical expressions have several parameters that need to be individually evaluated using multiple soil characterization tests. In the first part of this dissertation (Chapter 2), we have proposed a single parameter model that can be used to capture the variations in saturated hydraulic conductivity value of different types of porous media mixtures using a scalable modeling framework. Several laboratory tests were conducted to measure the saturated hydraulic conductivity values of

a variety of simulated coarse-fine and fine-coarse synthetic porous media mixtures. The model results were further validated using the data derived from experiments conducted with a fully hydrated natural clay and sand mixtures, and also using multiple literature-derived datasets.

The objective of the second part of this dissertation is to further our understanding of the Modified Philip–Dunne Infiltrometer (MPDI), which is used to determine the in situ K_s and the Green–Ampt suction head Ψ at the wetting front. The MPDI is inexpensive, easy to use, and requires a minimal amount of water. These advantages make the MPDI a useful method to rapidly estimate K_s and Ψ values throughout the infiltration practices since the hydraulic properties of the system have to be carefully measured from multiple locations during the construction and operation of the system. We have developed a forward-modeling algorithm that can be used to simulate water level changes inside the infiltrometer with time when the soil hydraulic properties K_s and Ψ are known. The forward model was used to generate 30,000 water level datasets using randomly generated values of K_s and Ψ. These model data were then compared against field-measured water level drawdown data collected for three types of soil. The Nash–Sutcliffe efficiency (NSE) was used to assess the quality of the fit.

Results from chapter 3 showed that the model fitted K_s and Ψ values are not sensitive to the moisture deficit $\Delta\theta$ but only sensitive to the measured drawdown data. Since the drawdown data can vary for a given soil when measured under varying initial soil moisture content, one has to carefully analyze the collected drawdown data and

correlate it with the soil moisture condition in order to get a unique estimate of K_s and Ψ. Also, data collected using the MPDI under wet condition should be carefully evaluated since the assumption that the flow is primarily driven by pressure and capillarity is no longer valid. In Chapter 4, we have studied the effect of varying the initial soil moisture content of a given soil on the measured drawdown curve and consequently on the uniqueness of the estimated K_s and Ψ values. Several sets of experiments on different soil texture classes were performed in the laboratory and in situ. We proposed a correction factor to be used in the governing equations of the MPDI that can help to obtain a unique estimate of K_s value of a given soil whatever the initial soil moisture content at the time of performing the test. All the experimental testing results were used to test the proposed factor.

5.2 Conclusions

The results of the first part of this dissertation showed that the proposed framework is a useful tool for modeling the hydraulic properties of various types of engineered mixtures. The model can help design optimal mixtures without conducting multiple experiments that could be time consuming and cost prohibitive. The model can estimate the saturated hydraulic conductivity values of coarse-fine mixtures with fine content varying between 0 and 100 percent without using multiple experimental data points. The proposed model successfully correlated the changes in the saturated hydraulic conductivity values of a variety of coarse-fine mixtures with the amount of fine material in the mixture. It is important to note that this method is suitable only for modeling artificial mixtures and

should not be used to predict the saturated hydraulic conductivity value of undisturbed, heterogeneous natural porous media where field-scale measurements are used.

Results from the forward-modeling algorithm in the second part of this dissertation showed that multiple sets of the MPDI model parameters K_s and Ψ can yield drawdown curves that can fit the field-measured data equally well. For the good fits (delineated by NSE $\geq$ the threshold value), the predicted K_s values converged to a valid range that is fully consistent with the tested soil texture class. However, Ψ values varied significantly and did not converge to a valid range even for good fits. Based on these results, we conclude that the MPDI is a useful method to estimate K_s but not a robust method to estimate Ψ. In addition, we found that the model fitted K_s and Ψ values are not sensitive to the assumed value of the moisture deficit $\Delta\theta$, therefore, the user of the MPDI can estimate $\Delta\theta$ based on qualitative field observations (i.e., wet or dry soil). Consequently, the MPDI is only sensitive to the measured drawdown data.

Results in Chapter 4 showed that the overall trend of K_s values estimated using the MPDI was decreasing with increasing the fine content (K_s is greater for the soil with 8% silt than soils with 15 and 30% when the initial soil moisture content is the same). For a given soil, the drawdown curve was different under varying initial soil moisture content. This results in different back-fitted K_s for a given soil using measured drawdown curves under varying initial soil moisture content. The lowest K_s values were observed when the MPDI was used in wet soil. That means an underestimate of K_s is the consequence of neglecting the gravity force as the infiltrated water from the MPDI into the soil is primarily

treated as driven by pressure and capillarity force. Previous studies have shown that the greater the effect of the gravitational force than the capillary force when the initial soil moisture content increases. Results showed that the proposed correction factor can help to obtain a unique estimate of K_s value of given soil when measured under varying initial moisture content but Ψ is still arbitrary and did not reflect the variation in the soil texture class and also the soil moisture content of a given soil.

5.3 Recommendations for Future Work

The third part of this dissertation (Chapter 4) investigated the effect of varying initial soil moisture content on the drawdown data measured using the MPDI and consequently on the estimated K_s and Ψ values. Several laboratory and field experiments on different soil texture classes using the MPDI were performed. We have tried to test the accuracy of the analysis in Chapter 4 using Hydrus (2D/3D) that can simulate water movement into the soil by numerically solving Richard's equation. Hydrus (2D/3D) was modified by Šimůnek et al. (2018) with a new computational module "Reservoir boundary condition" that can be used to simulate transient head boundary conditions. This module was used to generate the drawdown data inside the MPDI for the same soil under varying initial moisture content. Interestingly, the drawdown data varied slightly with the changes in the initial soil moisture content, which are much smaller variations than what we found in the laboratory and field data collection (Chapter 4) when the initial soil moisture was changed. It would be valuable to further test and understand the suitability of Hydrus (2D/3D) simulation model to generate the drawdown data inside the MPDI under varying initial soil moisture content and compare it with experimental testing results. If the Hydrus

(2D/3D) simulation model cannot do so, it is valuable to identify the reasons and the theoretical deficiency why Hydrus governing equations would not produce the drawdown curves varying with the initial soil moisture content. In Appendix-B, we provide a preliminary test example to illustrate the use of Hydrus (2D) for simulating the drawdown data inside the MPDI under varying initial soil moisture content conditions.

Appendix–A. Results of the Sensitivity Analysis in Chapter 3 using Three–Dimensional Plots

In this Appendix, the results of the sensitivity analysis of Applications 2 and 3 (see sections 3.3.2 and 3.3.3) are presented using the three–dimensional plots. Figures A.1 and A.2 are representing the 2D Figures 3.4 and 3.7, respectively. The two soil parameters (K_s and Ψ) of the MPDI model were sampled randomly using a uniform distribution within the range of 1×10^{-4} cm/s to 1×10^{-1} cm/s and −85 cm to −1 cm for K_s and Ψ, respectively; these ranges include all the soil types as reported in Clapp and Hornberger (1978). The value of Ψ will also be a function of the moisture content and can vary with the soil type (change of K_s), but randomly sampled parameters did not have any restriction to form these data pairs. The total 30,000 sets of generated parameters covered all possible random combinations of K_s and Ψ values. Only the data pairs that produced the positive NSE are presented in Figures A.1 and A.2, and most of the data pairs had negative NSE values

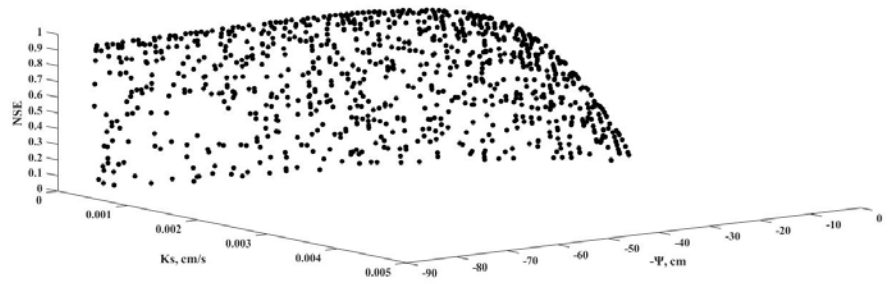

(a) Silt loam

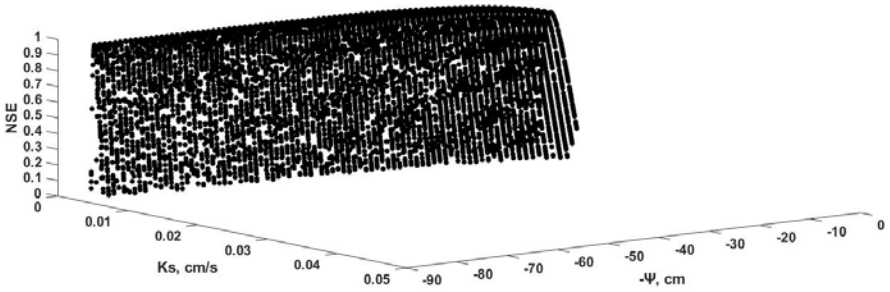

(b) Sandy loam

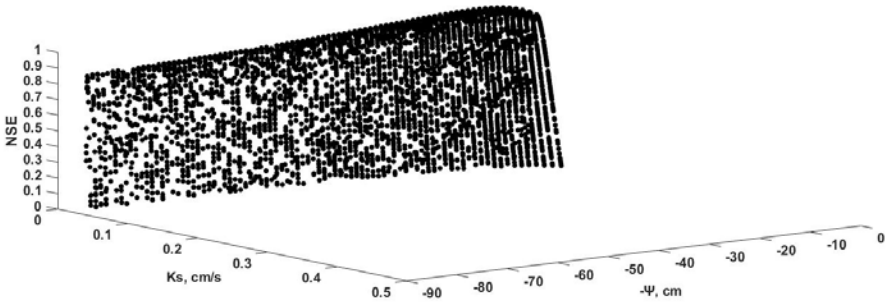

(c) Sand

Figure A.1. Scatter plots of the NSE calculated between Δt_{sj} determined by Equation 3.6 and the measured time intervals Δt_j for (**a**) silt loam, (**b**) sandy loam, and (**c**) sand. The scales for K_s are different for each of the three soils.

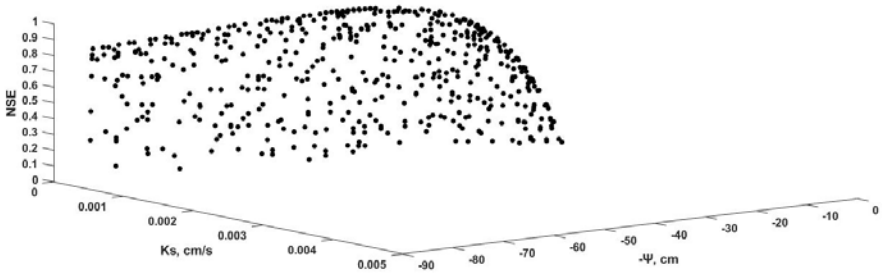

(a) Silt loam

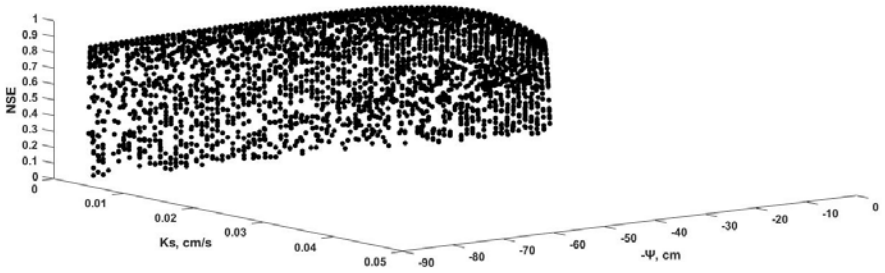

(b) Sandy loam

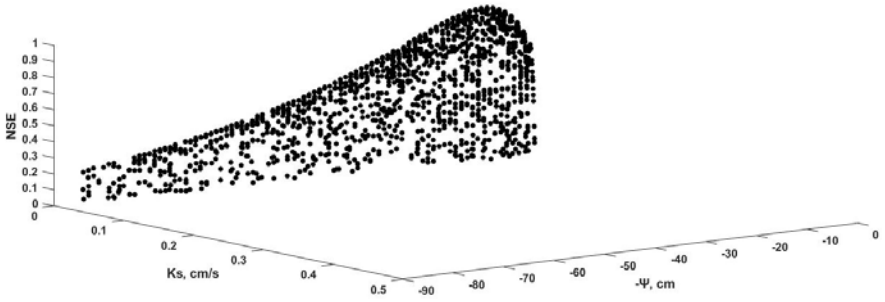

(c) Sand

Figure A.2. Scatter plots of the NSE calculated between $\Delta H_s(t_j)$ determined by Equation 3.5 and the changes in measured head $\Delta H(t_j)$ for (**a**) silt loam, (**b**) sandy loam, and (**c**) sand. The scales for K_s are different for each of the three soils.

Appendix–B. Example Simulation of the Drawdown Data inside the Modified Philip–Dunne Infiltrometer Using Hydrus (2D/3D)

In this Appendix, the drawdown data inside the MPDI were generated by applying Hydrus (2D/3D) software. The example was modeled using the axisymmetric option to simulate the three-dimensional domain with a symmetry around the vertical axis. Using the axisymmetric option, the user develops a 2-D domain that represents a volume results from revolving the 2-D domain around the vertical axis. For our example, the transport domain was 75 cm wide and 80 cm deep. That means we are modeling a soil cylinder with 150 cm diameter and 80 cm deep. The radius of the MPDI was 5 cm and the initial water height H_{in} inside the tube was 30 cm. The boundary condition at the soil surface where the MPDI is placed/inserted is seepage face. The lower boundary condition is a free drainage. All other surfaces including the MPDI insertion into the soil (5 cm) are no flux boundary conditions. The modeled soil was considered as a silt loam with the Hydrus default values of the Van Genuchten (1980) parameters. The simulation was conducted by changing the initial condition that was selected to be described in terms of water content. The initial water content θ_{in} were selected to represent varying soil conditions (i.e. dry and wet soil) with the values of 0.15, 0.25, and 0.35. Figure B.1 shows the drawdown curves of the selected soil under varying initial soil moisture content. The total time needed to infiltrate H_{in} = 30 cm water into the soil was 1127, 1160, and 1212 minutes for the θ_{in} values of 0.15, 0.25, and 0.35, respectively. Figure B.2 shows the calculated water content profile at 1080 minutes when water is still infiltrated into the soil for the three θ_{in} values. These drawdown curves are different from ones determined in the laboratory and the field. Therefore, further

study is necessary to determine why Hydrus (2D/3D) could not reproduce the drawdown curves as a function of soil initial moisture content.

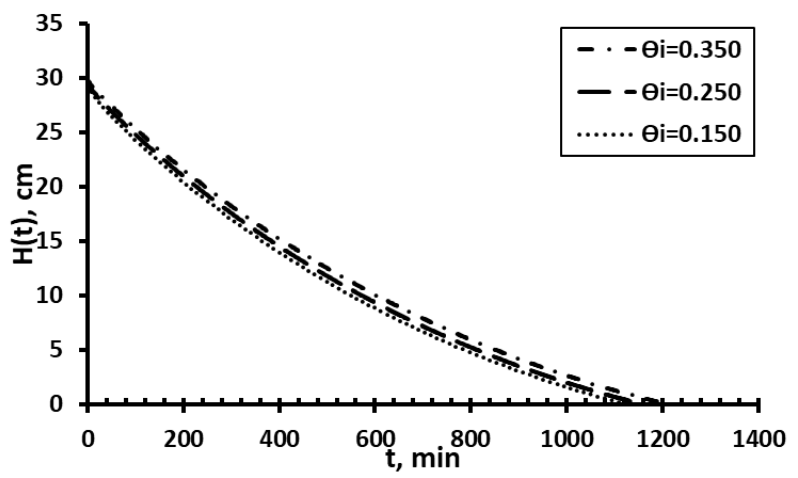

Figure B.1. Calculated drawdown curves inside the MPDI using Hydrus (2D/3D) under varying initial soil moisture content.

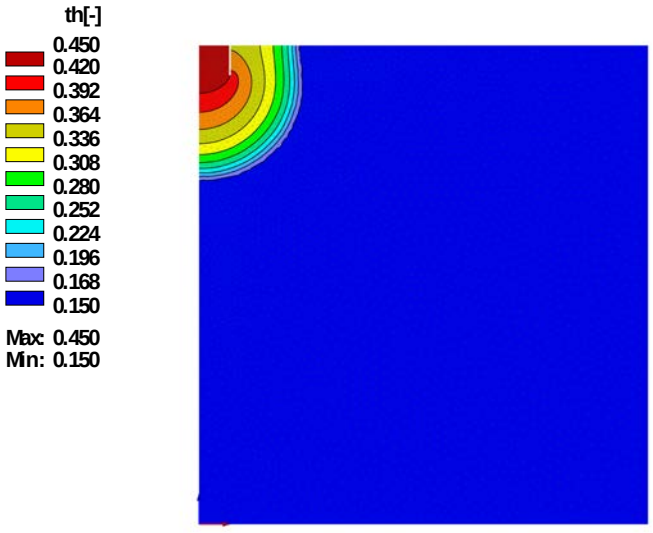

(a)

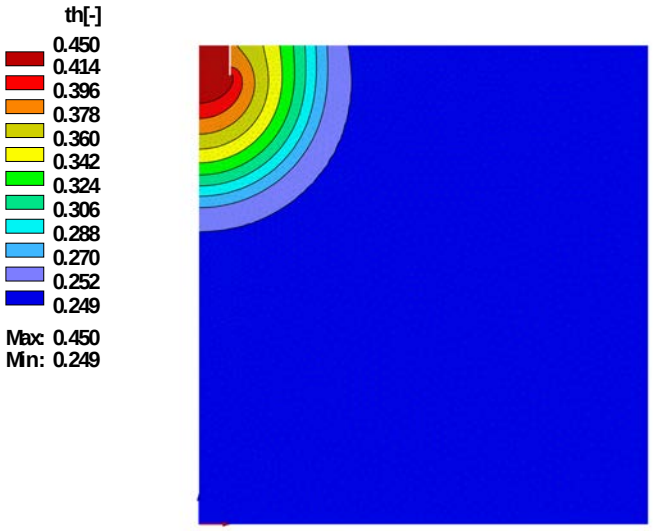

(b)

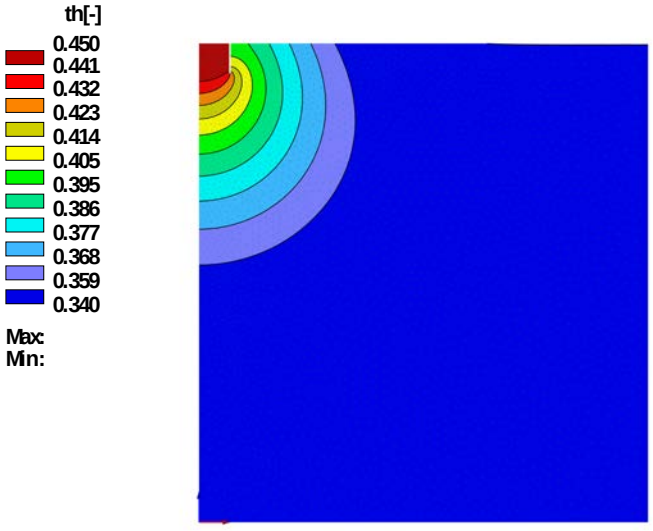

(c)

Figure B.2. Calculated water content profiles at 1080 minutes when the initial soil moisture content was (a) 0.15, (b) 0.25, and (c) 0.35.

References

Abeele, W. (1986). "The influence of bentonite on the permeability of sandy silts." *Nuclear and chemical waste management*, 6(1), 81-88.

Abichou, T., Benson, C. H., and Edil, T. B. (2002). "Micro-structure and hydraulic conductivity of simulated sand-bentonite mixtures." *Clays and clay minerals*, 50(5), 537-545.

Ahmed, F. (2014). "Characterizing the performance of a new iniltrometer and hydraulic properties of roadside swales."

Ahmed, F., Nestingen, R., Nieber, J., Gulliver, J., and Hozalski, R. (2014). "A Modified Philip–Dunne Infiltrometer for Measuring the Field-Saturated Hydraulic Conductivity of Surface Soil." *Vadose Zone Journal*, 13(10).

Ahmed, F., Nestingen, R., Nieber, J. L., Gulliver, J. S., and Hozalski, R. M. (2014). "A modified Philip–Dunne infiltrometer for measuring the field-saturated hydraulic conductivity of surface soil." *Vadose Zone Journal*, 13(10).

Akgün, H., Koçkar, M., and Aktürk, Ö. (2006). "Evaluation of a compacted bentonite/sand seal for underground waste repository isolation." *Environmental Geology*, 50(3), 331-337.

Alagna, V., Bagarello, V., Di Prima, S., and Iovino, M. (2016). "Determining hydraulic properties of a loam soil by alternative infiltrometer techniques." *Hydrological Processes*, 30(2), 263-275.

Alakayleh, Z., Clement, T. P., and Fang, X. (2018). "Understanding the Changes in Hydraulic Conductivity Values of Coarse-and Fine-Grained Porous Media Mixtures." *Water*, 10(3), 313.

Alakayleh, Z., Clement, T. P., and Fang, X. (2019). "A comprehensive Performace Assessment of the Modified Philip–Dunne Infiltrometer." *Water*, 11(9), 1881.

ASTM-D2216-10 (2010). "Standard Test Methods for Laboratory Determination of Water (Moisture) Content of Soil and Rock by Mass." *American Society for Testing and Materials: Philadelphia, USA*.

ASTM-D2423-68 (1968). "Standard Test Method for Permeability of Granular Soils (Constant Head)." *ASTM International, West Conshohocken, PA*.

ASTM-D5084-16a (2016). "Standard Test Methods for Measurement of Hydraulic Conductivity of Saturated Porous Materials Using a Flexible Wall Permeameter." *ASTM International, West Conshohocken, PA*.

ASTM-D5084-16a (2016). "Standard Test Methods for Measurement of Hydraulic Conductivity of Saturated Porous Materials Using a Flexible Wall Permeameter." *American Society for Testing and Materials: Philadelphia, USA*.

ASTM-D8152-18 (2018). "Standard Practice for Measuring Field Infiltration Rate and Calculating Field Hydraulic Conductivity Using the Modified Philip Dunne Infiltrometer Test. ." *American Society for Testing and Materials: Philadelphia, USA*.

ASTM-F1815-11 (2011). "Standard Test Methods for Saturated Hydraulic Conductivity, Water Retention, Porosity, and Bulk Density of Athletic Field Rootzones." *American Society for Testing and Materials: Philadelphia, USA*.

Bagarello, V., Iovino, M., and Elrick, D. (2004). "A simplified falling-head technique for rapid determination of field-saturated hydraulic conductivity." *Soil Science Society of America Journal*, 68(1), 66-73.

Benson, C. H., Daniel, D. E., and Boutwell, G. P. (1999). "Field performance of compacted clay liners." *Journal of Geotechnical and Geoenvironmental Engineering*, 125(5), 390-403.

Benson, C. H., and Trast, J. M. (1995). "Hydraulic conductivity of thirteen compacted clays." *Clays and clay minerals*, 43(6), 669-681.

Benson, C. H., Zhai, H., and Wang, X. (1994). "Estimating hydraulic conductivity of compacted clay liners." *Journal of Geotechnical Engineering*, 120(2), 366-387.

Bouwer, H. (1964). "Measuring Horizontal and Vertical Hydraulic Conductivity of Soil With the Double-Tube Method 1." *Soil Science Society of America Journal*, 28(1), 19-23.

Brooks, R. H., and Corey, A. T. (1966). "Properties of porous media affecting fluid flow." *Journal of the Irrigation and Drainage Division*, 92(2), 61-90.

Castelbaum, D., and Shackelford, C. D. (2009). "Hydraulic conductivity of bentonite slurry mixed sands." *Journal of geotechnical and geoenvironmental engineering*, 135(12), 1941-1956.

Chapuis, R. P. (1990). "Sand–bentonite liners: predicting permeability from laboratory tests." *Canadian Geotechnical Journal*, 27(1), 47-57.

Clapp, R. B., and Hornberger, G. M. (1978). "Empirical equations for some soil hydraulic properties." *Water Resources Research*, 14(4), 601-604.

Connolly, R. D., Silburn, D. M., Ciesiolka, C. A. A., and Foley, J. L. (1991). "Modelling hydrology of agricultural catchments using parameters derived from rainfall simulator data." *Soil and Tillage Research*, 20(1), 33-44.

Daniel, D. E. (1993). "Case histories of compacted clay liners and covers for waste disposal facilities."

Daniel, D. E. (1993). "Case histories of compacted clay liners and covers for waste disposal facilities." *International Conference on Case Histories in Geotechnical Engineering*. .

Denson, K. H., Shindala, A., and Fenn, C. D. (1968). "Permeability of sand with dispersed clay particles." *Water Resources Research*, 4(6), 1275-1276.

Dias, R. P., Fernandes, C. S., Teixeira, J. A., Mota, M., and Yelshin, A. (2008). "Permeability analysis in bisized porous media: Wall effect between particles of different size." *Journal of Hydrology*, 349(3), 470-474.

Dixon, D., Gray, M., and Thomas, A. (1985). "A study of the compaction properties of potential clay—sand buffer mixtures for use in nuclear fuel waste disposal." *Engineering geology*, 21(3-4), 247-255.

Doley, C., Das, U. K., Phukan, P. K., Dutta, D., and Bora, P. M. (2016). "A study on use of Brahmaputra river sand as a liner material for municipal landfills." *IOSR Journal of Mechanical and Civil Engineering*, 13, 91-96.

Durner, W., and Lipsius, K. (2005). "Determining Soil Hydraulic Properties." *Encyclopedia of Hydrological Sciences*, 1021-1144.

Ebina, T., Minja, R. J., Nagase, T., Onodera, Y., and Chatterjee, A. (2004). "Correlation of hydraulic conductivity of clay–sand compacted specimens with clay properties." *Applied Clay Science*, 26(1), 3-12.

Fan, Y.-W., Huang, N., Zhang, J., and Zhao, T. (2018). "Simulation of soil wetting pattern of vertical moistube-irrigation." *Water*, 10(5), 601.

Francisca, F. M., and Glatstein, D. A. (2010). "Long term hydraulic conductivity of compacted soils permeated with landfill leachate." *Applied Clay Science*, 49(3), 187-193.

Fredlund, D. G. (2006). "Unsaturated soil mechanics in engineering practice." *Journal of geotechnical and geoenvironmental engineering*, 132(3), 286-321.

García-Serrana, M., Gulliver, J. S., and Nieber, J. L. (2017). "Infiltration capacity of roadside filter strips with non-uniform overland flow." *Journal of Hydrology*, 545, 451-462.

Garlanger, J. E., Cheung, F. K., and Tannous, B. S. "Quality control testing for a sand-bentonite liner." *Proc., Geotechnical practice for waste disposal'87*, ASCE, 488-499.

Gleason, M. H., Daniel, D. E., and Eykholt, G. R. (1997). "Calcium and sodium bentonite for hydraulic containment applications." *Journal of geotechnical and geoenvironmental engineering*, 123(5), 438-445.

Gómez, J., Giráldez, J., and Fereres, E. (2001). "Analysis of infiltration and runoff in an olive orchard under no-till." *Soil Science Society of America Journal*, 65(2), 291-299.

Gómez, J., Giráldez, J. V., and Fereres, E. (2001). "Analysis of infiltration and runoff in an olive orchard under no-till." *Soil Science Society of America Journal*, 65(2), 291-299.

Gray, D. M., and Norum, D. "The effect of soil moisture on infiltration as related to runoff and recharge." *Proc., Proceedings of hydrology symposium*, Citeseer.

Gray, D. M., and Norum, D. "The effect of soil moisture on infiltration as related to runoff and recharge." *Proc., Proceedings of hydrology symposium*, Citeseer.

Green, W. H., and Ampt, G. (1911). "Studies on Soil Phyics." *The Journal of Agricultural Science*, 4(1), 1-24.

Gregory, J. H., Dukes, M. D., Jones, P. H., and Miller, G. L. (2006). "Effect of urban soil compaction on infiltration rate." *Journal of soil and water conservation*, 61(3), 117-124.

Hino, M., Odaka, Y., Nadaoka, K., and Sato, A. (1988). "Effect of initial soil moisture content on the vertical infiltration process—A guide to the problem of runoff-ratio and loss." *Journal of Hydrology*, 102(1-4), 267-284.

Horton, R. E. (1933). "The role of infiltration in the hydrologic cycle." *Eos, Transactions American Geophysical Union*, 14(1), 446-460.

Horton, R. E. "The interpretation and application of runoff plot experiments with reference to soil erosion problems." *Proc., Soil Science Society of America Proceedings*, 340-349.

Kanwar, R. S., Rizvi, H., Ahmed, M., Horton, R., and Marley, S. J. (1990). "Measurement of field-saturated hydraulic conductivity by using Guelph and velocity permeameters." *Transactions of the ASAE*, 32(6), 1885-1890.

Kenney, T., Veen, W. V., Swallow, M. A., and Sungaila, M. (1992). "Hydraulic conductivity of compacted bentonite–sand mixtures." *Canadian Geotechnical Journal*, 29(3), 364-374.

Komine, H. (2008). "Theoretical equations on hydraulic conductivities of bentonite-based buffer and backfill for underground disposal of radioactive wastes." *Journal of geotechnical and geoenvironmental engineering*, 134(4), 497-508.

Kristvik, E., Kleiven, G. H., Lohne, J., and Muthanna, T. M. (2018). "Assessing the robustness of raingardens under climate change using SDSM and temporal downscaling." *Water Science and Technology*, 77(6), 1640-1650.

Lee, D., Elrick, D., Reynolds, W., and Clothier, B. (1985). "A comparison of three field methods for measuring saturated hydraulic conductivity." *Canadian journal of soil science*, 65(3), 563-573.

Lipiec, J., Kuś, J., Słowińska-Jurkiewicz, A., and Nosalewicz, A. (2006). "Soil porosity and water infiltration as influenced by tillage methods." *Soil and Tillage research*, 89(2), 210-220.

Liu, H., Lei, T., Zhao, J., Yuan, C., Fan, Y., and Qu, L. (2011). "Effects of rainfall intensity and antecedent soil water content on soil infiltrability under rainfall conditions using the run off-on-out method." *Journal of Hydrology*, 396(1-2), 24-32.

Lundgren, T. "Some bentonite sealants in soil mixed blankets." *Proc., Proceedings, 10th International Conference on soil mechanics and foundation engineering, Stockholm*, 349-354.

Mallants, D., Jacques, D., Tseng, P.-H., van Genuchten, M. T., and Feyen, J. (1997). "Comparison of three hydraulic property measurement methods." *Journal of Hydrology*, 199(3-4), 295-318.

Malvern Panalytical (2018). "Mastersizer 3000 basic guide." *Malvern, United Kingdom*.

McKenzie, N., and Jacquier, D. (1997). "Improving the field estimation of saturated hydraulic conductivity in soil survey." *Soil Research*, 35(4), 803-827.

Merva, G. "The velocity permeameter technique for rapid determination of hydraulic conductivity in-situ." *Proc., Proceedings of 3rd Workshop on Land Drainage, Ohio State University*.

Meter Group Inc. (2018). "Mini Disk Infiltrometer User's Manual."

Mohanty, B., Kanwar, R. S., and Everts, C. (1994). "Comparison of saturated hydraulic conductivity measurement methods for a glacial-till soil." *Soil Science Society of America Journal*, 58(3), 672-677.

Mollins, L. H., Stewart, D. I., and Cousens, T. W. (1996). "Predicting the properties of bentonite-sand mixtures." *Clay Minerals*, 31(2), 243-252.

Mota, M., Teixeira, J., Bowen, W. R., and Yelshin, A. (2001). "Binary spherical particle mixed beds: porosity and permeability relationship measurement."

Muñoz-Carpena, R., Regalado, C. M., Álvarez-Benedi, J., and Bartoli, F. (2002). "Field evaluation of the new Philip-Dunne permeameter for measuring saturated hydraulic conductivity." *Soil Science*, 167(1), 9-24.

Nash, J. E., and Sutcliffe, J. V. (1970). "River flow forecasting through conceptual models part I—A discussion of principles." *Journal of Hydrology*, 10(3), 282-290.

Nestingen, R., Asleson, B. C., Gulliver, J. S., Hozalski, R. M., and Nieber, J. L. (2018). "Laboratory Comparison of Field Infiltrometers." *Journal of Sustainable Water in the Built Environment*, 4(3), 04018005.

Nestingen, R. S. (2007). "The comparison of infiltration devices and modification of the Philip-Dunne permeameter for the assessment of rain gardens." University of Minnesota.

Olson, N. C., Gulliver, J. S., Nieber, J. L., and Kayhanian, M. (2013). "Remediation to improve infiltration into compact soils." *Journal of environmental management*, 117, 85-95.

Perroux, K., and White, I. (1988). "Designs for Disc Permeameters." *Soil Science Society of America Journal*, 52(5), 1205-1215.

Philip, J. (1957). "The theory of infiltration: 1. The infiltration equation and its solution." *Soil science*, 83(5), 345-358.

Philip, J. (1957). "The theory of infiltration: 5. The influence of the initial moisture content." *Soil Science*, 84(4), 329-340.

Philip, J. (1993). "Approximate analysis of falling‐head lined borehole permeameter." *Water Resources Research*, 29(11), 3763-3768.

Pitt, R., Clark, S., and Field, R. (1999). "Groundwater contamination potential from stormwater infiltration practices." *Urban water*, 1(3), 217-236.

Rawls, W. J., Brakensiek, D. L., and Saxtonn, K. (1982). "Estimation of soil water properties." *Transactions of the ASAE*, 25(5), 1316-1320.

Regalado, C. M., Ritter, A., Alvarez-Benedi, J., and Munoz-Carpena, R. (2005). "Simplified method to estimate the Green–Ampt wetting front suction and soil sorptivity with the Philip–Dunne falling-head permeameter." *Vadose Zone Journal*, 4(2), 291-299.

Reynolds, W., Bowman, B., Brunke, R., Drury, C., and Tan, C. (2000). "Comparison of tension infiltrometer, pressure infiltrometer, and soil core estimates of saturated hydraulic conductivity." *Soil Science Society of America Journal*, 64(2), 478-484.

Reynolds, W., and Elrick, D. (1990). "Ponded infiltration from a single ring: I. Analysis of steady flow." *Soil Science Society of America Journal*, 54(5), 1233-1241.

Reynolds, W. D., and Elrick, D. E. (1986). "A Method for Simultaneous In Situ Measurement in the Vadose Zone of Field‐Saturated Hydraulic Conductivity, Sorptivity and the Conductivity‐Pressure Head Relationship." *Groundwater Monitoring & Remediation*, 6(1), 84-95.

Ruggenthaler, R., Meißl, G., Geitner, C., Leitinger, G., Endstrasser, N., and Schöberl, F. (2016). "Investigating the impact of initial soil moisture conditions on total infiltration by using an adapted double-ring infiltrometer." *Hydrological Sciences Journal*, 61(7), 1263-1279.

Sällfors, G., and Öberg-Högsta, A.-L. (2002). "Determination of hydraulic conductivity of sand-bentonite mixtures for engineering purposes." *Geotechnical and Geological Engineering*, 20(1), 65-80.

Sällfors, G., and Öberg-Högsta, A.-L. (2002). "Determination of hydraulic conductivity of sand-bentonite mixtures for engineering purposes." *Geotechnical & Geological Engineering*, 20(1), 65-80.

Schiff, L., and Dreibelbis, F. R. (1949). "Movement of water within the soil and surface runoff with reference to land use and soil properties." *Eos, Transactions American Geophysical Union*, 30(3), 401-411.

Shackelford, C. D., and Javed, F. (1991). "Large-scale laboratory permeability testing of a compacted clay soil."

Šimůnek, J., Šejna, M., and Van Genuchten, M. T. (2018). "New features of version 3 of the HYDRUS (2D/3D) computer software package." *Journal of Hydrology and Hydromechanics*, 66(2), 133-142.

Siriwardene, N., Deletic, A., and Fletcher, T. (2007). "Application of laboratory experiment results into practice: Clogging of stormwater infiltration systems." *Rainwater and Urban Design 2007*, 1035.

Sivapullaiah, P., Sridharan, A., and Stalin, V. (2000). "Hydraulic conductivity of bentonite-sand mixtures." *Canadian geotechnical journal*, 37(2), 406-413.

Soil Measurement Systems (2005). "Tension Infiltrometer User's Manual."

Soil Moisture Corp. (2012). "Guelph Permeameter Operating Instructions."

Taguchi, V. J., Carey, E. S., and Hunt III, W. F. (2018). "Field Monitoring of Downspout Disconnections to Reduce Runoff Volume and Improve Water Quality along the North Carolina Coast." *Journal of Sustainable Water in the Built Environment*, 5(1), 04018018.

Taylor, D. (1948). *Fundamentals of soil mechanics*, Chapman And Hall, Limited.; New York.

Van Genuchten, M. T. (1980). "A closed-form equation for predicting the hydraulic conductivity of unsaturated soils 1." *Soil science society of America journal*, 44(5), 892-898.

Weiss, P. T., and Gulliver, J. S. (2015). "Effective saturated hydraulic conductivity of an infiltration-based stormwater control measure." *Journal of Sustainable Water in the Built Environment*, 1(4), 04015005.

Wessolek, G., Plagge, R., Leij, F., and Van Genuchten, M. T. (1994). "Analysing problems in describing field and laboratory measured soil hydraulic properties." *Geoderma*, 64(1-2), 93-110.

Zhang, R. (1997). "Determination of soil sorptivity and hydraulic conductivity from the disk infiltrometer." *Soil Science Society of America Journal*, 61(4), 1024-1030.

Zhang, Y., and Schaap, M. G. (2019). "Estimation of saturated hydraulic conductivity with pedotransfer functions: A review." *Journal of Hydrology*, 575, 1011-1030.